Decoding Movement Direction for Brain-Computer Interfaces using Depth and Surface EEG Recordings

Project Report

Federico Bolner

Aalborg University,
Department of Health Science and Technology
Biomedical Engineering and Informatics
Fredrik Bajers Vej 7B
DK-9220 Aalborg

University of Padova,
Department of Information Engineering
Biomedical Engineering
Via Gradenigo, 6/B
35131 Padova, Italy

AALBORG UNIVERSITY

DEPARTMENT OF INFORMATION ENGINEERING
UNIVERSITY OF PADOVA

Department of Health Science and Technology
Fredrik Bajers Vej 7
DK-9220 Aalborg Ø
http://hst.aau.dk

Title:
Decoding Movement Direction for Brain-Computer Interfaces using Depth and Surface EEG Recordings

Theme:
Applied Biomedical Engineering & Informatics

Project Period:
Easter Semester 2012

Student:
Federico Bolner

Home university Supervisor:
Alfredo Ruggeri

Supervisors:
Dario Farina
Imran Khan Niazi

External Supervisor:
Karim Jerbi

Copies: 1

Page Number: 103

Date of Completion:
June 1^{st}, 2012

Abstract:

A Brain-Computer Interface (BCI) is a communication system between the brain and an external device. BCIs are often directed at assisting, augmenting, or repairing human cognitive or sensory-motor functions. In completely disabled patients, it may be used to recognize the patients' "will" directly from the brain in order to command a device, e.g. a prosthesis. The purpose of this project was to develop a decoder for a BCI system capable of providing a control output based on decoding of different directions of movement execution, which in turn will enhance the quality of the command to external systems to propitiate the restoration of more complex motor functions than the two-choice commands commonly available in literature. The system was based on classification of invasive and non-invasive brain signal recordings. The project was divided into sub-tasks: 1) experimental recording of a data bank of electroencephalographic (EEG) signals for testing the BCI; 2) development of a multi-class translation algorithm that decodes different movement directions based on EEG and intracranial recordings. The late step was subdivided in other two parts: a) time analysis for the detection of movement intention, and b) time frequency analysis for the classification of movement direction. Results of the detection of the intention of movement and the classification of the direction were significantly above the level of chance for both iEEG and scalp EEG data. The present study also enabled to set a comparison of different methods used for spatial filtering, normalization and classification. Merging detection and direction classification analyses seems a promising approach for the development of asynchronous brain–computer interface systems.

Acknowledgements

This report documents the work conducted during the 10th semester of the Master of Science in Biomedical Engineering and Informatics with speciality in Medical Systems at the Institute for Health Science and Technology at Aalborg University, Denmark.
Though only my name appears on the cover of this report, I would like to deeply thank many people who have contributed, directly or indirectly, to its production. My deepest gratitude goes to my supervisor Imran Khan Niazi, as well as Dario Farina and Karim Jerbi. I would also like to thank Victor, for his great contribution to this Master's thesis work. Finally, none of this would have been possible without the love and patience of my family and friends, who have sustained and encouraged me during my staying in Denmark. Sincere thanks go particularly to Nicola, Cristina, Martina, Claudio, Pablo, Andres and Yves-Rémi.

Aalborg University, June 1^{st} 2012

Contents

Chapter 1

Introduction

1.1 BCI systems

A brain-computer interface (BCI), also referred as brain-machine interface (BMI), is a device that translates neuronal signals reflecting a persons' intention into commands driving a machine (e.g. prosthesis, cursor, computer, robot, etc.) [Waldert et al., 2008; Birbaumer, 2006]. Typically, BCI control is achieved via classification of mental states or motor intentions using brain signals (such as EEG, iEEG, etc.). It is usually a closed-loop system, which acquires the signals, treats the data (preprocessing, feature extraction and classification are used to make a decision) and finally provides a feedback to the user through the device (e.g. movement of the prosthesis, etc.) [Pfurtscheller et al., 2008].

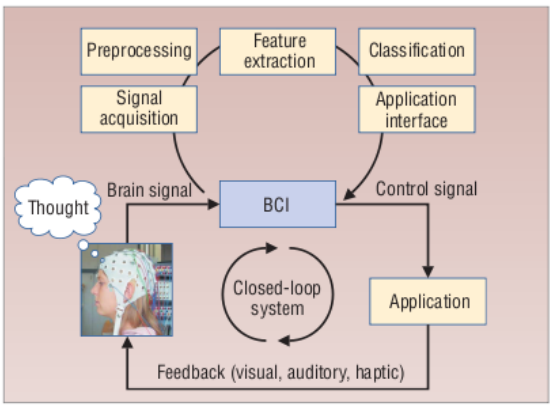

Figure 1.1: Elements of a BCI system. With the user's EEG recording as input, the system digitizes the brain signals, extracts and classifies signal features and feeds the results to the application interface. The user controls the application and receives visual, auditory, or haptic feedback on the accuracy of the focused thought. In this way, the system becomes a closed-loop [Pfurtscheller et al., 2008].

1.1.1 BCI for communication

The key part of a BCI system is to make brain and computer communicate with each other. To achieve this goal, several physiological phenomena and technical approaches are used. To date, the brain signals employed for invasive BCIs include: (1) action potentials from nerve cells or nerve fibers, (2) synaptic and extracellular field potentials and (3) electrocorticograms. The non invasive BCIs used include, instead: (1) the slow cortical potentials (SCP) component of the EEG, (2) other EEG and MEG oscillations, mainly sensorimotor rhythm (SMR), also called μ-rhythm, (3) P300 and other event-related brain potentials, (4) blood-oxygen-level-dependent (BOLD) response in functional magnetic resonance imaging (fMRI) and (5) near-infrared spectroscopy (NIRS), which measures cortical blood flow [Birbaumer, 2006].
A blind approach might also provide interesting results. Instead of using precise and well-known phenomena in given brain areas, classifiers can be trained on several 'random' features. Although this approach may be less efficient at first sight, it might provide new inputs about brain functional areas and physiology.

BCI systems are used in many different fields and applications. The main ones are rehabilitation and multi-media (e.g gaming, etc.).

1.1.2 BCI for rehabilitation

BCI systems have different medical applications. For instance, restorative BCI systems aim at normalization of neurophysiologic activity that might facilitate motor recovery. Rehabilitation methods based on neuroscience seek to stimulate spontaneous functional motor recovery by exploiting the brain potential for plastic reorganization. The example of stroke rehabilitation is meaningful. Motor impairment after stroke is the leading cause of permanent physical disability. A patient who has important difficulty to move his limbs, or can not even move them at all, can use a BCI system with visual feedback in order to improve his condition of disability. By triggering limb movements, even if the movement is not real (e.g. *motor imagery*), and adapting his will to the feedback, the patient activates sensorimotor networks that the lesions affected [Pfurtscheller et al., 2008; Soekadar et al., 2011].

Figure 1.2: Feedback training using virtual hands. The participant's task is to imagine left- and right-hand opening and closing tasks. The BCI generates movement of the right or left (virtual) hand according to classified brain patterns [Pfurtscheller et al., 2008].

Differently, the assistive technology (AT), using a BCI system, aims to provide assistance to disabled people in a daily environment (e.g. web browsing, prosthesis control, etc...). Because a BCI device alone is not able to provide 100 % reliable decoding of the real intention of the subject, BCI in AT is mainly used as an additional channel in a so-called hybrid BCI (hBCI) system [Millan et al., 2010].
However, examples of BCI-only AT systems are present in the literature. For instance, Leeb et al. succeeded to make a reliable brain-controlled wheelchair. When the tetraplegic user imagine movements of his paralysed feet, beta oscillations appear in the EEG recordings and are used to control the wheelchair in a virtual environment. The patient is then able to drive himself in a virtual street and move from avatar to avatar.

The navigation in a virtual environment may also have applications in the multi-media/gaming field.

1.1.3 BCI for gaming

Although BCI research will likely continue to focus on medical applications, BCIs may also be used by healthy users for different purposes [Allison et al., 2007].
For instance, the Berlin Brain Computer Interface (BBCI) provides intuitive control strategies in plausible gaming applications through the use of bio-feedbacks. In addition, the BBCI paradigm shows encouraging result for patients without previous experiences with BCI systems. Indeed, even an untrained subject can navigate through the Pacman labyrinth (see figure 1.3) in about 40 seconds [Krepki et al., 2003].

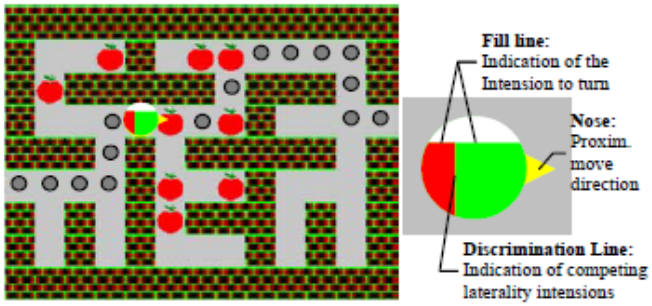

Figure 1.3: Feedback "Brain Pacman" and the head filling strategy for indication of user's upcoming intentions. The Pacman moves every 2 seconds [Krepki et al., 2007].

On top of this, many other applications can be imagined. Middendorf et al. presented a BCI that allowed people to bank a full motion aircraft simulator; some other games or virtual environments allow users to turn or lean left or right. However, this particular kind of BCI usually only allows one degree of freedom with a binary choice [Allison et al., 2007].
A few companies have sold BCIs intended to enable healthy subjects to play simple games (e.g. ibva.com, cyberlink.com and smartbraingames.com). Although the state

of art of BCI gaming usually allows only one degree of freedom with a binary choice, further developments are expected in this field [Allison et al., 2007].

1.1.4 Types of BCI systems

BCIs can be categorized according to two main characteristics: synchronization and invasiveness [Besserve, 2007].

1.1.4.1 Synchronous - asynchronous BCIs

The main difference between synchronous and asynchronous BCIs stands in the fact that synchronous BCI uses the response of the brain to a given stimulus, while asynchronous BCI analyses the signal in continue. The synchronous paradigm is usually used more often [Besserve, 2007]. For example, Leeb et al. uses an asynchronous paradigm, which screens the brain in continue, in order to control a wheelchair in real-time by imagination of feet movements.
In this report the brain response to a given signal off-line was analysed: the preparation of the movement is triggered by a visual cue, then actual movement initiated by a *"Go signal"*. It involves, therefore, a synchronous BCI.

1.1.4.2 Invasive - non invasive BCIs

Invasive BCI uses intracranial techniques to acquire the signal, such as electrocorticography (ECoG, in which electrodes are on the surface of the cortex) or stereoelectroencephalography (SEEG, where electrodes are placed inside the grey matter). Non-invasive BCI instead uses extracranial recordings of the brain activity, such as electroencephalography (EEG, electrodes on the scalp), magnetoencephalography (MEG) or functional magnetic resonance imaging (fMRI) [Besserve, 2007]. Unlike invasive systems, which entail the risks associated with brain surgery, non invasive systems are basically harmless [Pfurtscheller et al., 2008].
For practical reasons, non invasive BCI are more common: from 2007 to 2011, 14.992 publications have cited EEG or MEG, while only 337 mention intracranial EEG [Dalal et al., 2011].

1.2 State of the art

The following report was written with the goal of detecting the movement intention and classification of four different directions of hand movement, both during the actual movement and the preparation phase, by means of invasive and non-invasive synchronous BCIs.

1.2.1 Overview

Directional tuning of hand/arm movement is present in iEEG, in the low-pass filtered signals (Mehring et al. 2004, Ball et al. 2009; see also figure 1.5) and in the ampli-

tude modulations of different frequency bands (Leuthardt et al. 2004, Ball et al. 2009). Tuning strength is sufficient for relatively accurate directional decoding from low-pass filtered signals as well as from amplitude modulations of different frequency bands.
As for non invasive EEG, it has been shown that directional tuning for hand/arm movement can also be observed both in low-pass filtered signals and in amplitude modulations of different frequency bands (Waldert et al. 2008, figure 1.6). However, it seems that EEG are less capable of revealing high frequencies (Dalal et al. 2008, Waldert et al. 2008) and only few publications clearly show movement dependent high γ modulations above 90 Hz that are unlikely due to artefacts (Gonzalez et al. 2006, Ball et al. 2008).
The common time-frequency pattern during center-out movements (see figure 1.4) is the following: change of amplitude in a low frequency band ($<$ 2 Hz for iEEG, $<$ 7 Hz for EEG) during the movement, decrease of amplitude in an intermediate frequency band (6-30 Hz for iEEG, 10-30 Hz for EEG) shortly before and lasting until the end of the movement, and movement related amplitude increase in high frequency band (34-128 Hz for iEEG, 62-87 Hz for EEG) [Waldert et al., 2009].

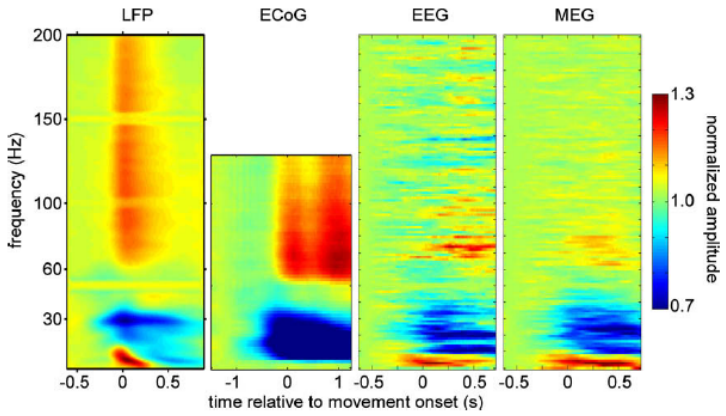

Figure 1.4: Grand-average time-resolved amplitude spectrograms during centre-out movements for the different recording techniques (LFP, ECoG, EEG, MEG) [Waldert et al., 2009].

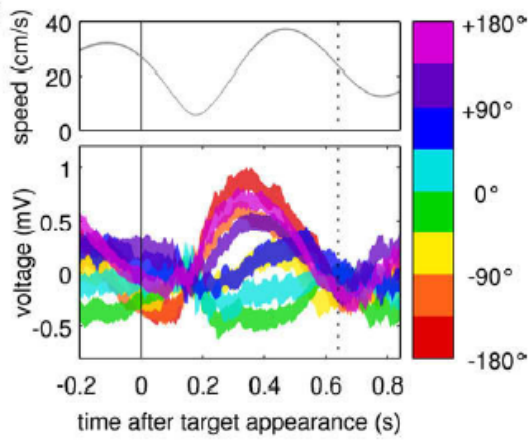

Figure 1.5: Average human ECoG recorded from one electrode placed over the hand/arm motor cortex, measured during continuous target-to-target movement and sorted for eight different movement directions (lower plot). The vertical solid line shows the time of a new target appearance (t = 0) while the dotted line indicates the median time of target reaching. Coloured bands display the mean over all single traces of one direction +/- standard-error of the mean. The upper inset shows the average magnitude of hand velocity [Waldert et al., 2009].

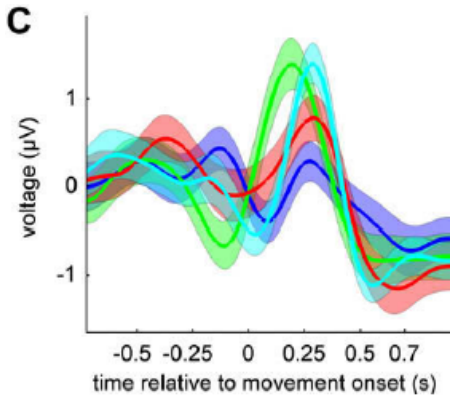

Figure 1.6: Averaged movement related potential recorded with one EEG electrode above the contralateral motor area of one subject (average +/- standard-error of the mean across all trials for each direction, blue – right, green – up, red – left, cyan – down) [Waldert et al., 2009].

1.2.2 Particular cases

Rickert et al. showed that the local field potential (LFP) recorded by an intracranial procedure can be used to discriminate 8 directions in a centre-out arm movement. Analysis of the LFPs in the time domain showed that the amplitude of a slow complex waveform beginning shortly before the onset or arm movement is modulated with the direction of the movement (see figure 1.7. Direction-dependant modulations are also found in other frequency ranges (<4 Hz, 6-13 Hz and 63-200 Hz), where the components of the signal typically increase their amplitudes before and during movement execution (see figure

1.8). As shown in figure 1.9, the analysis of the low frequency band yields the best decoding power (DP = 0.24 on < 4 Hz and 1 electrode) and the combination of the high frequency band and the low frequency band (63-200 Hz and < 4 Hz) can increase the decoding power.

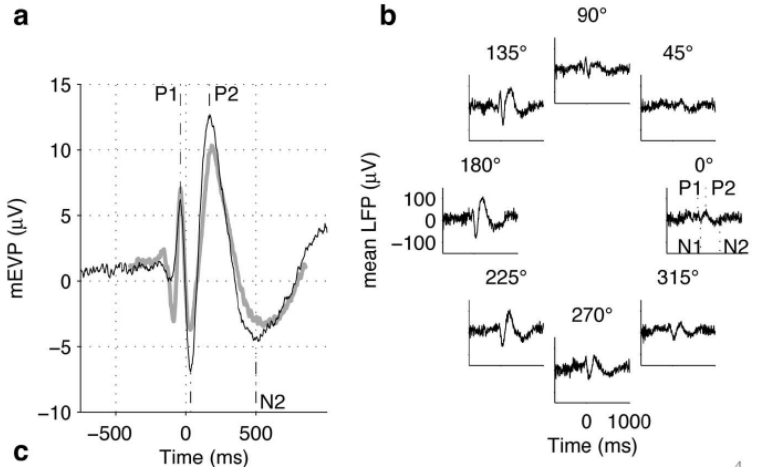

Figure 1.7: Tuning of the movement-evoked potential. Time 0 ms indicates movement onset. (a) Grand average movement evoked potentials (averaged across all recorded LFPs). Trials were aligned either to movement onset (black curve) or to cue onset (grey curve). P1, P2, N1, and N2 indicate the points in time of the positive and negative peaks of the average LFP. (b) Directional tuning of a movement evoked potential obtained from a single electrode: trial-averaged activity shown separately for each movement direction [Rickert et al., 2005].

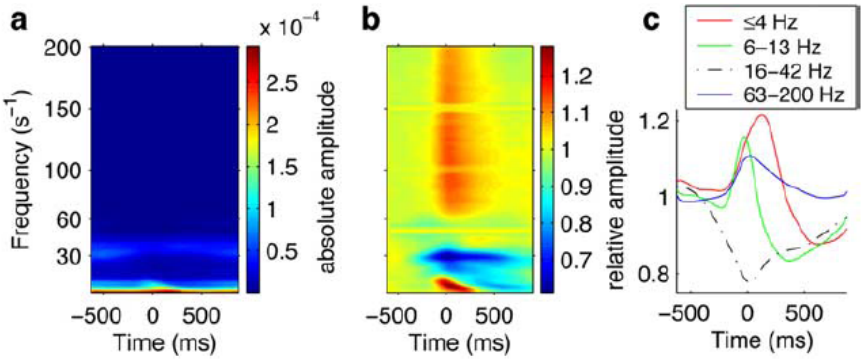

Figure 1.8: (a) Time-resolved amplitude spectrum. (b) Each frequency bin normalized by its baseline amplitude, (c) Changes in the amplitude exhibited in four different frequency bands (<4, 6–13, 16–42, and 63–200 Hz) during the task [Rickert et al., 2005].

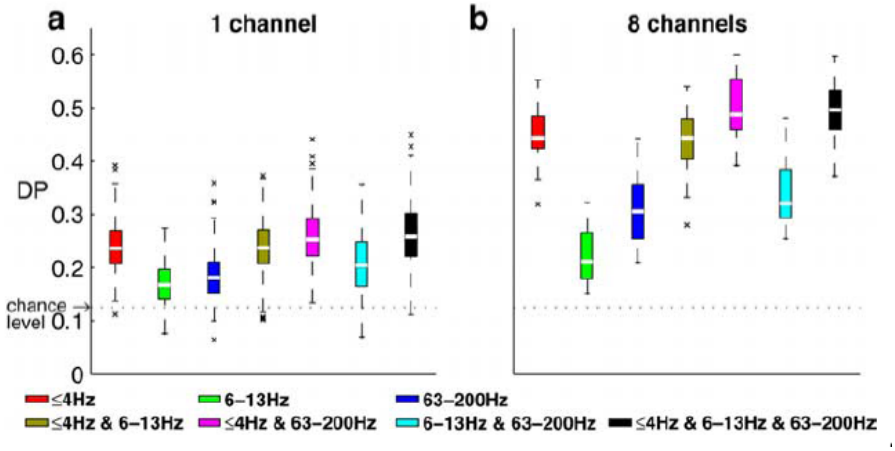

Figure 1.9: Decoding power in different frequency bands [Rickert et al., 2005].

Leuthardt et al. used ECoG recordings to control a one-dimensional computer cursor. This binary task can be a achieved with up to 74 % accuracy while opening and closing the right hand (combination of frequency bands within 10.5 and 50.5 Hz) and 83 % of accuracy while imagining opening and closing right hand (showing a decrease in 30.5-32.5 Hz band). This result may seem curious, as the best result is achieved with the imagination task. This can be explained by the effort Leuthardt et al. of optimising the imaginary task, which is indeed more relevant for BCI. Direction-dependant modulations are also found for a bidimensional joystick movement direction task (4 directions), particularly in the 40-180 Hz band (see figure 1.10).

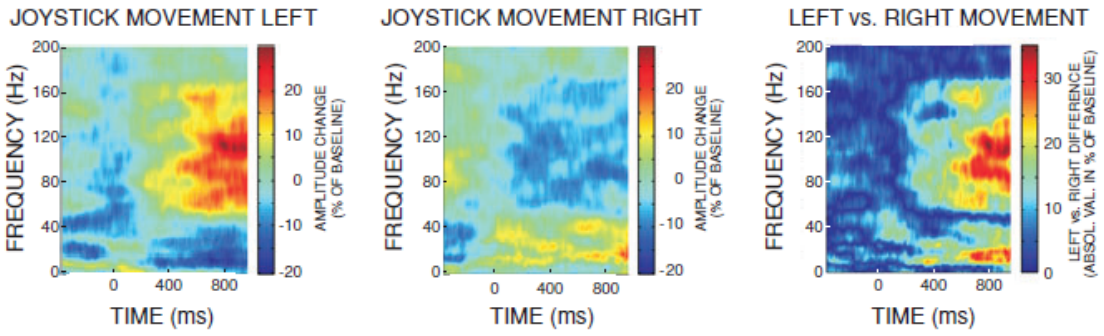

Figure 1.10: ECoG correlations with joystick movement direction before and during movement [Leuthardt et al., 2004].

Ball et al. proposed a general study on how arm movement direction in neuronal activity of the cerebral cortex (ECoG technique) can be used for movement control mediated by a BCI. The results shown in figures 1.11 and 1.12 are found using regularized linear discriminant analysis (RLDA) in a center-out arm movement task in 4 directions.

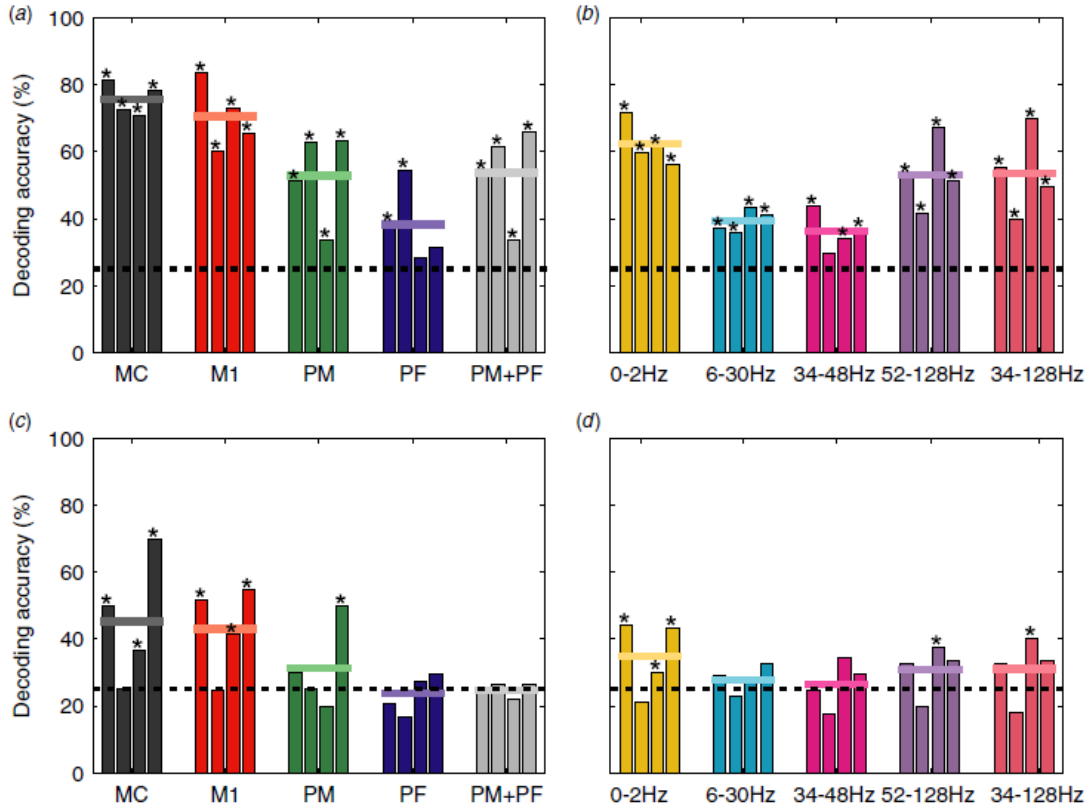

Figure 1.11: Decoding accuracy from different frontal anatomical subregions and signal frequency bands (four movement directions). The dashed line depicts the chance level. Stars indicate bars with significant decoding accuracy. (a) Decoding results for the movement-related potentials from the whole mean duration of the reaching movement, including activity up to 250 ms prior to movement onset. The five groups of bars correspond to the anatomical subdivisions MC (entire motor cortex = M1 + PM), M1 (primary motor cortex), PM (premotor cortex), PF (prefrontal cortex) and PM + PF (premotor and prefrontal cortex). Each of the five bars in the individual groups of bars represents one recording session (two sessions from subject 1, and one session from each of the subjects 2, 3 and 4). Horizontal coloured lines mark the mean DA for each anatomical subdivision. (b) Frequency domain decoding results for MC, for the same time window as in (a), for the low, intermediate and different *gamma* bands (low, high and broad). In (c) and (d), the corresponding results as in (a) and (b) are given for activity during the pre-movement time window only, ranging from 250 ms to 0 ms before the arm movement onset [Ball et al., 2009].

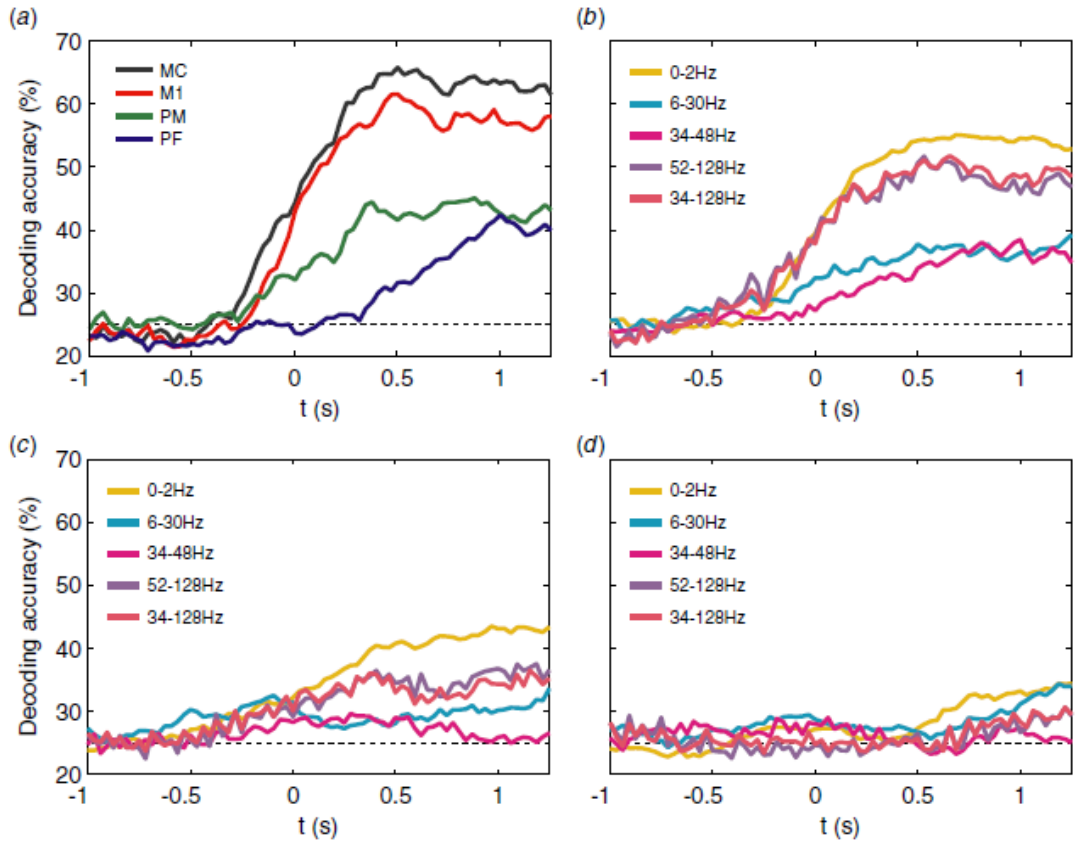

Figure 1.12: Temporal evolution of decoding accuracy. Graphs show the DA of the time window lasting from 500 ms before until the time indicated on the x-axis. Time is given relative to movement onset. (a) Time course for decoding of the movement-related potentials for M1, PM, MC and PF. (b) Time course of DA for decoding from the amplitude spectra using the low, intermediate and different *gamma* bands for M1. The black line indicates the chance level. (c) Time course for PM and (d) for PF [Ball et al., 2009].

1.3 Problem statement

Movement intention detection can be achieved studying EEG waveforms which occur before the movement onset. One of the major challenges in detecting EEG waveforms from single trials is the poor signal to noise ratio (SNR) of the EEG. Since EEG signals represent the summation of potentials generated by a large population of cortical neurons, the amplitude of the spontaneous EEG activity is relatively large (in the range of 100 μV) with respect to the activity related to motor planning and execution, such as the initial negative phase of MRCP (range 8–10 μV, see appendix C for a MRPC insight). In order to improve the SNR of EEG signals, spatial filtering can be used. However, commonly used spacial filters such as Laplacian filters, may not be optimal for detection of MRCPs from single trials [Niazi et al., 2011].

Once the movement intention is confirmed, the decoding of the direction is the next challenge. By considering the signal in the frequency domain, new information about the movement direction might be found. The ability to decode the direction of upper-limb motor tasks from its underlying neural signature is even more intriguing for brain computer interface used for rehabilitation. Although a lot of progress has been achieved in the recent years, numerous methodological and physiological questions remain open or need deeper exploration. Specifically, what type of information about movement direction can be extracted from surface and invasive recordings of brain activity? Which brain signals provide the best decoding of limb movements direction? What signal classification algorithms are best suited for this endeavour and how can we optimize them to achieve efficient BCIs in the future?

Aim

The goal of this research project is to implement and apply multiple detection and decoding techniques to scalp and depth EEG recorded in subjects performing center-out motor task in four different directions. The accuracy of the various decoding strategies will be compared at various levels: (a) the classification methods, (b) the discriminant neuronal signatures, known as the features, (c) the type of EEG recordings and (d) robustness to artifacts and noise.

Methods

This interdisciplinary project consists of two main parts: (1) electrophysiological recordings of brain activity such as MRCPs, LFPs and different brainwaves, both from iEEG and scalp EEG; and (2) implementation and comparison of signal detection, classification and decoding approaches to infer movement intention and direction from invasive and non-invasive brain signal recordings.

Part 1

Experimental data acquisition in subjects performing a delayed motor task was conducted. In addition to already existing intracranial EEG recordings acquired from an epileptic patient (Grenoble hospital, France), new surface EEG recordings were acquired (Aalborg University laboratory, Denmark). The latter experiment used scalp EEG in a delayed center-out motor task. The scalp EEG data were cleaned from blinks or muscle artifacts and were pre-processed prior to implementation of detection and classification tests.

Part 2

- Two types of signals were explored: (a) surface EEG (acquired in Aalborg University laboratory), and (b) depth intracranial EEG (provided by Lyon laboratory).

- Two types of analyses were considered, (a) movement intention detection and (b) movement direction detection, either intended (during the preparation period) or executed (during real movement).
- Two types of features were assessed: (a) time-domain features such as motor cortical potentials for movement intention detection, and (b) frequency-domain features for movement detection/direction decoding.
- Different spatial filter were used in the time-domain analysis. For the frequency-domain, features were examined with a number of appropriate signal processing tools that include: (i) wavelet transforms, to compute the frequency features from the EEG signals, (ii) Linear Discriminant Analysis (LDA), Support Vector Machine (SVM), k-Nearest Neighbor (KNN) and Neural Network (NN) for classification of (intended/executed) movement directions.

Expected impact

The results of this ambitious project may have implications at least at three levels: (a) from a methodological point of view, the comparison of the classification approaches on experimental data can provide important insights into the strengths and limitations of existing methods and might suggest how to improve them; (b) from a physiological perspective, identification of the best discriminant features will advance our knowledge of motor encoding/decoding in the context of motor-related BCIs; (c) in the long-term, the expertise and results obtained in this project may have useful implications on the future use of BCI to control a robotic prosthesis (neural prosthesis) on one hand, and on the use of BCI in the context of neuro-rehabilitation in patients with motor deficiencies on the other.

Chapter 2

Methods

In this chapter are reported the experimental protocol, the methods used for time analysis (movement intention detection) and, finally, the methods used for the time frequency analysis (movement direction classification).

2.1 Experimental protocol

2.1.1 Subjects

2.1.1.1 Intracortical EEG

The subject is a patient affected by a drug-resistant epilepsy who decided to be operated. As the EEG/MEG investigations are not sufficient to find the epileptic focus, in-depth electrodes were used until the site was located. During the investigation period, the patient gave her agreement to carry the present experiment.

2.1.1.2 Scalp EEG

Five subjects were used for this purpose. The subjects were all right-handed males with an age that ranged from 23 to 30. None of the subject suffered from hand or arm pathologies or neurological disorders. The participants gave their informed written consent before inclusion in the study. The entire test was conducted accordingly to "The Rights of a Volunteer in a Biomedical Research Project", issued by the Danish National Committee on Biomedical Research Ethics.

2.1.2 Experimental setup

2.1.2.1 Intracortical EEG

Intra-cerebral recordings were conducted using a video-SEEG monitoring system (Micromed, Treviso, Italy), which allowed the simultaneous data recording from 128 depth-EEG electrode sites. The data from the recorded patient were bandpass filtered online from 0.1 to 200 Hz and sampled at 1024 Hz During the acquisition, the data were

recorded using a reference electrode located in the white matter.
The in-depth electrodes were placed in agreement with the surgeon needs so as to identify the epileptic focus. As a result, they were spread in the brain without any relations to the investigated task.
As shown in figures 2.1 and 2.2, each electrode is labelled by a letter and each dot represents an electrode site where a signal was recorded. On each electrode, the different sites are labelled by a number: from 1 (closer from the scalp), to usually 16, depending on the specific electrode (e.g. *v14* is the 14^{th} site on electrode *v*).

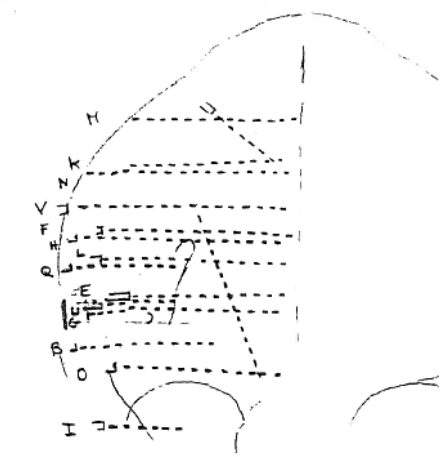

Figure 2.1: Electrodes implantation diagram, each dot represents a recording site (Image from Lyon).

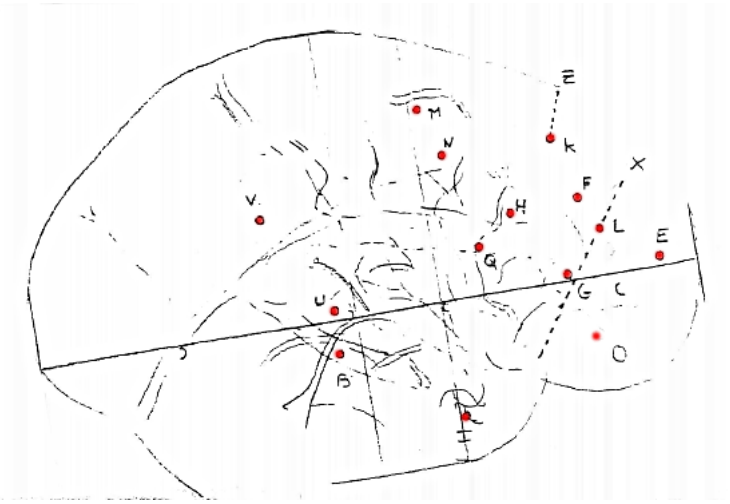

Figure 2.2: Electrodes implantation diagram, each dot represents a recording site (Image from Lyon).

2.1.2.2 Scalp EEG

The experiment took place in an electrically shielded room. Subjects were seated on a chair, in front of a LCD screen placed on a table, with the arm on the table and the hand holding a mouse. EEG signals were recorded from Ag/AgCl scalp electrodes (trying to keep the impedance below 5 $k\Omega$). Twenty electrodes were placed accordingly to the International 10-20 system, located in F3, F1, Fz, F2, F4, FC3, FC1, FCz, FC2, FC4, C3, C1, Cz, C2, C4, CP3, CP1, CPz, CP2, CP4, P3, P1, Pz, P2, P4. The subjects were grounded at the forehead. The right ear lobe (A2) was used as a reference, while the EOG was measured from FP1. The EEG and EOG signals were sampled with a rate of 500 Hz and amplified with a gain of 19, using a forty channels digital DC EEG amplifier (Nuamps Express, Neuroscan, USA) and data were recorded with the Acquire Software Scan 4.5 (Neuro Scan Labs).Presentation software was used in order to follow the exact same protocol used and provided from Lyon. The signals were converted by a 32-bit A/D converter. Early preprocessing has been performed with EEGLAB and Neuroscan.

2.1.3 Task

The experimental task consisted in a center-out movement of the hand in four different direction. The subjects were to perform a simple movement of the hand in the given direction, while holding the mouse (no constraints on the speed of the movement), reaching a given target on the screen and then coming back to the central starting point. Presentation software was used to display synchronized cues on the screen both for the iEEG and surface EEG recordings. The task consisted, in detail, of:

- A "rest period", from 0 to 1 sec, during which the screen was blank.
- At 1 sec a visual cue (illuminated target) in a random direction, was given to the subject.
- A "preparation period", from 1 to 2.5 sec, during which the subject was previously instructed not to perform the movement.
- At 2.5 sec a "go signal" was displayed. This meant that the subject could start the movement in the suggested direction.
- A "movement period", starting from 2.5 to 3.9 sec. The subject moved the pointer of the mouse towards the target, reached it, and came back to the central starting target on the screen.

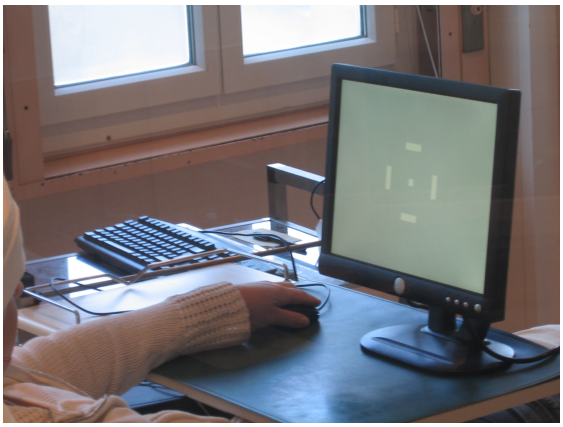

Figure 2.3: Experiment setup. The central point and the 4 different targets (up, down, right, left) can be seen on the screen.

This protocol was used both for the iEEG and surface EEG, with some differences between the number of direction and number of trials recorded. As for the iEEG recordings, the subject performed 50 trials (movement tasks) for each of the four directions (up, down, left and right), both for the left and the right hand. As for the surface EEG recordings, 100 trials for each of the four directions (up, down, left and right) were collected for the right hand, whereas only two directions (up and down, 100 trials) were collected from the left hand. The increase in the number of trails recorded from the scalp EEG can be justified by the loss of quality of the scalp recordings with respect to the intracortical ones.

2.2 Artifact removal

2.2.1 Detrend

The iEEG signal is 0.1 to 200 Hz bandpassed online then detrendend to remove the continuous part (offset). The scalp EEG signal is 0.05 - 150 Hz bandpass filtered offline then detrended. However, the bandpassing and detrending do not remove the muscular artifacts.

2.2.2 Artifact removal

2.2.2.1 iEEG data

As the muscular artifacts were widespread into the brain, their influence could partially removed their by using bipolarization on iEEG data. I.e., instead of using the voltage of site 6 and site 7 of electrode n (calculated from a reference electrode in the white matter) as two signals, n7-n6 was used. If an artifact was present, it most likely appeared on both the two sites due to the short inter-site distance (around 3 mm). Thus, these artifacts could removed by bipolarization [Jerbi et al., 2009]. After bipolarization, the

isolated recording sites (those without any adjacent sites) were removed as well.
In order to remove the remaining artifacts (e.g. channels corrupted by or used for synchronization purposes), for each channel, an averaged time-frequency (TF) map (average across all the trials and all the movement tasks) was built and visually inspected. The procedure allowed to discard those channels which did not contain useful information (see figures 2.4 and 2.5) Performing the procedures described above, 91 sources of signal out of the starting 128, were kept.

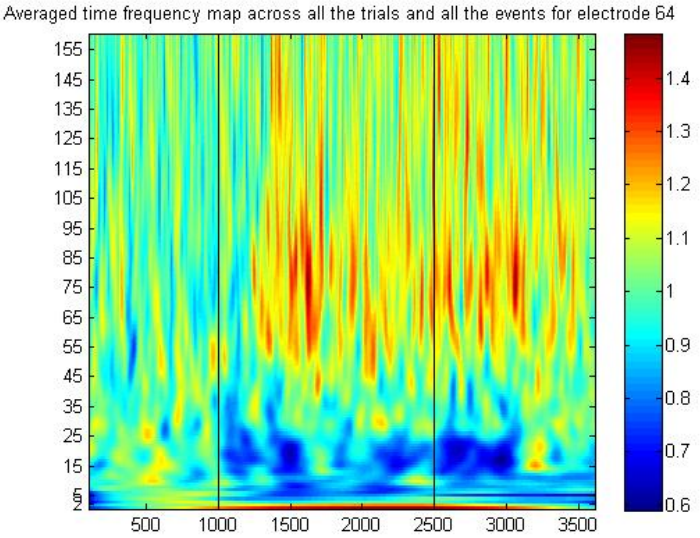

Figure 2.4: Averaged TF map for channel f10-f9. The vertical black lines show respectively the visual cue and the go signal. The channel does not show any particularly evident artifact.

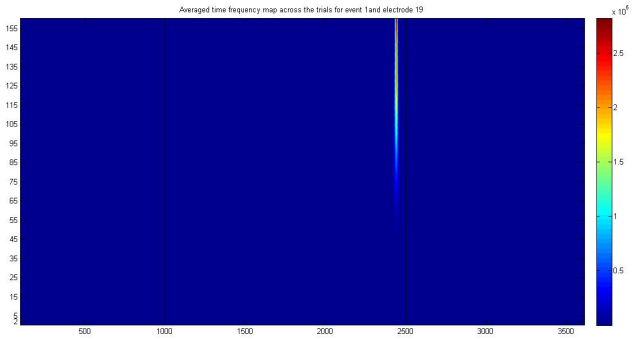

Figure 2.5: Example of a synchronous high amplitude artifact around 2450 ms. This artifact was found on channels i5-i4 and i6-i5, which were probably used to send trigger signals to the system.

2.2.2.2 Scalp EEG data

A 75 μV threshold was used for the detection of eyes artifacts in the EEG signal. For each epoch, if the signal acquired from any electrode was above the threshold, the entire epoch was discharged (and not only the couple epoch-electrode). Indeed, if an artifact was above the threshold level on one electrode, it was also present on other electrodes, maybe without being strong enough to cross the threshold. It is worth mentioning that a bipolarized iEEG signal is generally far less vulnerable to muscular artifacts than EEG signal Leuthardt et al. [2004].

2.3 Signal processing

2.3.1 Movement intention detection

Here follows a brief introduction to the protocol and the techniques used to analyse the data set, which are later treated more extensively. The experimental data were analysed with two different spatial filters and a cross-correlation approach was used to determine the movement intention detection accuracy. Since the aim is detecting the *intention* of the movement, only the initial negative phase of the MRCP was used (see appendix C for a MRPC insight). The signal analysis methods are discussed in the following subsections. The procedure was divided in two steps: first, the MRCP template extraction from the training data, and then the movement intention detection accuracy calculus.
The aim of spatial filtering is to improve the signal-to-noise ratio by creating a virtual channel which is a (linear, in the following cases) combination of the input channels of the filter. The first filter was a large Laplacian spatial filter (LSF), which has been proved to be a valuable choice among other fixed coefficient spatial filters [Niazi et al., 2011]. The second filter was an optimized spatial filter (OSF), where the optimization process is achieved with the aim of maximizing the SNR of the filtered data. After the spatial filtering, the MRCP template was extracted from the resulting channel (named surrogate channel from now on).
In the second part of the analysis, the negative phase of the MRCP template was compared to the data to calculate the movement intention detection accuracy. This was achieved by measuring the cross-correlation between template and signal and obtaining the number of correct and incorrect detections. The results are expressed using statistical parameters as true positive rate (TPR) and false positives rate (FPR). Finally, the performance of the different spatial filters was compared.
The protocol described above was applied on: (a) each data set containing the single task performed by each subject (e.g 'down' movement with the right hand for subject no. 3), and (b) combining for each hand (and subject) the data of all the movement tasks (e.g all the epochs from left hand of subject no. 3), allowing to use more epochs for the averaging, but losing the information about the direction.

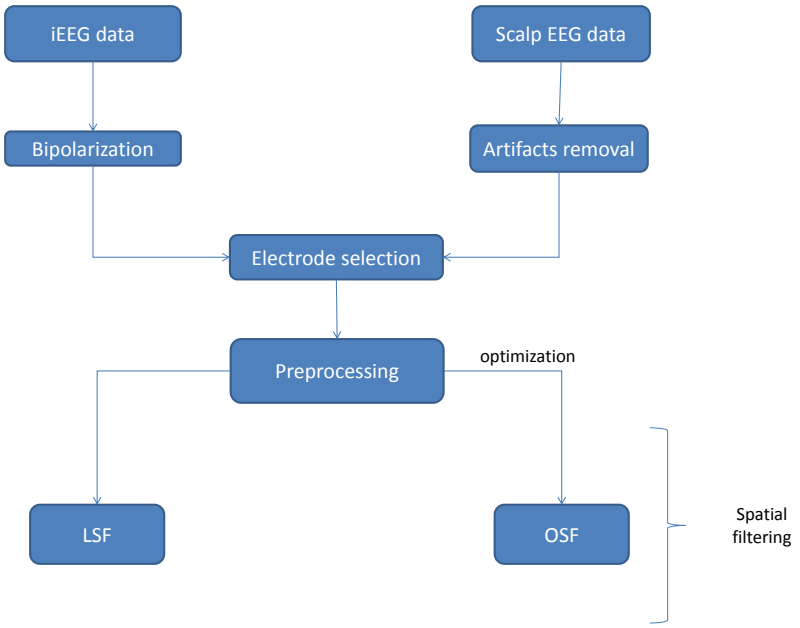

Figure 2.6: The flux diagram describes the first part of the protocol (signal processing)

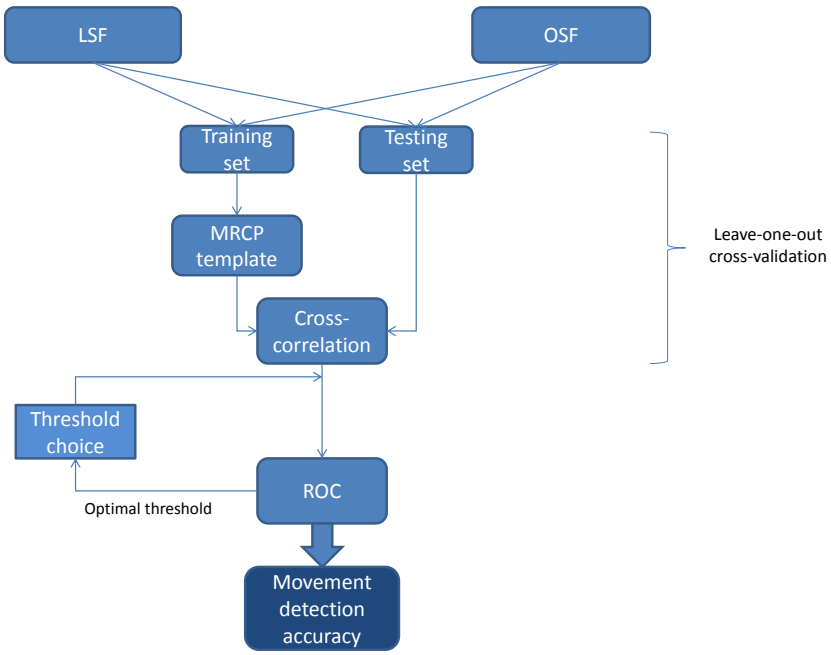

Figure 2.7: The flux diagram describes the second part of the protocol (template extraction and movement detection)

2.3.1.1 Electrode selection

iEEG After the bipolarization process, 91 channels located in 16 electrodes (see figure 2.8) were available. Out of these 91, 7 channels were selected to be used in the analysis; their location is showed in figure 2.8. This amount of channels may seem restricted compared to the starting number, but this selection was necessary for at least two reasons: (a) the optimization process for the OSF filter on 91 channels would have required a very long computation, and (b) from an MRCP extraction point of view, these seven channels were the ones showing a shape that reminded the one of the MRCP.
Among these seven channels, two channels were chosen from two electrodes near sensorimotor areas, three channels from other two electrodes located in the frontal lobe and the two last channels came from two electrodes which passed through the temporal lobe. The locations of the chosen electrodes are near the motor cortex, the prefrontal areas and basal ganglia, places in which the MRCP is likely to be generated (see appendix C).

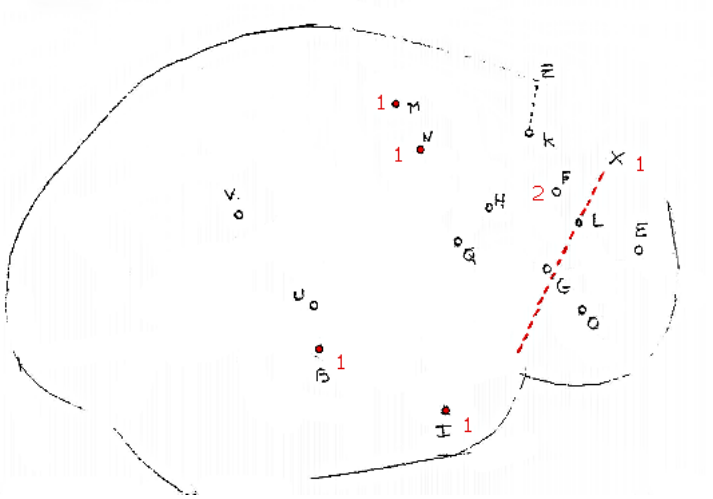

Figure 2.8: Electrodes location and number of the channels chosen for the iEEG data analysis.

Scalp EEG For the spatial filtering, 9 channels out of 20 were chosen as input for the filter. As figure 2.9 shows, they were:

- C3, C1, Cz, CP3, CP1, CPz, P3, P1, Pz for right hand movements and
- Cz, C2, C4, CPz, CP2, CP4, Pz, P2, P4 for left hand movements.

The choice is justified by the fact that these electrodes are located above the premotor, motor and somatosensory cortices and are not expected to be easily contaminated by task related auditory or visual artifacts. Electrodes F3, F1, Fz, F2 and F4 electrodes were not used, both to make the optimization process faster and because they are the nearest to the subject face.

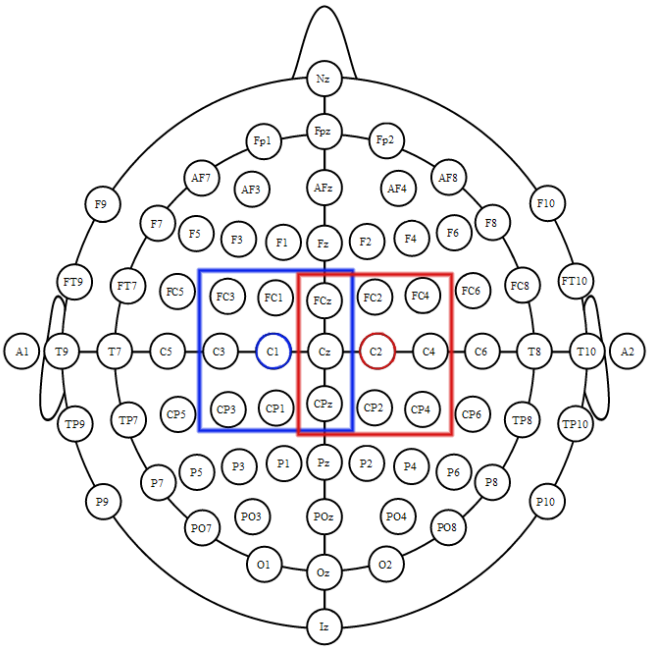

Figure 2.9: Electrodes selection for the scalp EEG. The squares indicate which electrodes were selected for the analysis, depending on the hand used during the movement (right hand:blue square, left hand:red square). The circle indicated which electrode had 1 as weight coefficient in the Laplacian filtering process.

2.3.1.2 Preprocessing

iEEG and scalp EEG data was band-pass filtered with a third order Butterworth zero-phase filter from 0.05 Hz to 5 Hz to isolate the nìabnd of interest prior to the application of the spatial filter.

2.3.1.3 Spatial filtering

In the past years, spatial filtering has been used in the BCI context especially for source localization in EEG recordings. In particular, the surface Laplacian is a technique which is applied in order to improve the spatial resolution of electroencephalographic signals. Through a liner combination of the input channels, the filtering process results in a single virtual channel (later referred as *surrogate channel*) which contains greater spatial information than the raw potentials measured by EEG montages [Bradshaw and Wikswo, 2001].
A spatial filter is defined and changes its characteristics depending on its set of coefficients. In this study, two different spatial filters were investigated: a Laplacian spatial filter (LSF) and an optimal spatial filter (OSF) [Niazi et al., 2011].
The two spatial filters (LSF and OSF, see next paragraph) were applied on the preprocessed data (both iEEG channels and EEG channels) and resulted in a surrogate channel for each one of them.

Laplacian filter The Laplacian filter has fixed coefficients. The channel coefficients used in this study, were:

$$x_i = \begin{cases} 1, & i = 1 \\ -\frac{1}{(N_{ch}-1))}, & \forall i \neq 1, \end{cases}$$

where N_{ch} is the number of channels. Thus, $N_{ch} = 7$ for the iEEG data and $N_{ch} = 9$ for the scalp EEG. The sum of the N_{ch} coefficients was zero so that the spatial dc (mean value of the waveform) components were rejected [Niazi et al., 2011]. Channel 1, which has weight equal to 1 in the Laplacian filter ($x_1 = 1$), was chosen and changed according to the type of data which was processed.

As for iEEG data, channel 1 was chosen empirically among the sources located in the frontal areas and above the motor cortex. Because of their location, a preference was initially reserved to M and N electrodes (see figure 2.8 for detailed position). As it could be expected, the signal recorded from these sites presented a good source of information about the movement phase (after the 'go' signal in the protocol), but they did not show the MRCP negativity phase. A more recurrent negative phase was instead present in a channel located on electrode F, placed over the frontal lobe of the brain. A preliminary analysis was anyway conducted and confirmed that channel F performed from 0 % up to 10-15 % better in terms of TPR compared to channels located in M or N (see section 2.3.1.4). Thus, the channel in the F electrode was finally chosen as channel 1 for the Laplacian filter for the final analysis.

As for the scalp EEG, instead, channel 1 corresponded to C1 for right hand movements and C3 for left hand movement. As shown in figure 2.9, C1 and C3 were respectively at the center of the of the two sets of electrodes positioned contralaterally with respect to the hand used during the task. Their positions, overlaying the hand area in the brain, were the ones that could most likely provide a good source of information [Ramoser et al., 2000].
Here follows an example for the scalp EEG data (right hand movement):

$$surrogate\ channel = \begin{bmatrix} x_1 & x_2 & ... & x_{N_{ch}} \end{bmatrix} \begin{bmatrix} channel\ C1 \\ channel\ C3 \\ ... \\ channel\ Pz \end{bmatrix}$$

Optimized Laplacian Filter The Optimal Spatial Filter (OSF) provides an optimized coefficient set so to maximize the signal-to-noise ratio in the surrogate channel.
The filter coefficients were optimized on the data set with the following procedure. First, 'signal' epochs of about 1 s were selected (approximately equal to the entire MRCP length). These epochs contained the initial negative phase of the MRCP. More precisely, they started from the beginning of the negativity phase of the MRCP and finished shortly before its peak positivity in the movement period. Then, 'noise' epochs of 1 second (by protocol it corresponded to the whole *rest period*) were selected.

The aim of the optimization process was to find a set of channels that maximizes the 'signal' energy while minimizing the 'noise' energy, with the constraint that the sum of the coefficients was zero. This can be translated in maximizing the SNR, which was calculated as:

$$SNR = \frac{P_{signal}}{P_{noise}},$$

where P_{signal} and P_{noise} are respectively the power of the signal and noise.
A quasi-Newton method was used for the optimization and the BFGS (Broyden–Fletcher–Goldfarb–Shanno) method was applied for the Hessian update. From an initial guess, a series of steps were repeated iteratively until the set of the filter coefficients $\mathbf{x}$ converged to the solution. The initial vector of coefficients $\mathbf{x_0}$ was based on the EEG large Laplacian montage [Niazi et al., 2011].

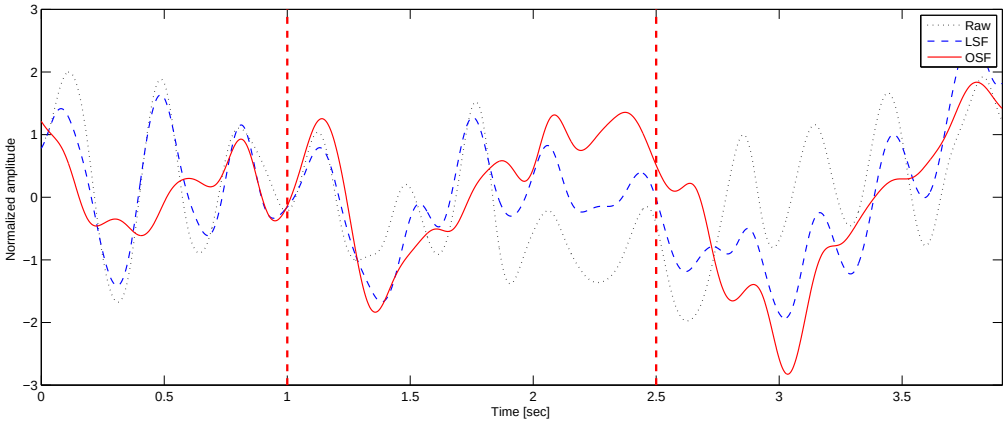

Figure 2.10: Normalized epoch traces (mean over all the epochs) for the movement in the 'up' direction, with the left hand (**iEEG data**). The plot displays the raw signal and the two spacial filters outputs. More precisely: (a) normalized 'raw' signal (after preprocessing) acquired from the 'channel 1' of the Laplacian filtering (coefficient $x_1 = 1$)('Raw', dotted line), (b) normalized surrogate channel of the Laplacian filter ('LSF', dashed line), and (c) normalized surrogate channel of the Optimized Spacial Filter ('OSF', continuous line). The vertical dashed lines correspond to the 'visual cue' and the 'go signal',respectively.
The descending phase of the MRCP was later used as template for the movement detection.

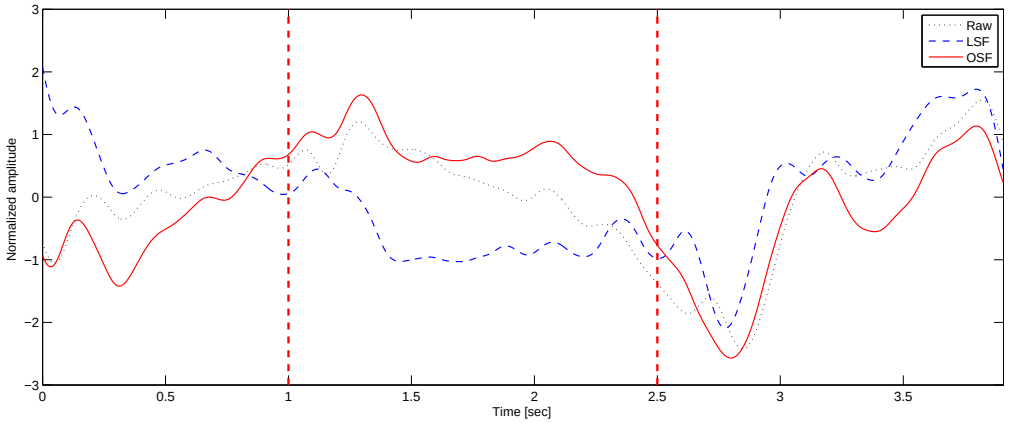

Figure 2.11: Normalized epoch traces (mean over all the epochs) for the movement in the 'up' direction, with the left hand (**scalp EEG data** recorded from subject no. 2). The plot displays the raw signal and the two spacial filters outputs. More precisely: (a) normalized 'raw' signal (after preprocessing) acquired from the 'channel 1' of the Laplacian filtering (coefficient $x_1 = 1$)('Raw', dotted line), (b) normalized surrogate channel of the Laplacian filter ('LSF', dashed line), and (c) normalized surrogate channel of the Optimized Spacial Filter ('OSF', continuous line). The vertical dashed lines correspond to the 'visual cue' and the 'go signal',respectively.
The descending phase of the MRCP was later used as template for the movement detection.

2.3.1.4 Template extraction and movement intention detection

The template was built on the descending phase of the MRCP extracted from the training data (referred to leave one-out cross-validation) of the surrogate channels of the two differnt filters (LSF and OSF), allowing later comparison. Then, through cross-validation (using the leave-one-out technique, see D.2.5) between template and testing signal epochs was calculated and a ROC curve was built. The ROC allowed to measure the true positive rate and false positive rate of the movement intention detection. The threshold for the cross-correlation, above which a 'detection' occurred, was selected on the midpoint of the turning phase of the ROC. This allowed to obtain a balance between number of correct detections and number of false positives.

Template extraction The templates were obtained from the OSF and LSF surrogate channels, averaging the epochs of the training set, and then extracting the MRCP portion of interest: from about the start of the depression phase till the negativity peak (see figure 2.12). The length of this template was in most cases of less or equal to 1 second of signal, depending on the subject, the hand and the movement in question.

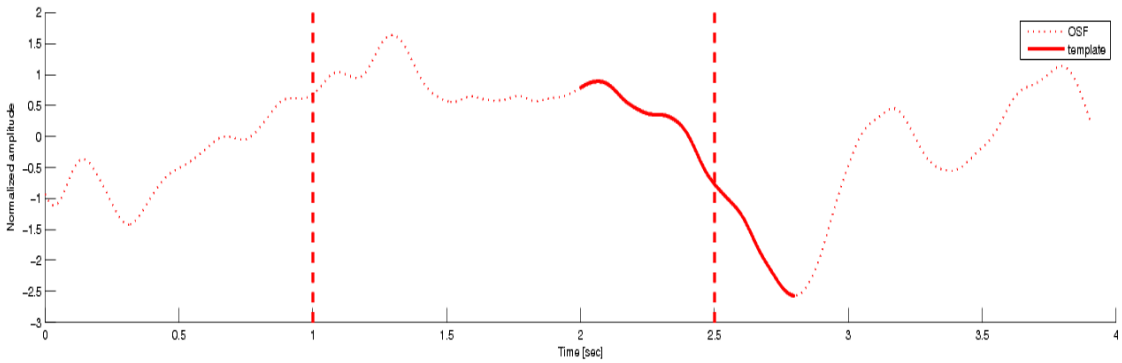

Figure 2.12: Example of template extracted from the training set (subject 2, left hand movement in the 'up' direction from scalp EEG data). The template corresponds to the descending phase of the MRCP (thick line).

Movement detection For the movement detection, a leave-one-out cross-validation approach was used (more information can be found in section D.2.5). The cross-correlation between the template (built on the training data) and testing epoch was calculated. After setting a certain threshold, the true and false positive rates could be measured. The TPR and FPR were calculated as:

$$TPR = tp/(tp + fn), \quad FPR = fp/(fp + tn),$$

where tp, tn, fp, fn indicate the number of true positives, true negatives, false positives and false negatives, respectively.

- tp (true positive): a movement is detected in the 'signal' portion of the epoch (in the protocol it corresponded to 'preparation' + 'movement' phase)
- tn (true negative): an absence of movement is detected in the 'noise' portion of the epoch ('rest period' in the protocol description)
- fp (false positive): a movement is detected in the 'noise' portion of the epoch
- fn (false negative): absence of movement is detected in the 'signal' portion of the epoch

The "detection" corresponded to finding a cross-correlation value higher than the set threshold.
The process was repeated with different threshold values, and resulted in a receiver operating characteristic (ROC). Finally the "optimal" threshold was chosen as the one that allowed to obtain the highest number of correct movement detections while having the lowest of incorrect detections; this translated in reaching the highest TPR while minimizing the FPR. It was decided to identified the 'optimal' threshold as the one which provides the nearest value (Euclidean distance) to $(TPR, FPR) = (100\%, 0\%)$ in the ROC curve. This value lay in the well known midpoint of the turning phase of the

ROC. By doing this, a balance between TPR and FPR can be obtained.
After selecting the optimal threshold, the corresponding optimal TPR and FPR were calculated. They represented a measure of the movement intention detection accuracy.

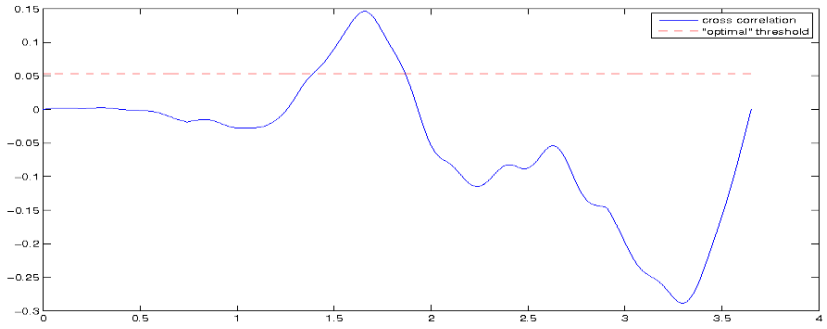

Figure 2.13: Example of cross correlation signal between template and the portion of the 'signal' portion of one epoch. The dotted red line shows the optimal threshold. In this case, the graph shows a *tp*.

Artificially generated noise By protocol, the rest period (here referred also as 'noise' signal) lasted 1 second. This duration is almost three times shorter than the remaining part of the signal (2.9 sec) and it is nearly the same as the MRCP template. Thus, it is probably not long enough to lead to a correct detection accuracy. In order to obtain a more realistic result, epochs of artificial noise of the same length of the rest of the epoch (2.9 sec) were generated.
This was done estimating an auto-regressive (AR) model of every 'noise' epoch and using it to build new noise for the epoch under exam, in place of the real noise. By doing this, the new 'noise' and 'signal' portions were of the same length.
The order of the model was set using the Akaike Final Prediction Error estimate (FPE). When the FPE did not improve in a significant way, the model could not be enhanced by incrementing its order. Using this criteria, the order was set at 15, with the provided set of data. Burger's method, which has been proved to be a valid method to estimate the parameters of an AR model, was used [De Hoon et al., 1996].
Since the AR model input was white noise, the noise estimate was slightly different every time the algorithm was run. The TPR and FPR, which changed in the same way, were thus calculated as the mean over the values of TPRs and FPRs obtained by running the algorithm 10 times.

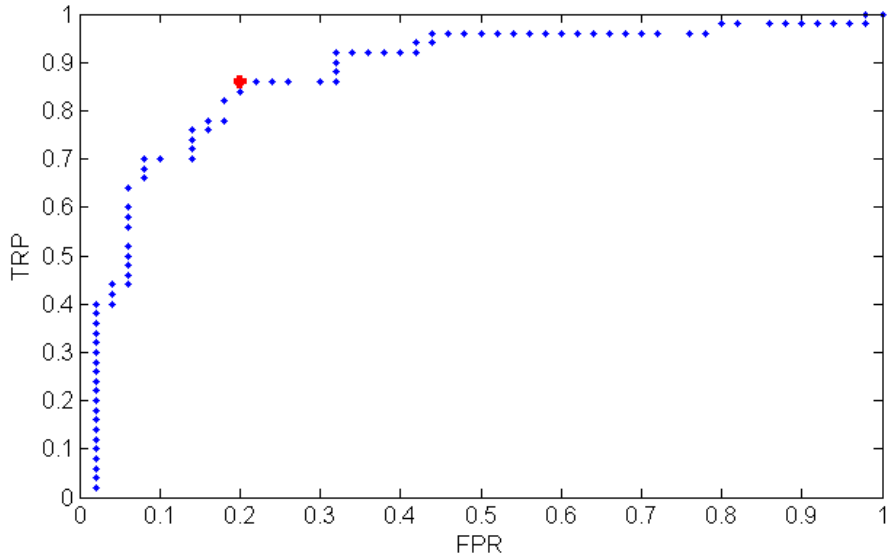

Figure 2.14: The figure shows an example of ROC curve, which gives direct information about the detection accuracy.

2.3.2 Movement direction classification

Both iEEG and scalp EEG recordings were cleaned from artifacts as described in section 2.2. The time-frequency approach was mainly used to investigate the decoding accuracy of the movement direction (for two and four directions). Other types of analyses were conducted on the decoding of movement intention and the discrimination of the hand used during the task, comparing both the data of the preparation period and movement period to the rest period.
First, normalized time-frequency maps of the power spectral density of the epochs were built for each electrode, then features were extracted from the maps and finally used for classification. Four classification algorithms were used and compared for this purpose: linear discriminant analysis (LDA), support vector machine (SVM), k-nearest neighbor (kNN) and neural network (NN) (see figure 2.15).
Following, each one of the mentioned steps is explained in detail.

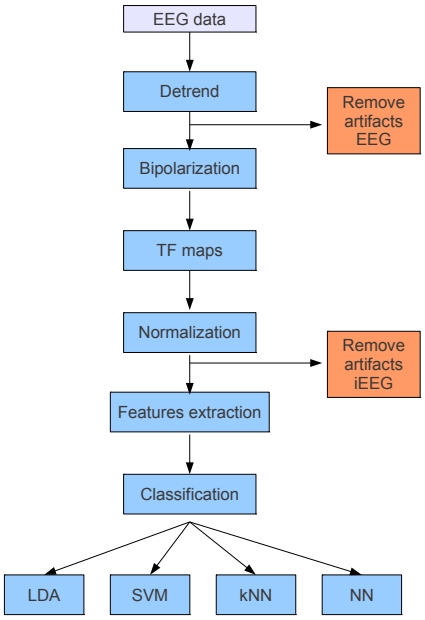

Figure 2.15: The flux diagram presents the methods used for the time-frequency analysis. (1) pre-processing: detrend and bipolarization, (2) time-frequency (TF) maps and normalization, (3) feature extraction, (4) classification with different methods: linear discriminant analysis (LDA), support vector machine (SVM), k-nearest neighbour (kNN), neural network (NN). The artifacts removal is performed at different levels with respect to the origin of the recordings.

2.3.2.1 Time-frequency maps

Time-frequency (TF) maps of the Power Spectral Density (PSD) for each channel and epoch were calculated using the wavelet transform. Despite a demanding computation, wavelet transform ensures better resolution for both time and frequency compared to the windowed Fourier transform (see appendix D.1). Furthermore, the computational issue was of minor importance because the analysis was performed offline. Morlet windows were used for the wavelet transform, as they are the most used in the BCI context. In figure 2.16 there is an example of how a TF map looked like.

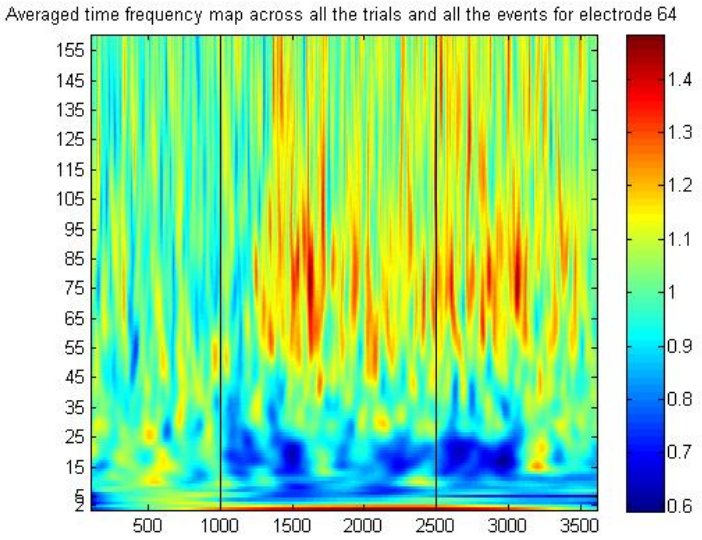

Figure 2.16: Example of a TF map. The effect of wavelet transform in high frequencies (stretching) and low frequencies (crushing) is evident. Note the increase of power in the high frequencies during preparation and the movement, while the power of the intermediate frequency band decreases. The power of the very low frequencies is particularly high during the movement preparation. Vertical black lines are the visual cue and the go signal, respectively.

Normalization In order to enhance the relative power within an epoch, the power spectra was normalized with the following method:

$$\frac{TF - baseline}{baseline},$$

where the baseline represents the PSD at rest (corresponding, by protocol, to the first second of the epoch). The power spectral density was first divided in frequency bins of 1 Hz. Then, the PSDs of each frequency bin are subtracted and then dived by the baseline PSD of the corresponding bin. TF maps were calculated in order to extracte the features of interest for the classification.

2.3.2.2 Feature extraction

Averaged PSD values in certain time and frequency windows were chosen as the features. The selected time-windows were common for iEEG and scalp EEG data: 100-800 ms for the rest period, 1000-2300 ms for the preparation period and 2700-3700 ms for the movement period. Because of the different nature of the recordings, instead, the frequency ranges choice was treated separately.

Usual frequency bands are extensively referenced in the iEEG-related literature. Normally, frequencies up to 200 Hz can be used for iEEG avoiding major noise issues ([Leuthardt et al., 2004]).
Using multiple references, the following frequency ranges were chosen for iEEG recordings: 2-4, 2-7, 4-7, 8-13, 6-30, 15-30, 30-130, 60-130 and 60-160 Hz. Very low and very high bands (0-2 Hz, 160-200 Hz) were not considered because of the wavelet transform's lack of resolution in extreme frequencies ([Leuthardt et al., 2004; Rickert et al., 2005; Ball et al., 2009; Waldert et al., 2009; Jerbi et al., 2011]).

Usual frequency bands are extensively referenced in the EEG-related literature as well. Usually, the maximal frequency is around 90 Hz, but recent references report the use of frequencies up to 150 Hz. The following frequency ranges were selected for scalp EEG recordings: < 3 Hz, < 5 Hz, < 7 Hz, 2-4 Hz, 10-30 Hz, 15-30 Hz, 30-50 Hz, 60-85 Hz, 62-87 Hz, 50-128 Hz, 30-130 Hz, which was supported by other studies ([Ball et al., 2008; Waldert et al., 2008, 2009; Jerbi et al., 2011]). The 50-128 Hz and 30-130 Hz were particularly high, but it was interesting to test them anyway.

2.3.2.3 Classification

Classification algorithms Linear discriminant analysis (LDA), Support Vector Machine (SVM), k-Nearest Neighbor and Neural Network (NN) were the classification algorithms applied to this study. A supervised approach were employed, since there was prior knowledge of which sample belonged to which class.
A review wrote by Lotte et al. helped the decision of the classifiers. LDA, RFLDA, SVM, KNN and Perceptrons provide good results in several studies (see table 2.17). However, the RFLDA is only useful if the sample size is small compared to the size of the feature vector [Dai and Yuen, 2003], which is not our case. It should also be remarked that perceptron does not actually refer to the historical perceptron, but to pattern recognition feedforward neural networks.
KNN algorithms are not very popular in the BCI community, probably because they are known to be very sensitive to the dimensionality of the feature space. However, when used in BCI systems with low-dimensionality feature vectors, kNN can be efficient [Lotte et al., 2007]. Due to its low computational requirements and good performance, LDA is particularly well suited for online classification or multi-class analysis [Lotte et al., 2007]. In addition, many references use LDA for the classification of hand movement using EEG signals [Rickert et al., 2005; Mehring et al., 2004]. As mentioned above, NN was also included. More precisely, a four-layer feedforward neural network, using a widespread supervised training method called back-propagation, was used.

Protocol	Preprocessing	Features	Classification	Accuracy (%)	References
Finger: on BCI competition 2003 data set IV	CSSD	ERD and Bereitschaftspotential based features	Perceptron	84	[48]
	14–26 Hz band pass + CSP	Activity in two brain regions with sLORETA	Perceptron	83	[18]
	bandpass	PCA+CSP+OLS	SVM	90	[77]
Speech muscles	0.5–15 Hz band pass	Raw EEG	MLP	100	[43]
Finger/toe		Raw EEG	TDNN	<90	[57]
			GDNN	≃90	
Finger: on different data sets	0–5 Hz band pass	Amplitude values of smoothed EEG	kNN	78.4	[38]
			Linear SVM	96.8	
			RFLDA	96.7	
			LDA	96.3	
		Amplitude values of smoothed EEG	Gaussian SVM	93.3	[39]
			Linear SVM	92.6	
			RFLDA	93.7	
			LDA	90.7	
			kNN	78	
		BP	Voting with LVQ NN	≃85	[54]
Finger: in asynchronous mode	1–4 Hz band pass	Bi-scale wavelet features	1-NN	up to 81	[76]
	1–4 Hz band pass + PCA	Normalized bi-scale wavelet features		97	[67]

Figure 2.17: Accuracy of classifiers in movement intention based BCI [Lotte et al., 2007].

Evaluation of the classifier performances The limited amount of data suggested the application of a method that reuses the training data for the testing. The popular leave-one-out cross-validation was selected for this purpose.
The decoding accuracy (DA) was picked as the parameter used to characterize the classifier performances. The DA is defined as the percentage of correctly decoded trials (samples, epochs) over the total number of the trials:

$$DA = \frac{N_c}{N},$$

where N_c is the number of samples which is correctly classified and N is the total number of samples [Waldert et al., 2009; Mehring et al., 2004].

2.3.2.4 Classification on iEEG recordings

As the iEEG data was available from the beginning, a deeper and more extensive examination was operated. In order to select the channels on which to run a more detailed analysis (see the end of this section), the following hypothesis was made: if a good DA for a couple channel-task (e.g. channel 1 is good to discriminate the 4 movements task)

can be found using a large time window, the DA could be improved by choosing different time windows, other frequency bands or by using a multi-feature approach, for the same couple channel-task. On the contrary, a good DA using a narrow time-window will not necessarily lead to a better DA on a wider one. As a result, the first analysis was performed on the widest time-windows.
The main goal of this first analysis was to find the channels which provided the best results for each classification method. In fact, at the end of this procedure, the three best channels were kept aside for further investigation. Besides that, a secondary goal was to provide a comparison of the different classifiers and their parameters, e.g. the parameter k in kNN. $K = 3$ was chosen as it can provide great sensitivity, and $k = 5$ because it can be more robust to the noise.
Following, you can find a summary of the methods used for this analysis:

- 'subtraction and division by baseline' normalization
- investigation of all the channels (91)
- use of the largest time windows: 100-800 ms, 1000-2300 ms and 2700-3700 ms for the rest, preparation and movement period, respectively)
- single-feature analysis
- LDA, SVM, kNN (k=3 and k=5) classification algorithms

Regarding NN, due to long computation time, an extensive analysis as was done on LDA, SVM and kNN was impossible (more than 10 days of computation). As a result, it was decided to test the NN only on the best features (couples channel-frequency range) for each task of both LDA and kNN.

This time-frequency approach was not only used to find the decoding accuracy of the movement direction, both for two directiona (discrimination between movement towards 'up' direction vs 'down' direction) and for four directions (discrimination of movements towards 'up', 'left', 'right' and 'down' direction), but also to examine the decoding of movement intention (comparing rest vs preparation period and rest vs movement period) and the discrimination of the hand used during the task (comparing the two different preparation periods for the left hand vs right hand, as well as the two movement periods).

Further analysis was conducted on the iEEG recordings. Unless otherwise specified, these analyses were not conducted from scratch on each channel, but rather on the three channels which gave the best DA with the procedure described above.

Influence of the normalization In addition to the 'subtraction and division by baseline' method, the following were also studied on kNN (k=3) and LDA:

- absence of normalization
- $TF - baseline$
- $\frac{TF}{baseline}$

Time-windows influence For each period of the task, other two shorter time windows besides the largest were considered: 100-500 ms and 400-800 ms for the rest period; 1000-1400 ms and 200-2500 ms for the preparation period; 2500-300 ms and 3200-3700 ms for the movement period.

Two-feature analysis Multi-feature approaches are highly referenced in literature, so a two-feature analysis (two different frequency ranges at the same time) was conducted on LDA and kNN. The DA was obtained by examining only the three best channels provided by the first single-feature analysis, but did not lead to a better DA. This was quite unexpected, thus a second analysis from scratch scanning all the possible channels was performed with LDA (the DA, indeed, improved using this approach).

Combination of channels The signals supplied by the three channels found in the first classification analysis were combined by summation as follows: chann1 + chann2, chann2 + chann3, chann3 + chann1, chann1 + chann2 + chann3, with the aim of improving the DA.

2.3.2.5 Classification on scalp EEG recordings

As scalp EEG recordings have been performed in the last weeks of the project, the results found for intracortical data were applied to scalp EEG classification. So, the protocol included the use of the 'subtraction and division by the baseline' normalization method, the largest time windows (100-800, 1000-2300 and 2700-3700 ms), one feature (frequency band), a single channel, and LDA and kNN (k=3 and k=5) classification algorithms. Due to this time issues, SVM an NN were not used.
Further analysis was anyway briefly performed on the first data provided by the Aalborg's laboratories (subject 1) and included the use of different time windows and SVM. As for the time windows, no improvement of the DA was shown. Regarding SVM, instead, the results were very similar to those provided by LDA, as happened in the iEEG analysis. So, as SVM was a time consuming algorithm, it was not kept.

Chapter 3

Results

Time and time-frequency results are successively displayed in this chapter.

3.1 Movement intention detection

In general, the results demonstrated that it is possible to detect voluntary movement intentions using the descending phase of the MRCPs. The TPR (true positive rate) was always above 70% (OSF data) and often above 75 %, which roughly translates in the correct detection of three intended movement out of four. The TPRs sometimes reach values above 80% or 90% (using real noise and estimated noise, respectively). Most of the FPRs (false positive rate) were, instead, around 20-25%. Considering the complexity of the task the subject had to perform, and the amount of 'noise signal' available, the results were considered rather satisfactory.

The following tables present the TPRs (%) and FPRs (%) for the datasets already described in chapter 2. They point out the detection performances on (a) the particular movement (4 directions) performed by each subject (e.g. movement towards 'down' direction, with the right hand of subject no. 3), and (b) the combined data that came from the hand (left and right) of a subject, with no distinction of the direction.
An average over the different movements for every subject can also be evaluated easily (see tables 3.1, 3.2, 3.5, 3.6 and 3.3, 3.4 3.7, 3.8).
The analysis was performed both on iEEG and EEG data (Tables from 3.1 to 3.4 and from 3.5 to 3.9, respectively). The detection accuracy has been calculated for two data sets: the first provided by purely by the recordings unchanged, and the second by using estimated 'noise signals' of 3 seconds, built from the 'real' noise signals (corresponding to the first second of the recorded epochs). In the latter case, an average of the TPRs and FPRs has been calculated over the values (TPRs and FPRs) that were given running the algorithm 10 times. The standard deviation of the mentioned average was not reported in the tables to avoid confusion and because it was always lower than 5%. As expected, using only the rest period (or 'real noise') as the noise signal provided greater performances.

A comparison between the performance of the two spatial filters is highlighted in the tables as well, finding no relevant improvement using the OSF. In particular, table 3.9 shows the detection accuracy for the two filters, averaging the TPRs and FPRs over all the movements and all the subjects.
Finally, Table 3.10 shows the mean over the five subjects for the six tasks (scalp EEG recordings), using estimated noise.

Since the legend is common for every table, it will be listed here:

- OSF Optimized Spatial Filter
- LSF Laplacian Spatial Filter
- LH Left Hand
- RH Right Hand
- u movement towards 'up' direction
- d movement towards 'down' direction
- l movement towards 'left' direction
- r movement towards 'right' direction

Mov.	**OSF - TPR (%)**	**LSF - TPR (%)**
LH_u	84.0	80.0
LH_r	90.0	82.0
LH_d	96.0	82.0
LH_l	90.0	72.0
RH_u	80.0	70.0
RH_r	94.0	80.0
RH_d	86.0	74.0
RH_l	80.0	88.0
sd	6.0	6.0
Mean	**87.5**	**78.5**

Mov.	**OSF - FPR (%)**	**LSF - FPR (%)**
LH_u	18.0	20.0
LH_r	12.0	24.0
LH_d	30.0	26.0
LH_l	12.0	10.0
RH_u	18.0	32.0
RH_r	18.0	24.0
RH_d	32.0	38.0
RH_l	20.0	32.0
sd	7.4	8.6
Mean	**20.0**	**25.8**

Table 3.1: The table shows the detection accuracy for the iEEG data for the particular movement task performed by the subject.

Mov.	**OSF - TPR (%)**	**LSF - TPR (%)**
LH_u	79.9	70.1
LH_r	79.6	74.1
LH_d	71.4	81.5
LH_l	81.5	69.9
RH_u	72.7	78.0
RH_r	73.4	75.3
RH_d	68.3	72.4
RH_l	75.0	77.9
sd	4.7	4.1
Mean	**75.2**	**74.9**

Mov.	**OSF - FPR (%)**	**LSF - FPR (%)**
LH_u	26.7	38.9
LH_r	34.7	42.2
LH_d	34.4	36.7
LH_l	29.3	32.8
RH_u	34.8	45.6
RH_r	35.0	38.2
RH_d	52.5	43.6
RH_l	31.4	41.1
sd	7.8	4.1
Mean	**34.9**	**39.9**

Table 3.2: The table shows the detection accuracy for the iEEG data for the particular movement task performed by the subject, using estimated noise signal for the analysis.

Mov.	OSF - TPR (%)	LSF - TPR (%)
LH	81.5	84.5
RH	83.0	83.0
sd	1.1	1.1
Mean	**82.3**	**83.8**

Mov.	OSF - FPR (%)	LSF - FPR (%)
LH	14.5	23.5
RH	20.5	27.0
sd	4.2	2.5
Mean	**17.5**	**25.3**

Table 3.3: The table shows the detection accuracy for the iEEG data, for the joined movement tasks performed by the subject, for both hands.

Mov.	OSF - TPR (%)	LSF - TPR (%)
LH	75.2	77.9
RH	78.7	80.3
sd	2.5	1.7
Mean	**77.0**	**79.1**

Mov.	OSF - FPR (%)	LSF - FPR (%)
LH	31.9	32.0
RH	35.2	34.3
sd	2.3	1.6
Mean	**33.6**	**33.2**

Table 3.4: The table shows the detection accuracy for the iEEG data, for the joined movement tasks performed by the subject, for both hands, using estimated noise in analysis.

	OSF - TPR (%)					LSF - TPR (%)				
Mov.	**sub1**	**sub2**	**sub3**	**sub4**	**sub5**	**sub1**	**sub2**	**sub3**	**sub4**	**sub5**
LH_u	66.3	60.0	76.6	57.1	71.7	70.4	64.7	64.9	66.3	71.7
LH_d	83.4	79.3	61.3	77.9	77.3	63.6	70.1	54.8	72.6	75.3
RH_u	70.4	87.8	69.0	75.2	81.0	68.4	79.6	75.0	65.0	66.0
RH_r	69.0	72.4	72.2	84.0	91.2	75.0	78.6	58.8	69.0	84.3
RH_d	63.3	78.8	75.3	65.0	86.5	79.6	88.9	69.1	65.0	64.4
RH_l	69.4	81.2	85.7	82.0	78.8	80.6	68.7	65.3	64.0	73.1
sd	6.9	9.5	8.2	10.4	6.9	6.7	8.9	7.2	3.3	7.2
Mean	**70.3**	**76.6**	**73.4**	**73.5**	**81.1**	**72.9**	**75.1**	**64.7**	**67.0**	**72.5**

	OSF - FPR (%)					LSF - FPR (%)				
Mov.	**sub1**	**sub2**	**sub3**	**sub4**	**sub5**	**sub1**	**sub2**	**sub3**	**sub4**	**sub5**
LH_u	45.9	31.8	45.7	27.6	44.6	45.9	36.5	40.4	36.7	29.3
LH_d	21.2	44.8	35.4	42.1	26.8	33.3	51.7	37.6	35.8	39.1
RH_u	17.3	25.5	24.0	30.9	21.0	27.6	34.7	50.0	25.8	38.0
RH_r	27.0	27.6	26.8	27.0	3.9	31.0	35.7	21.6	34.0	17.6
RH_d	33.7	20.2	29.9	36.0	19.2	19.4	39.4	27.8	27.0	50.0
RH_l	48.0	36.4	32.7	26.0	22.1	21.4	25.2	18.3	23.0	52.9
sd	11.3	9.3	8.6	6.3	14.7	9.6	7.0	11.1	5.1	12.1
Mean	**32.2**	**31.1**	**32.4**	**31.6**	**22.9**	**29.8**	**37.2**	**32.6**	**30.4**	**37.8**

Table 3.5: The table shows the detection accuracy for the scalp EEG data for the particular movement task performed by the subject.

	OSF - TPR (%)					LSF - TPR (%)				
Mov.	**sub1**	**sub2**	**sub3**	**sub4**	**sub5**	**sub1**	**sub2**	**sub3**	**sub4**	**sub5**
LH_u	70.0	62.0	73.7	65.3	65.7	73.8	62.6	65.1	58.1	69.3
LH_d	80.9	84.8	72.8	70.6	69.6	56.4	84.0	57.7	66.1	63.7
RH_u	76.7	78.0	69.7	69.8	75.9	68.8	79.0	76.7	63.6	58.3
RH_r	81.4	77.1	80.7	69.2	86.1	80.0	78.3	66.5	69.3	77.2
RH_d	57.7	77.0	70.0	78.5	78.8	68.6	85.1	64.1	64.4	64.6
RH_l	61.2	64.7	60.7	69.0	72.0	73.2	74.6	60.5	64.6	66.0
sd	10.1	8.7	6.5	4.4	7.2	7.9	8.2	6.5	3.7	6.3
Mean	**71.3**	**73.9**	**71.3**	**70.4**	**74.7**	**70.1**	**77.3**	**65.1**	**64.4**	**66.5**
	OSF - FPR (%)					**LSF - FPR (%)**				
Mov.	**sub1**	**sub2**	**sub3**	**sub4**	**sub5**	**sub1**	**sub2**	**sub3**	**sub4**	**sub5**
LH_u	40.1	20.2	32.2	28.7	19.7	19.8	18.8	17.1	16.9	23.6
LH_d	30.0	19.3	27.8	33.4	22.2	23.3	29.4	32.7	30.8	28.2
RH_u	19.4	22.2	16.9	21.6	21.5	18.0	25.3	25.1	22.5	21.8
RH_r	26.5	22.1	25.6	25.9	17.5	15.3	23.1	24.0	22.5	21.5
RH_d	20.4	18.3	23.3	23.3	17.2	19.8	25.1	24.7	19.5	29.9
RH_l	31.9	29.6	22.4	25.1	25.0	24.2	25.0	25.6	24.8	32.4
sd	7.7	4.1	5.2	4.2	3.0	3.3	3.5	5.0	4.8	4.6
Mean	**28.1**	**22.0**	**24.7**	**26.3**	**20.5**	**20.1**	**24.5**	**24.9**	**22.8**	**26.2**

Table 3.6: The table shows the detection accuracy for the scalp EEG data for the particular movement task performed by the subject, using estimated noise signal for the analysis.

	OSF - TPR (%)					LSF - TPR (%)				
Mov.	**sub 1**	**sub 2**	**sub3**	**sub4**	**sub5**	**sub 1**	**sub 2**	**sub3**	**sub4**	**sub5**
LH	74.5	87.8	70.0	84.0	81.0	69.4	79.6	78.0	69.0	66.0
RH	75.0	72.4	72.1	75.3	91.2	80.0	78.6	58.8	64.9	84.3
sd	0.4	10.9	1.5	6.2	7.2	7.5	0.7	13.6	2.9	12.9
Mean	**74.8**	**80.1**	**71.1**	**79.7**	**86.1**	**74.7**	**79.1**	**68.4**	**67.0**	**75.2**
	OSF - FPR (%)					**LSF - FPR (%)**				
Mov.	**sub 1**	**sub 2**	**sub3**	**sub4**	**sub5**	**sub 1**	**sub 2**	**sub3**	**sub4**	**sub5**
LH	24.5	25.5	23.0	27.0	21.0	23.5	34.7	51.0	34.0	38.0
RH	35.0	27.6	27.8	30.1	3.9	35.0	35.7	21.6	25.8	17.6
sd	7.4	1.5	3.4	2.2	12.1	8.1	0.7	20.8	5.8	14.4
Mean	**29.8**	**26.6**	**25.4**	**28.6**	**12.5**	**29.3**	**35.2**	**36.3**	**29.9**	**27.8**

Table 3.7: The table shows the detection accuracy for the iEEG data, for the joined movement tasks performed by the subject, for both hands.

	OSF - TPR (%)					LSF - TPR (%)				
Mov.	**sub 1**	**sub 2**	**sub3**	**sub4**	**sub5**	**sub 1**	**sub 2**	**sub3**	**sub4**	**sub5**
LH	80.8	76.7	67.3	69.8	76.4	69.4	81.0	76.0	63.9	58.5
RH	74.4	76.2	80.1	72.4	85.1	82.7	78.0	66.3	69.1	76.4
sd	4.5	0.4	9.1	1.8	6.2	9.4	2.1	6.9	3.7	12.7
Mean	**77.6**	**76.5**	**73.7**	**71.1**	**80.8**	**76.1**	**79.5**	**71.2**	**66.5**	**67.5**
	OSF - FPR (%)					**LSF - FPR (%)**				
Mov.	**sub 1**	**sub 2**	**sub3**	**sub4**	**sub5**	**sub 1**	**sub 2**	**sub3**	**sub4**	**sub5**
LH	29.8	23.2	16.8	24.3	24.3	24.2	28.1	25.5	22.3	20.4
RH	25.8	19.8	26.3	29.1	19.5	19.7	21.5	26.6	22.4	20.1
sd	2.8	2.4	6.7	3.4	3.4	3.2	4.7	0.8	0.1	0.2
Mean	**27.8**	**21.5**	**21.6**	**26.7**	**21.9**	**22.0**	**24.8**	**26.1**	**22.4**	**20.3**

Table 3.8: The table shows the detection accuracy for the iEEG data, for the joined movement tasks performed by the subject, for both hands, using estimated noise in analysis.

TPR (%)		FPR (%)	
OSF	**LSF**	**OSF**	**LSF**
72.3	69.7	24.3	23.2

Table 3.9: Mean over all the movement tasks and all the subjects, for the same spatial filter (estimated noise data)

	TPR (%)		FPR (%)	
Mov.	**OSF**	**LSF**	**OSF**	**LSF**
LH_u	67.3	65.8	28.2	19.2
LH_d	75.7	65.6	26.5	28.9
RH_u	74.0	69.3	20.3	22.5
RH_r	78.9	74.3	23.5	21.3
RH_d	72.4	69.4	20.5	23.8
RH_l	65.5	67.8	26.8	26.4

Table 3.10: The table shows the mean over the five subjects of the everyone of the six tasks performed during scalp EEG recordings (estimated noise data).

3.2 Movement direction classification

3.2.1 iEEG data

The following tables display the results of the decoding accuracy (DA) obtained from the first analysis performed on iEEG recordings (see section 2.3.2). A summary of the analysis can be found in figures 3.4 and 3.5, which respectively display the best DAs found for each comparative analysis and each classifier, and the number of occurrences of each frequency band which belongs to the best discriminant features across the classifiers. Some representative TF-maps are reported in figures 3.6, 3.7 and 3.8.

	LDA			**SVM**		
	DA(%)	*freq. band (Hz)*	*chann.*	*DA(%)*	*freq. band (Hz)*	*chann.*
RM	82.25	60-130	v14-v13	86	2-7	i2-i1
RP	81.5	6-30	b2-b1	86.25	2-7	v14-v13
LRM	67	60-160	u2-u1	67	60-160	u2-u1
LRP	64	60-130	v3-v2	63	60-130	v3-v2
UDM	66	60-160	g13-g12	65	60-160	g13-g12
UDP	64	8-13	u2-u1	63	2-4	x14-x13
4M	36	15-30	o10-o9			
4P	35	30-130	x14-x13			

Figure 3.1: For LDA and SVM classifiers, the best decoding accuracy (DA) found using all channels and all the frequency bands is displayed. The type of analysis is shown in the first column. RM: rest vs movement; RP: rest vs preparation; LRM: left vs right hand, using the movement period; LRP: left vs right hand, using the preparation period; UDM: movement towards 'up' direction vs movement towards 'down' direction, using the movement period; UDP: movement towards 'up' direction vs movement towards 'down' direction, using the preparation period; 4M: 4-directions classification, using the movement period; 4P: 4-directions classification, using the preparation period.

	kNN, k=3			**kNN**, k=5		
	DA(%)	*freq. band (Hz)*	*chann.*	*DA(%)*	*freq. band (Hz)*	*chann.*
RM	99.5	60-130	x13-x12	99	15-30	g14-g13
RP	99.75	2-7	k11-k10	98.75	30-130	m11-m10
LRM	78	8-13	f3-f2	78	8-13	f3-f2
LRP	71	2-7	e8-e7	69	60-160	o9-o8
UDM	73	15-30	q7-q6	66	60-130	v2-v1
UDP	68	2-4	e6-e5	71	4-7	o2-o1
4M	37	60-130	f9-f8	40.5	15-30	o9-o8
4P	40	2-7	q8-q7	36.5	2-7	e8-e7

Figure 3.2: For kNN classifiers (k=3 and k=5), the best decoding accuracy (DA) found using all channels and all the frequency bands is displayed. The type of analysis is shown in the first column. RM: rest vs movement; RP: rest vs preparation; LRM: left vs right hand, using the movement period; LRP: left vs right hand, using the preparation period; UDM: movement towards 'up' direction vs movement towards 'down' direction, using the movement period; UDP: movement towards 'up' direction vs movement towards 'down' direction, using the preparation period; 4M: 4-directions classification, using the movement period; 4P: 4-directions classification, using the preparation period.

	NN for LDA	**NN** for kNN
	DA(%)	*DA(%)*
RM	95.7	95.7
RP	95.2	94
LRM	55	50
LRP	59	44
UDM	50	50
UDP	50	41

Figure 3.3: For NN, the decoding accuracy (DA) found using only the couple channel-frequency that leads to the best DA with the previous analyses conducted using LDA and kNN (k=3) is displayed. The type of analysis is shown in the first column. RM: rest vs movement; RP: rest vs preparation; LRM: left vs right hand, using the movement period; LRP: left vs right hand, using the preparation period; UDM: movement towards 'up' direction vs movement towards 'down' direction, using the movement period; UDP: movement towards 'up' direction vs movement towards 'down' direction, using the preparation period.

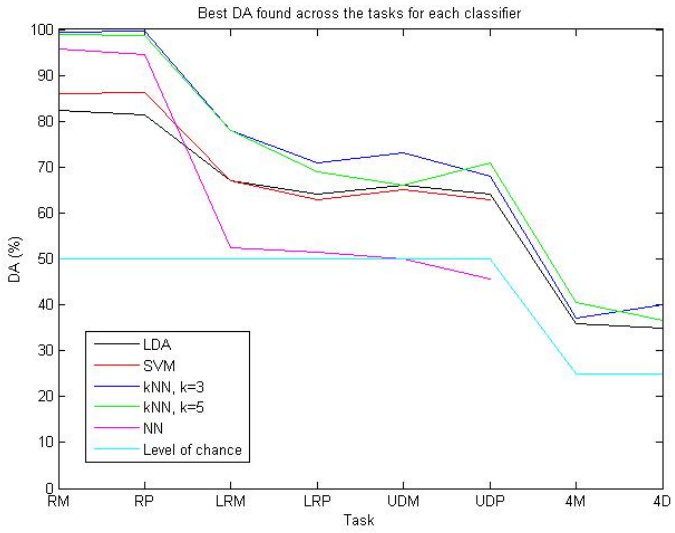

Figure 3.4: Best decoding accuracy (DA) found for each type of analysis and each classifier. For the NN classifier, the average of the DA found with NN-LDA and NN-kNN is displayed (see figure 3.3). RM: rest vs movement; RP: rest vs preparation; LRM: left vs right hand, using the movement period; LRP: left vs right hand, using the preparation period; UDM: movement towards 'up' direction vs movement towards 'down' direction, using the movement period; UDP: movement towards 'up' direction vs movement towards 'down' direction, using the preparation period; 4M: 4-directions classification, using the movement period; 4P: 4-directions classification, using the preparation period.

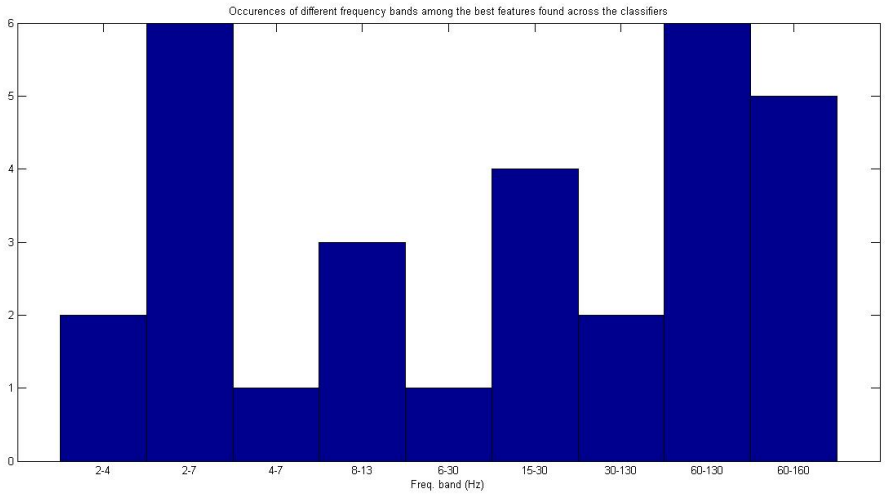

Figure 3.5: Number of occurrences of each frequency band which belongs to the best discriminant features across the classifiers.

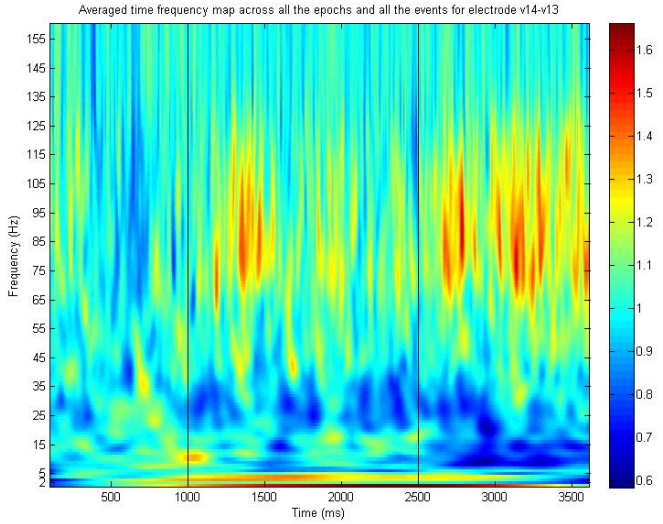

Figure 3.6: Averaged time-frequency map across all the events and all the epochs of channel v14-v13. Note how the power in high and low frequencies increases during the preparation and the movement period. This channel yields to a $DA = 82.25\%$ for rest vs movement using the 60-130 Hz frequency band and LDA, and a $DA = 86.25\%$ for rest vs preparation using the 2-7 Hz and SVM.

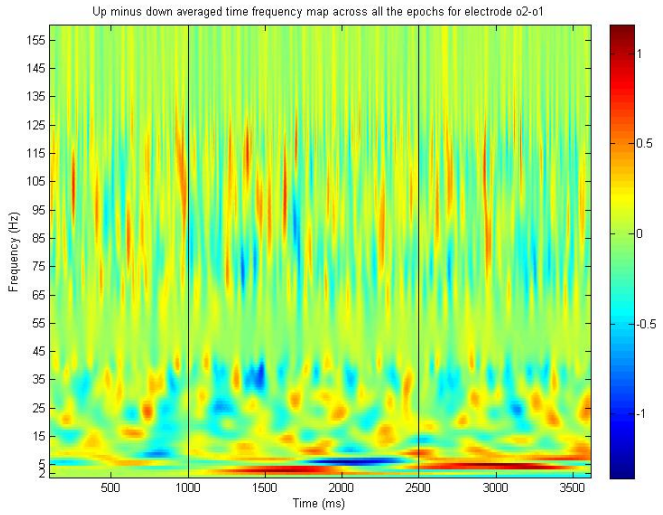

Figure 3.7: The figure displays the subtraction of the averaged (on all the epochs) time-frequency maps of movement towards 'up' direction and towards 'down' direction (channel o2-o1). We notice an increase of power in the 2-5 Hz frequency band and a decrease of power in the 5-8 Hz frequency band during the preparation period, and an increase of power in 3-7 Hz frequency band during the movement. This channel yields to a $DA = 71\%$ movement towards 'up' direction vs movement towards 'down' direction, using the preparation period, 4-7 Hz frequency band, and kNN (k=5).

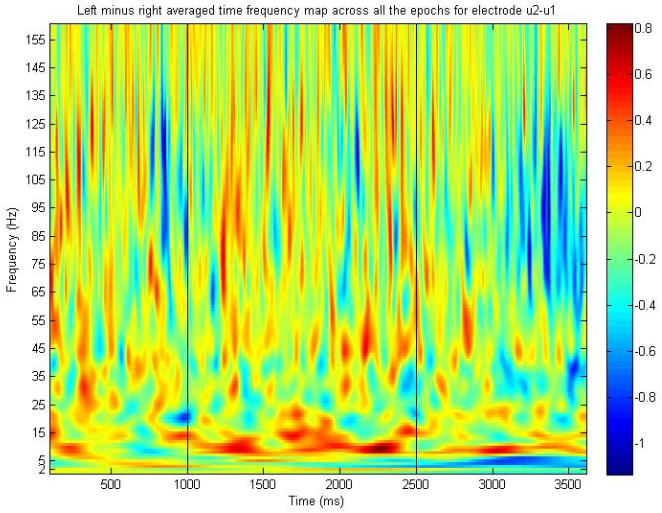

Figure 3.8: The figure displays the subtraction of the averaged (on all the epochs) time-frequency maps of left vs right hand (channel u2-u1). This channel yields to a $DA = 67\%$ using the preparation period, 60-160 Hz frequency band, LDA and SVM.

3.2.1.1 Influence of normalization

The influence of the absence and three types of normalization for kNN (k=3) and LDA classifiers is displayed in tables 3.9 and 3.10, respectively (see section 2.3.2.4 for details on the normalization techniques). The 'subtraction and then division by the baseline' method, provided the best results in terms of DA. This method and the 'division by the baseline' method led to very similar DAs (but different TF maps). Results using SVM are also very similar to the ones obtained with LDA. Thus, the results regarding the normalization method 2) and using SVM classification are not displayed.

kNN, k=3			
	no norm.	*sub. & div.*	*sub.*
	DA(%) / chann.	*DA(%) / chann.*	*DA(%) / chann.*
RM	57/x13-x12	99.5/x13-x12	99/n14-n13
RP	58.75/h13-h12	99.25/v3-v2	99.25/g14-g13
LRM	68/e8-e7	78/e8-e7	64/q3-q2
LRP	64/f3-f4	71/f3-f4	62/i5-i4
UDM	61/e12-e11	73/q7-q6	62/q7-q6
UDP	63/b3-b2	68/e6-e5	66/f11-f10
4M	32/v3-v2	37/q8-q7	34.5/q8-q7
4P	33/f9-f8	40/f9-f8	32.5/e7-e5

Figure 3.9: The best DA and the corresponding channel are displayed for kNN (k=3) classification. No norm: absence of normalization; sub & div: subtraction and division by the baseline; sub: subtraction of the baseline. RM: rest vs movement; RP: rest vs preparation; LRM: left vs right hand, using the movement period; LRP: left vs right hand, using the preparation period; UDM: movement towards 'up' direction vs movement towards 'down' direction, using the movement period; UDP: movement towards 'up' direction vs movement towards 'down' direction, using the preparation period, 4P: 4-directions classification, using the preparation period.

LDA			
	no norm.	*sub. & div.*	*sub.*
	DA(%) / chann.	*DA(%) / chann.*	*DA(%) / chann.*
RM	66.5/l14-l13	82.25/k7-k6	83.75/v14-v13
RP	58.75/b2-b1	81.5/b2-b1	80.25/b2-b1
LRM	64/u7-u6	67/v3-v2	66/v3-v2
LRP	62/e3-e2	64/u2-u1	62/e3-e2
UDM	62/i4-i3	66/g13-g12	63/v2-v1
UDP	60/x14-x13	64/u2-u1	60/u2-u1
4M	33/x14-x13	29.5/x14-x13	33/x14-x13
4P	32.5/o10-o9	35/o10-o9	31.5/o10-o9

Figure 3.10: The best DA and the corresponding channel are displayed for LDA classification. No norm: absence of normalization; sub & div: subtraction and division by the baseline; sub: subtraction of the baseline. RM: rest vs movement; RP: rest vs preparation; LRM: left vs right hand, using the movement period; LRP: left vs right hand, using the preparation period; UDM: movement towards 'up' direction vs movement towards 'down' direction, using the movement period; UDP: movement towards 'up' direction vs movement towards 'down' direction, using the preparation period, 4P: 4-directions classification, using the preparation period.

3.2.1.2 Time windows influence

The time-windows influence on the feature choice process was evaluated by calculating the DA for LDA and kNN (k=3) classification (see figures 3.12 and 3.11, respectively) using several combinations of the time-windows for each period of the task. They were 100-500 ms, 100-800 ms and 400-800 ms for the rest period; 1000-1400 ms, 1000-2300 ms and 2000-2500 ms for the preparation period; 2500-3000 ms, 2700-3700 ms and 3200-3700 ms for the movement period. Large time windows (222 in the tables) led to the best DA. See section 2.3.2.4 for further information.

kNN, k=3									
	111	*122*	*133*	*211*	*222*	*233*	*311*	*322*	*333*
	DA(%)	*DA(%)*	*DA(%)*	*DA(%)*	*DA(%)*	*DA(%)*	*DA(%)*	*DA(%)*	*DA(%)*
RM	98.5	98.75	99	98.75	99.5	98.75	99	99.25	99.25
RP	98.75	99	99	99	99.75	99	98.75	99.25	99
LRM	62	65	63	62	78	60	62	57	63
LRP	61	64	69	73	71	65	60	69	64
UDM	65	64	63	63	73	63	59	61	65
UDP	64	58	67	62	69	62	64	65	58
4M	31.5	33	31	34.5	37	32.5	30	32	31
4P	33	30.5	31	31	40	32	31	33	30

Figure 3.11: The table displays the best DA found for each type of analysis and several windows combinations for kNN (k=3). The considered time windows are referenced as a code of three numbers, where the position of the digit corresponds to the period and the digit itself corresponds to the chosen time-window among the three of them (with respect to the period). E.g., 122 means: **1**22 first time window for the rest period (100-500 ms); 1**2**2 second time window for the preparation period (2700-3700 ms) and 12**2** the second time window for the movement period (2700-3700 ms). Other notations remain the same.

LDA									
	111	*122*	*133*	*211*	*222*	*233*	*311*	*322*	*333*
	DA(%)	*DA(%)*	*DA(%)*	*DA(%)*	*DA(%)*	*DA(%)*	*DA(%)*	*DA(%)*	*DA(%)*
RM	78.75	81.75	81.75	77.5	82.25	80.25	81.25	79.75	83.25
RP	81	81.25	78.75	77.75	81.5	80.75	79	79.25	82
LRM	60	62	63	61	67	66	62	64	65
LRP	64	61	62	61	64	61	63	59	61
UDM	59	67	62	61	64	61	60	64	65
UDP	61	60	61	61	64	61	58	64	62
4M	31	32.5	32.5	30.5	36	32.5	30	31.5	34
4P	31.5	30.5	30	32	33	33.5	32.5	36	33

Figure 3.12: The table displays the best DA found for each type of analysis and several windows combinations for LDA. The considered time windows are referenced as a code of three numbers, where the position of the digit corresponds to the period and the digit itself corresponds to the chosen time-window among the three of them (with respect to the period). E.g., 122 means: **1**22 first time window for the rest period (100-500 ms); 1**2**2 second time window for the preparation period (2700-3700 ms) and 12**2** the second time window for the movement period (2700-3700 ms). Other notations remain the same.

3.2.1.3 Two-feature analysis

The two-feature analysis (two different frequency ranges at the same time) for LDA and kNN (see figures 3.13 and 3.15, respectively) can be compared with the analysis performed with a single-feature analysis (see figure 3.1, 3.2 and 3.3). In tables from 3.13 to 3.16, the DA was obtained investigating only the three best channels provided by the single-feature analysis, while in table 3.17 all the possible channels were used using LDA. The DA improves only by performing the latter approach. Refer to chapter 2.3.2.4 for further information.

LDA, 2 features			
	DA(%)	*chann.*	*freq.(Hz)*
RM	84.25	v14-v14	2-4 – 60-160
RP	82.75	b3-b2	2-7 – 30-130
LRM	66	u2-u1	2-4 – 30-130
LRP	65	g13-g12	4-7 – 60 160
UDM	65	v3-v2	2-4 – 60-160
UDP	68	x14-x13	2-4 – 6-30
4M	33	o10-o9	2-7 – 30-130
4P	36	x14-x13	2-4 – 4-7

Figure 3.13: Display the best results found using LDA with two features applied on the 3 best channels provided by the single-feature analysis. Other notations remain the same.

SVM, 2 features			
	DA(%)	*chann.*	*freq.(Hz)*
RM	88.5	i2-i1	2-7 – 6-30
RP	90	v14-v13	2-7 – 30-130
LRM	66	u2-u1	4-7 – 60-160
LRP	63	v3-v2	2-4 – 60 130
UDM	64	g13-g12	60-130 – 60-160
UDP	66	x14-x13	2-4 – 6-30

Figure 3.14: Display the best results found using SVM with two features applied on the 3 best channels provided by the single-feature analysis. Other notations remain the same.

kNN, k=3, 2 features			
	DA(%)	*chann.*	*freq.(Hz)*
RM	97.75	x13-x12	2-4 – 15-30
RP	97.75	v3-v2	15-30 – 30-130
LRM	74	f3-f2	8-13 – 60-160
LRP	66	e8-e7	6-30 – 15-30
UDM	64	n9-n8	2-4 – 30-130
UDP	62	b3-b2	2-4 – 2-7
4M	35	f10-f9	2-7 – 60-160
4P	36	q8-q7	2-7 – 30-130

Figure 3.15: Display the best results found using kNN (k=3) with two features applied on the 3 best channels provided by the single-feature analysis. Other notations remain the same.

kNN, k=5, 2 features			
	DA(%)	*chann.*	*freq.(Hz)*
RM	97.75	g14-g13	6-30 – 15-30
RP	98	m11-m10	2-7 – 15-30
LRM	74	f3-f2	8-13 – 60-160
LRP	68	o9-o8	15-30 – 60-130
UDM	64	n9-n8	2-4 – 30-130
UDP	62	n9-n8	6-30 – 30-130
4M	40	g12-g11	4-7 – 60-130
4P	37	e8-e7	2-7 – 30-130

Figure 3.16: Display the best results found using kNN (k=5) with two features applied on the 3 best channels provided by the single-feature analysis. Other notations remain the same.

LDA, 2 features			
	DA(%)	*chann.*	*freq.(Hz)*
RM	84.25	v14-v13	2-4 – 60-160
RP	83.75	v14-v13	2-7 – 60-130
LRM	68	n2-n1	2-7 – 4-7
LRP	66	k12-k11	8-13 – 6-30
UDM	66	o10-o9	2-7 – 30-130
UDP	69	e7-e6	30-130 – 60-160
4M	39.5	z5-z4	8-13 – 6-30
4P	36.5	n10-n9	4-7 – 60-130

Figure 3.17: Display the best results found using LDA with two features applied on the **all** the channels ("from scratch"). Other notations remain the same.

3.2.1.4 Combination of channels

As reported in section 2.3.2.4, the information supplied by two (or three) channels was combined by summation of the signals from the channels, for each type of comparison (RM, RP, LRM, LRP, UDM and UDP), as follows: chann1 + chann2, chann2 + chann3, chann3 + chann1, chann1 + chann2 + chann3. All the possible combinations of the three best channels provided by the initial single-feature analysis were investigated on LDA, SVM and kNN classifiers. Compared to the initial findings, the DA remained the same or decreased, thus the results are not displayed.

3.2.2 EEG data

The protocol can be found in section 2.3.2.5. The results for the 4-direction classification were close to the level of the chance (25%) and are consequently not displayed.
The analysis was conducted on the right hand of the 5 subjects (apart when investigating the classification of the two hands, of course). A summary of the results is displayed in figures 3.23 and 3.24. Some TF maps are displayed in figures 3.25, 3.26 and 3.27.

Subject 1									
	LDA			**KNN**, k=3			**KNN**, k=5		
	DA(%)	*freq.(Hz)*	*chann.*	*DA(%)*	*freq.(Hz)*	*chann.*	*DA(%)*	*freq.(Hz)*	*chann.*
RM	81.6	30-130	C3	99.6	60-85	C3	99.5	30-130	C2
RP	81.6	62-87	F3	99.6	15-30	CZ	99.3	2-3	CP1
LRM	65.3	50-128	CZ	63.2	15-30	C1	64.3	15-30	C1
LRP	60.7	62-87	F3	66.3	50-128	CP4	64.3	50-128	C4
UDM	63.8	30-50	FZ	62.2	2-4	F3	63.8	60-85	F1
UDP	58	15-30	CPZ	62.2	50-128	F4	64.8	50-128	F4

Figure 3.18: For LDA classification conducted on subject 1, the best decoding accuracy (DA) found using all channels and all the frequency bands is displayed. The type of analysis is shown in the first column. RM: rest vs movement; RP: rest vs preparation; LRM: left vs right hand, using the movement period; LRP: left vs right hand, using the preparation period; UDM: movement towards 'up' direction vs movement towards 'down' direction, using the movement period; UDP: movement towards 'up' direction vs movement towards 'down' direction, using the preparation period.

Subject 2									
	LDA			**KNN**, k=3			**KNN**, k=5		
	DA(%)	*freq.(Hz)*	*chann.*	*DA(%)*	*freq.(Hz)*	*chann.*	*DA(%)*	*freq.(Hz)*	*chann.*
RM	83.5	30-130	CP1	99.6	15-30	FCZ	99.6	60-85	CP2
RP	79.6	2-7	FC1	99.6	2-4	C3	99.5	4-7	F1
LRM	61.3	30-130	CZ	66.5	4-7	C1	64.4	15-30	C1
LRP	61.3	2-5	FC1	65.5	4-7	C1	64.9	50-128	C1
UDM	60.8	15-30	FZ	63.9	60-85	CP4	64.9	50-128	FC3
UDP	59.8	15-30	F1	62.9	60-85	C1	69	60-85	C1

Figure 3.19: For LDA classification conducted on subject 2, the best decoding accuracy (DA) found using all channels and all the frequency bands is displayed. The type of analysis is shown in the first column. RM: rest vs movement; RP: rest vs preparation; LRM: left vs right hand, using the movement period; LRP: left vs right hand, using the preparation period; UDM: movement towards 'up' direction vs movement towards 'down' direction, using the movement period; UDP: movement towards 'up' direction vs movement towards 'down' direction, using the preparation period.

Subject 3									
	LDA			**KNN**, k=3			**KNN**, k=5		
	DA(%)	*freq.(Hz)*	*chann.*	*DA(%)*	*freq.(Hz)*	*chann.*	*DA(%)*	*freq.(Hz)*	*chann.*
RM	88.7	15-30	F4	99.7	10-30	C4	99.4	30-130	FC4
RP	79.1	2-7	FC2	99.7	30-130	FCZ	99.3	2-3	FC1
LRM	62.4	30-130	FC1	61.3	4-7	F3	63.9	30-130	F1
LRP	61.3	30-50	CZ	61.9	4-7	F2	63.9	60-85	CP1
UDM	58.2	60-85	F3	63.9	60-85	CPZ	63.4	2-4	FC4
UDP	60.8	62-87	CP3	69	2-3	F3	65.4	2-5	C1

Figure 3.20: For LDA classification conducted on subject 3, the best decoding accuracy (DA) found using all channels and all the frequency bands is displayed. The type of analysis is shown in the first column. RM: rest vs movement; RP: rest vs preparation; LRM: left vs right hand, using the movement period; LRP: left vs right hand, using the preparation period; UDM: movement towards 'up' direction vs movement towards 'down' direction, using the movement period; UDP: movement towards 'up' direction vs movement towards 'down' direction, using the preparation period.

Subject 4									
	LDA			**KNN**, k=3			**KNN**, k=5		
	DA(%)	*freq.(Hz)*	*chann.*	*DA(%)*	*freq.(Hz)*	*chann.*	*DA(%)*	*freq.(Hz)*	*chann.*
RM	78.3	30-130	CZ	99.6	30-50	CP1	99.5	30-50	CP1
RP	79.7	10-30	FZ	99.6	30-50	FC2	99	30-130	FC2
LRM	62.8	30-50	FC2	62.3	30-130	CZ	63.9	30-50	FC2
LRP	60.8	10-30	CZ	64.9	2-7	CP3	66.5	50-128	C3
UDM	62.9	2-5	F1	63.4	30-50	CZ	62.9	2-5	F1
UDP	58.8	10-30	C3	66.5	2-5	FZ	68.6	2-5	FZ

Figure 3.21: For LDA classification conducted on subject 4, the best decoding accuracy (DA) found using all channels and all the frequency bands is displayed. The type of analysis is shown in the first column. RM: rest vs movement; RP: rest vs preparation; LRM: left vs right hand, using the movement period; LRP: left vs right hand, using the preparation period; UDM: movement towards 'up' direction vs movement towards 'down' direction, using the movement period; UDP: movement towards 'up' direction vs movement towards 'down' direction, using the preparation period..

Subject 5									
	LDA			**KNN**, k=3			**KNN**, k=5		
	DA(%)	*freq.(Hz)*	*chann.*	*DA(%)*	*freq.(Hz)*	*chann.*	*DA(%)*	*freq.(Hz)*	*chann.*
RM	82	30-130	F3	99.7	10-30	CP1	99.2	2-5	C3
RP	79.8	60-85	CPZ	99.9	2-4	CP3	99.4	60-85	F4
LRM	70.6	60-85	F3	65.5	2-7	CP2	64.4	2-7	FC2
LRP	64.9	30-130	F3	66	2-4	CP1	65.5	10-30	CP4
UDM	72.7	50-128	F3	71.6	50-128	F3	69.6	50-128	F3
UDP	64.4	50-128	F1	63.4	15-30	FC4	64.9	60-85	CZ

Figure 3.22: For LDA classification conducted on subject 5, the best decoding accuracy (DA) found using all channels and all the frequency bands is displayed. The type of analysis is shown in the first column. RM: rest vs movement; RP: rest vs preparation; LRM: left vs right hand, using the movement period; LRP: left vs right hand, using the preparation period; UDM: movement towards 'up' direction vs movement towards 'down' direction, using the movement period; UDP: movement towards 'up' direction vs movement towards 'down' direction, using the preparation period.

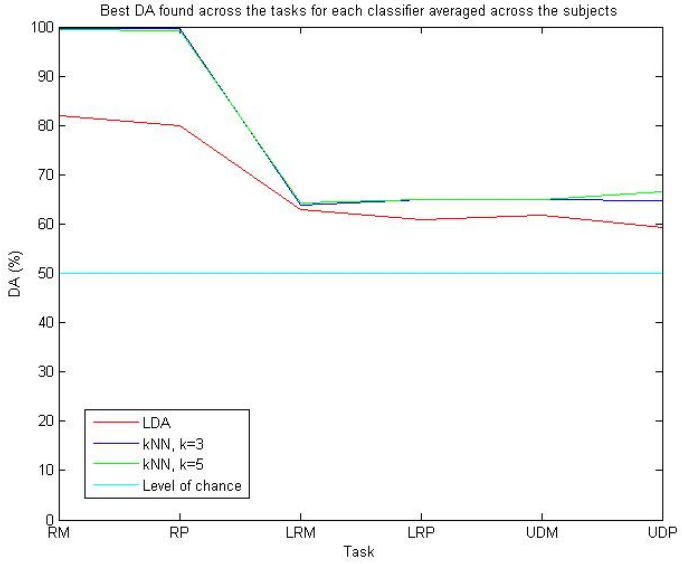

Figure 3.23: Average over the subjects of the best decoding accuracy (DA) found for each type of analysis and each classifier. RM: rest vs movement; RP: rest vs preparation; LRM: left vs right hand, using the movement period; LRP: left vs right hand, using the preparation period; UDM: movement towards 'up' direction vs movement towards 'down' direction, using the movement period; UDP: movement towards 'up' direction vs movement towards 'down' direction, using the preparation period.

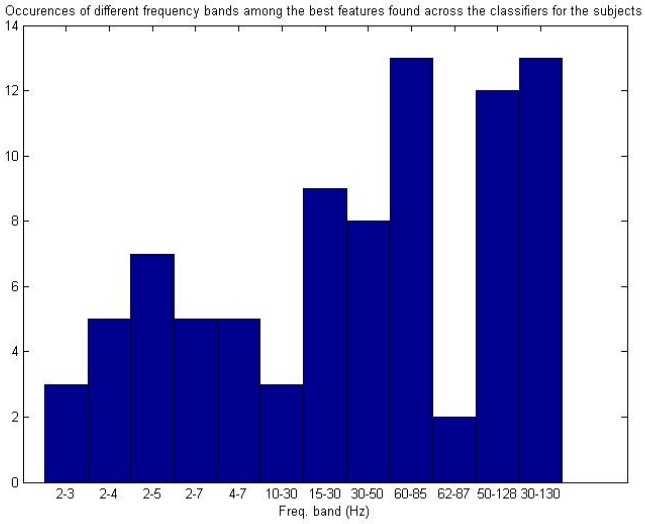

Figure 3.24: Number of occurrences of each frequency band which belongs to the best discriminant features across the classifiers (data from all the 5 subjects is included).

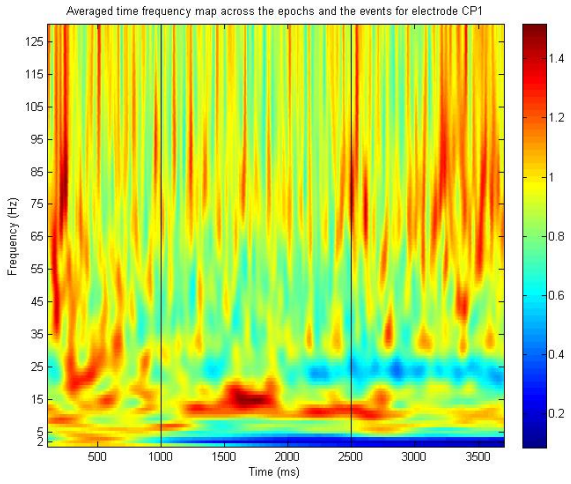

Figure 3.25: Averaged time-frequency map across all the events and all the epochs of channel CP1 (subject 1). Note how the power in low frequencies decreases during the preparation and the movement period, while the power in the intermediate frequencies increases only during the preparation period, and the power in the higher frequencies increases only during the movement period. This channel yields to a $DA = 99.3\%$ for rest vs movement using the 2-3 Hz frequency band and kNN (k=5).

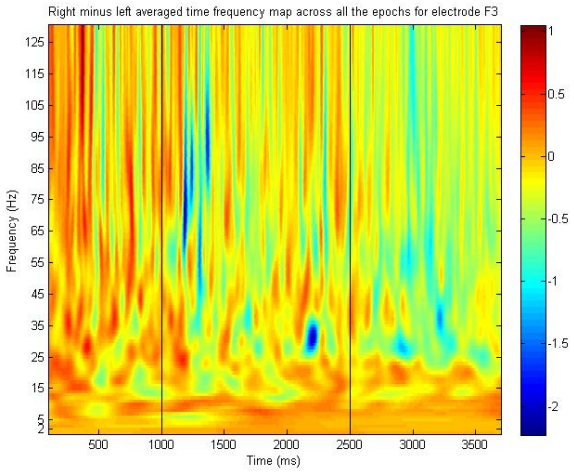

Figure 3.27: The figure displays the subtraction of the averaged (on all the epochs) time-frequency maps of left vs right hand (channel F3, subject 5). We notice a first decrease of intermediate and higher frequencies during the preparation period, then a clearer decrease of intermediate and higher frequencies during the movement period. This channel yields to a $DA = 70.6\%$ using the movement period, 60-85 Hz frequency band and LDA, and a $DA = 64.9\%$ using the preparation period, 30-13 Hz frequency band and LDA.

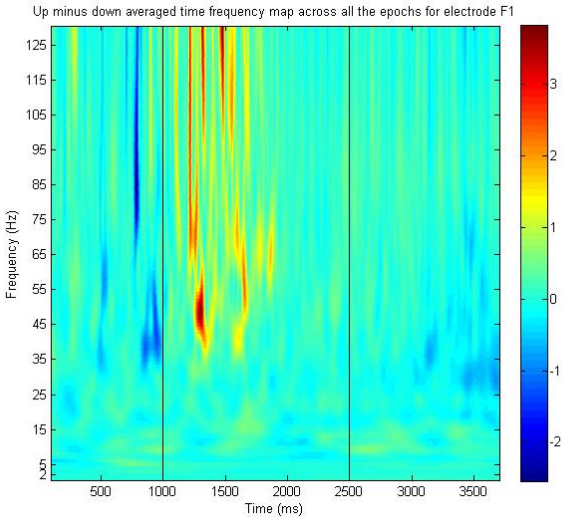

Figure 3.26: The figure displays the subtraction of the averaged (on all the epochs) time-frequency maps of movement towards 'up' direction and towards 'down' direction (channel F1, subject 1). We notice a decrease of power in the higher frequencies during the preparation period. This channel yields to a $DA = 63.8\%$ movement towards 'up' direction vs movement towards 'down' direction, using the movement period, 60-85 Hz frequency band, and kNN (k=5).

Chapter 4

Discussion

4.1 Results summary

In general, the results demonstrated the feasibility to detect a user's voluntary intention of movement using the negative phase of MRCPs or the time-frequency maps from executed movements trials in four directions. Despite the relative complexity of the protocol followed by the subject during the task (see Chapter 2), the true positive rates obtained from both iEEG data and scalp EEG with time analysis showed that spatial filtering is a robust and valuable technique with respect to movement intention detection purposes. The average TPR (true positive rate) was around 70-75% (OSF filter), reaching values above 80% or 90% (real noise and estimated noise, respectively), while the majority of the false positive rates were around 20-25%. Finally, a consideration about the detection accuracies of movement in the four directions can be made. The tables show (in particular, but not only, Table 3.10) no general trend of a better detection accuracy for a particular direction rather than another.
It was also possible to use time-frequency analysis for the detection of movement intention, although it is a far less robust method. Indeed, important changes in the power spectral density may be induced by mental states of the user and can be mistaken as movement intentions. The decoding accuracy obtained from both iEEG and EEG data was above 80% (LDA and SVM) and goes up to 99% (kNN).
Once the movement intention is validated, the movement direction analysis can be taken into account. Time-frequency analysis enables the classification of the intended direction of movement on intracortical EEG. Using the data from the preparation phase, the DA was about 70% (kNN) and 64% (LDA and SVM) in a two-direction classification, whether for a four-directions classification it was around 38% (kNN) and 35% (LDA). Using the data form the actual movement period, the DA was instead about 75% (kNN) and 67% (LDA or SVM) for two directions, and around 39% (kNN) and 36% (LDA) for four directions classification. A two-directions classification was possible on scalp EEG data as well. On average the DA was 66% (kNN) and 62% (LDA), while the four-directions classification is around the level of chance.

An interesting outcome was the difference observed across the subjects with respect to frequency ranges and classifiers performances. As for the employed methods, the DA greatly benefited from the normalization applied to the time-frequency maps. In particular, 'subtraction and division' normalization (see chapter 2.3.2.4) led to the best accuracy. It can be therefore concluded that normalization enhances the decoding accuracy. Concerning the time windows, the choice of the three longer time windows yielded to the best results. Moreover, the effort of combining more channels did not gave the expected improvement. Finally, with the use of a multi-feature analysis, the decoding accuracy of movement direction increased with LDA and SVM classifiers, whereas it led to a globally decreased DA using kNN.

4.2 Similar BCI paradigms

The novelty of the **detection of movement intention** analysis stands in the application of the movement *intention* detection based on the negative phase of the MRCP for four different directions of movement, with no prior training of the subjects. Since there are no similar studies, a direct comparison is not possible. Several studies can be though reported, which concentrated their attention on low frequencies (1-4 Hz) switch designs, mainly intended for communication purposes [Bashashati et al., 2006; Yom-Tov and Inbar, 2003]. Their results showed a lower TPR (50 -70%), but one of the goals relied in having a minimal FPR (which was around 1-2%).
A similar study, conducted by Niazi et al. on scalp EEG recordings, has been of great inspiration for the design of the detection of movement intention. In this study, the accuracy of the detection of movement intention from single trial MRCPs for both movement imagination and execution, was measured applying a similar spatial filtering technique: a portion of the negative phase of the MRCP (until movement onset) was used as a template. A similar Optimized Laplacian Filter (OSF) was used to improve the SNR of the MRCP over the noise. The mean of TPR was 82.5% (FPR were not reported). However, the subject performed always the same task (ankle dorsiflexion), instead of a four direction task, Moreover, it was shown that the OSF outperformed the LSF.
As the results of this project work suggest, the Optimized Spatial Filter brings an improvement over the Large Laplacian filter, but it often was not high. One of the reasons may stand in the fact that, by protocol, only of 1 second of noise signal (the 'rest period') was available in the SNR optimization. The results anyway confirmed the robustness of the Optimized Spatial filter in this kind of analysis, where four different movement directions were performed by 5 (scalp EEG) + 1 (iEEG) subjects at their preferred speed, following a rather "complex" set of instructions. The validity of the OSF was also confirmed in a study conducted on MRCP classification by Boye et al., on imagination of plantar-flexions with the right foot. Features were extracted with principal component analysis and the classification of MRCPs over the noise was performed with kNN and SVM. In this case, the TPR were high (80-90%), but given the differences in the protocol (e.g. a larger data set, only one task rather than four, and usage of the entire MRCP waveform), a direct comparison appears inappropriate.

Some of papers mentioned above tend to give a priority to a low FPR rather than high TPRs. Depending on the purpose of the BCI system, a different threshold can be set, which would result in a different weight of TPRs over FPRs. In this study, the threshold was set in order to reach the highest TPR while minimizing the FPR, but other approaches can be used. For instance, a higher TPR could be achieved increasing the number of false positives, or also using the entire MRCP as template instead of the negative phase. In the latter case, thought, the detection could only be made once the movement is already started, loosing the predictive properties of the study.

Moving to **direction classification**, it should be specified that in the time-frequency analysis different classification methods (LDA, SVM, kNN, NN) were compared, both on scalp and intracranial EEG recordings, which has not been done in such an extensive way before. In addition, the different normalization methods comparison is not referenced in current literature as well. As a result, the studies mentioned below only partially cover the analysis performed in this report. Is is again important to stress that one of the main goals was to compare different classifiers, rather than spending time to optimize only one, as the majority of the published studies did.

From the reported findings, it can be concluded that normalization enhances the decoding accuracy for time frequency analysis. The best results were found with the 'subtranction and division' normalization (see 2.3.2.4).
A multi-channel classification approach was also carried out on the iEEG recordings. This analysis is indeed supported by current BCI literature. For example, in a similar experiment on EEG recordings, Jerbi et al. reported a peak of the DA when 34 out of 55 channels were used, while a drop of DA occurred using more electrodes. Moreover, they hypothesised that simultaneous multichannel recordings from large neuronal ensembles used in the context of brain machine interfaces, which further supports the notion of a distributed representation of limb kinematics in multiple cortical areas. According to Waldert et al., the decoding performance on iEEG data could be increased by using additional recording sites; indeed, the weaker inter-channel correlation and thus less redundancy between channels, could lead to an improvement of the system. In another study, Waldert et al. reported that the use of few sensors placed exclusively above contralateral motor-related areas can improve the DA of a similar EEG experiment. Also Mehring et al., as shown in figure 4.1, supported the use of multiple channels in order to increase the DA. In addition, Rickert et al. showed that combining two frequency bands at the same time can increase the DA (e.g. <4 Hz and 63-200 Hz, see figure 4.2), but also noticed that the combination of all the frequency bands did not further increase the DA because of the relatively low amount of additional information added by the intermediate frequency band competes with the decrease in performance of the decoder as a result of the higher complexity of the feature space. So, a trade-off between a) the number of features, b)an increase of complexity in the feature space and c) the computation time -a major issue, in our case- has to be found.
The cited studies suggested the use a multi-channel and multi-feature approach, however

these procedures not always brought a benefit to the DA, as already mentioned at the beginning of this chapter and as it is explained in section 4.3.3.

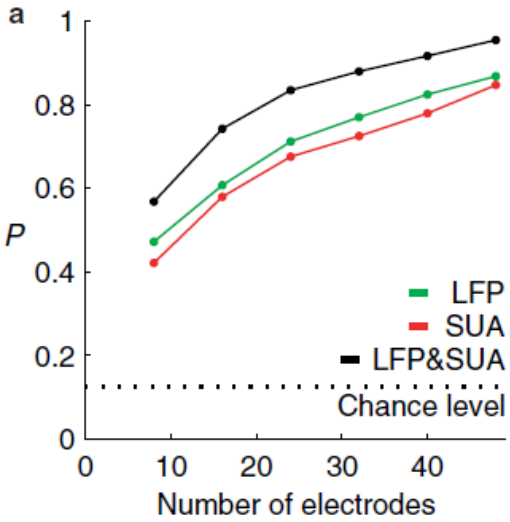

Figure 4.1: Decoding of movement target and trajectories from multiple local field potentials (LFP). Average probability of correctly discriminating between eight targets as a function of the number of recording electrodes. LFPs (green) and single-unit activity (SUA, red), both recorded simultaneously from identical sets of micro-electrodes yielded a similar decoding power. Using LFPs in conjunction with simultaneously recorded SUAs (black) further increased the average decoding power [Mehring et al., 2004].

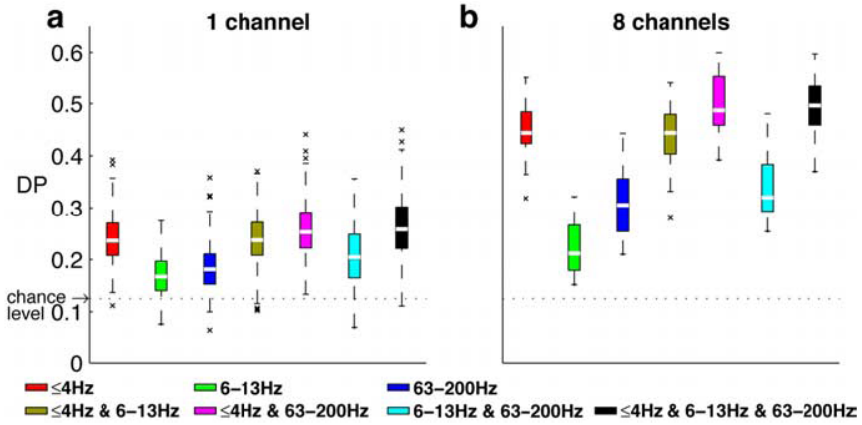

Figure 4.2: Decoding power of different frequency bands. a) The box plots show the distribution of decoding power of single LFPs for various frequency bands and their combinations indicated at the bottom. White bars depict the median, the box ranges from the lower to the upper quartiles, the dashed whiskers extend to the most extreme decoding power within the 1.5-fold interquartile range from the borders of the bars, and the symbols mark outliers. b) Decoding power of simultaneous LFP recordings from eight electrodes [Rickert et al., 2005].

According to Jerbi et al., the highest directional tuning information can be found in <4 Hz and 60-140 Hz frequency bands. With the project's results in mind (see section 3), it can be noticed that most of the frequencies ranges which provided the best DAs ware either in the lower or in the higher frequency bands. Yet, some intermediate bands also yielded to interesting DAs, especially for kNN and LDA classification. The use of intermediate frequency bands is e.g. supported by Rickert et al., who showed that the amplitude of the LFPs in the <13 Hz band was modulated with the direction of movement and that it decreased during movement execution in the 16–42 Hz band. Also Mehring et al. used the changes of relative spectral power in the 8-30 Hz band in order to classify limb movements.

In conclusion, the reached level of DA, particularly looking at the kNN classifier, can be seen as satisfactory and can be compared to what is found in literature. For example, Leuthardt et al. used ECoG recordings decoding to control a one-dimensional computer cursor. This binary task was achieved with up to 74% accuracy while performing opening and closing movements of the right hand, and with 83% of accuracy while the subject was performing imagination of the same task. Other binary tasks referenced by Leuthardt et al. were performed with a 60 to 70% DA before training. However, these papers focused on the classification 4 or 8 directions classification (see figure 4.2) and use ECoG recording, thus a direct comparison is not possible.

Concerning EEG results, the DA of the detection of four directions was instead at the level of chance. The decoding of movement direction from EEG recordings, indeed, is considered to be still an open challenge and was only performed with encouraging results by Waldert et al. (see figure 4.3). In this study, scalp EEG and MEG recordings were used to decode four different directions of movement. They obtained a decoding accuracy of 67% on average across the subjects, using information from the low-pass filtered (<3 Hz) MEG activity during the movement. Their study is unfortunately isolated. Thus, it has been largely assumed that non invasive recordings cannot decode limb movement directions because of the low SNR and bandwidth limitation [Jerbi et al., 2011].

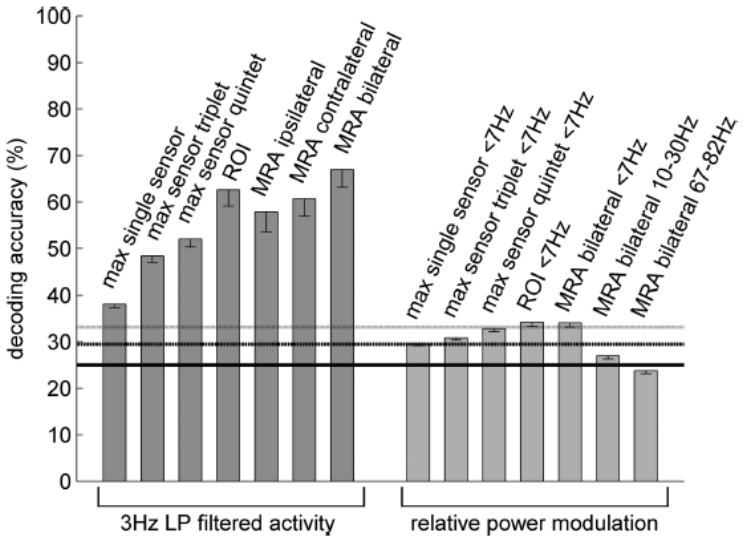

Figure 4.3: DA (averaged across all subjects, decoded time window: 0–500 ms) using signals from different groups of sensors ranging from single sensor-based decoding to decoding of all sensors above motor-related areas. The DA values for both the 3 Hz low-pass (LP) filtered MEG activity and the three frequency bands with significant power modulations are shown. Error bars indicate SEM. MRA, Motor-related area; ROI, regions of interest derived from the single sensor-based decoding. The three horizontal lines indicate the chance, $p<0.05$, and $p<0.001$ levels [Waldert et al., 2008].

4.3 Limitations

4.3.1 Recordings reliability

For obvious reasons, iEEG recordings in the human are only performed on non-healthy subject during pre-surgical investigations. iEEG is therefore recorded mostly in patients with intractable epilepsy who are sometimes cognitively impaired due to various pain/sedating medication or frequent seizures. In addition, the period between channel implantation and channel removal is often very limited and sometimes the patients do not have interest to participate in BCI experiments [Waldert et al., 2009]. Furthermore, epileptic EEG shows characteristic peaks from time to time during the 'normal' state. During a crisis, those peaks gain in amplitude and the different EEG channels begin to synchronize with each other. If there is a crisis during an experiment, the data have of course to discarded. However, the 'normal state' peaks remain and might induce a bias in the data. Because the placement of the electrodes is solely determined by the requirements of the surgeon, some areas (e.g. motor cortex) which could be relevant for BCI-systems purposes might be missing. Indeed, according to Leuthardt et al., the decoding performance is dependant on the location of the implanted electrodes, the number of electrodes, and the inter-electrodes distance. Again, these parameters are determined on neurosurgical evaluations.
Based on the limited availability of intracranial recordings, their invasiveness and re-

liability, the used of such data in a day to day environment for BCI systems seems inappropriate and improbable. On top of this, in case of low DA, a general conclusion about whether iEEG is able to decode limb movements or not, can not be drawn. Nevertheless, the use iEEG data seemed to allow better decoding of the movement direction compared to EEG, probably because of its better spatial resolution, and low / absent influence of muscle artifacts and low-pass filtering effect of other tissues (e.g. the skull).

Concerning scalp EEG data, we face the opposite problem: the area recorded with each electrode is wide. Although EEG enables to cover the entire surface of the scalp, it is not able to isolate a very specific zone.
As reviewed by Jerbi et al., the presence of eye artifacts induces a notable drop in the accuracy. Even if eye blinks are discarded with the use of a threshold, some eye saccades might remain and impact the results [Waldert et al., 2008]. In addition, at least another person was present in the same room while the experiment was running, leading to an increased risk of eye saccades.

4.3.2 Experimental protocol

There were limitations related to the experimental protocol, which were common for EEG and iEEG. In the protocol, visual cues triggered the execution of a task (the first visual cue to indicate the direction and the 'go signal'). The impact of visual triggers on the EEG signals is not known. Indeed, a punctual drop in the power of a given frequency band right after the visual cue could have been mistaken as movement preparation. Furthermore, after a visual cues, each subject reacted differently: some performed the movement quickly, some more slowly, some with a constant speed during the experiment, some increasing or decreasing it. As a result, the protocol was not exactly the same and some results might have been biased, e.g. particularly in the averaging across the MRCP templates. The mouse position information could have been used in order to locate precisely the movement onset, however using such a technique would have raised algorithmic issues due to a different length of each sample for every trial. Finally, although a great effort was made in order to carefully reproduce the intracranial experimental protocol ran in Grenoble (France), the two setups were not exactly the same: positions (the subject sat in a bed in France, sat on a chair in Denmark), distance from the screen, etc. These differences might lead to unknown bias.

Further considerations can be made on the detection of movement intention. As a first note, by protocol, only 1 sec. of rest period (also referred as 'noise' in chapter 2) was available. This led to the decision to generate estimated noise based on the real one. As it might be expected, the performances decreased using the estimated noise. Nevertheless, most of the drawn considerations were based on those results, because the same length of 'noise' and 'signal' ensured greater reliability of the results. Only 50 epochs were collected for each movement for iEEG recordings, while they were 100 for scalp EEG. These numbers could be increased. It is in fact worth mentioning that combining all the epochs from one hand in one dataset, with no distinction of the

direction, led to higher TPRs and lower FPRs, increasing the decoding accuracy. This result can be explained by the fact that a larger training set allowed to built a better MRCP template. This difference was indeed more beneficial to the iEEG, as only half of epochs were recorded with respect to scalp EEG data. On top of this, the limited number of epochs "forced" to reuse the training data also for the testing (leave-one-out cross-validation). Finally, the results from iEEG analysis generally showed higher FPRs (using estimated noise), despite the fact that intracortical recordings have greater spatial resolution than standard scalp EEG. This might have happened because the electrodes were placed in order to treat the epileptic subject's illness, rather than in optimal locations (e.g the motor cortex), and were not spatially disposed on a surface like for the scalp EEG data, nor one next to the other, but spread around the brain. This probably affected the performance, since spatial filtering was used for the analysis on the iEEG data as well. On top of this, bipolarisation might have deleted some important components of the MRCP.

4.3.3 Methods

The limitations mainly regarded the time-frequency approach, due to the more extensive analysis proposed in the decoding of movement direction part.

A limit (and a strength) of normalization was the fact that it was conducted specifically for each epoch. In a real-time online analysis, such a method cannot been used (a common baseline should be used for all the epochs). In a previous study conducted by Rohu et al., it has been shown that the use of an averaged baseline across the epochs led to a decrease of the DA for the movement classification.
Results showed that the DA decreased by narrowing the time windows. However, as the analysis was conducted only on the 3 channels which gave the best DA using the longest time-windows, a conclusion cannot be generalized or extended on the other electrodes. Furthermore, due to data storage limitations, a more refined time-window analysis could not be performed.
As for time-windows, the combination of the channels was carried only on the 3 channels resulting from the first long time-windows results. An analysis from scratch, trying all the possible combinations of two or more channels, was not conducted due to obvious time and computational issues.
The combination of two or three features showed different behavior of kNN and LDA-SVM in a two-feature analysis. This is not surprising, as LDA and SVM are close methods. Yet, a decrease of the DA is more unexpected. This can be explained again by the choice of the 3 channels relevant for a single feature analysis. If those channels provided a good result in a single-feature analysis, it is not implicit they can do it also for a multi-feature approach. In fact, as shown by a further analysis of two-feature classification applied on *all* the channels (see figure 3.17), the DA actually increased.

Classifier comparison As first notice, an objective classifier comparison is extremely difficult due to all the parameters which have to be taken into account (particularly in

NN and SVM). In addition, the choice of the classifier is highly dependant of both the data set and the goal of the classification (e.g. offline vs. online).
For both iEEG and EEG data, results showed that kNN classifiers (both for $k = 3$ and $k = 5$) globally led to better results than LDA, SVM or NN. The impact of k is not obvious. According to Lotte et al., kNN algorithms are not popular in the BCI community, probably because of their sensitivity to the curse-of-dimensionality (when the number of training data is small compared to the size of the feature vectors), which makes them perform poorly in several BCI experiments. However, when kNN is used in BCI systems with low dimensional feature vectors, it may prove itself to be efficient, as it did in this study
Neural Networks are very sensitive to overtraining, especially with noisy and non-stationary data as EEGs. Therefore, careful architecture selection and regularization is required [Lotte et al., 2007]. This could partially explain the poor DA obtained in the classification of the direction, where the features space is more complex and noisy than for the 'rest vs movement' classification. Furthermore, due to time issues, the neural network classification was run only on the best features previously found for LDA and kNN, which might not necessarily be the most relevant for this type of classifier.
Finally, LDA generally provided slightly worse results than SVM, with the benefit of a lower computational effort. Further optimization on SVM classifier could have increase the DA.
Ideally, classifiers should be tested within the same context (i.e. with the same users, using the same feature extraction method and the same protocol). One of the problems would be to apply to each classifier the same level of optimization and pre-established parameters (number of layers and learning function for NN, k and distance measure for kNN, a-priori assumptions for LDA and parameters for SVM). For this reason Schalk et al. have proposed the use of a general purpose BCI system, the BCI2000 toolkit. This toolkit is a modular framework which allows to easily change the classification, preprocessing or feature extraction modules. With such a system, it becomes possible to test several classifiers with the same features and preprocessing. The use of BCI2000 could help to choose the best a-priori classifier which has to be further optimized.

4.4 Prospectives

The two techniques proposed in this study (time and time frequency analysis) could be both applied in the same BCI system. Indeed, the two methods might be complementary. Even if time frequency analysis performs equally or better than time analysis for the detection of movement intention, it is a far less robust method. E.g., a mental calculation task or state may lead to important changes in the time-frequency domain, and could thus be mistaken as a movement intention. On the contrary, MRCPs are specifically linked to motor tasks.
A way of improving the system would be the use of not only the early phase, but the whole MRCP, which may also enable the decoding of the movement direction. Modifying the experimental protocol might also lead to better and more reliable outcomes. For

instance, a longer rest and preparation period would bring benefit to the time-based approach. The visual cues should also be eliminated to avoid possible and undesired contributions on the MRCPs and time-frequency maps, and the mouse position could be used to precisely detect the movement onset and course.
In order to be used such a system in real life application, another important aspect should be further investigated. Considering the heterogeneous results found among the subjects, it seems difficult to design a system which could be efficient without fitting itself to the user (choice of a classifier, features, optimized filter coefficients, etc...). Two paths might be followed: try to find patterns with cross comparison on a large population of subjects, or, better, trying to adapt the techniques of choice on a specific user, quickly and efficiently.
The use of a training session also seems a valuable approach in order to improve the results. Closed loop systems have shown to improve quickly also with short training periods. Leuthardt et al. reported 74-100% final accuracy for a binary task performed across all subjects after short training periods (3-24 min) (see figure 4.4).

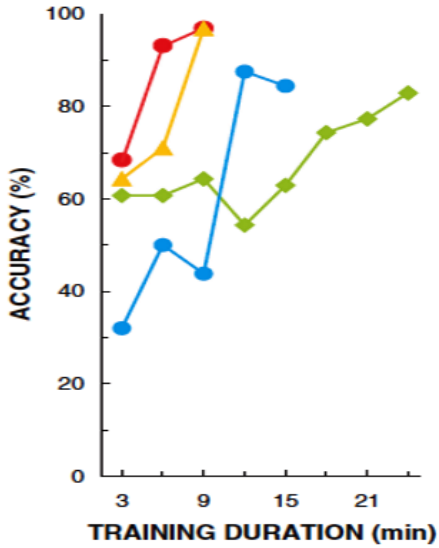

Figure 4.4: Learning curves for ECoG control of vertical cursor movement using motor imagery to move up and rest to move down). (Accuracy in the absence of control would be 50%) [Leuthardt et al., 2004]

A study conducted by Leuthardt et al. reported a substantial improvement from 71% to 94% of correct classification using a closed loop system. For a future application in a real-time system, the use of a closed loop system seems very appealing, both for the selection of the features of interest and the optimization of the classifier.

Chapter 5

Conclusion

The goal of this research project was to implement and apply multiple detection and decoding techniques to scalp and depth EEG recorded in subjects performing a 4-directions center-out motor task. Two main techniques have been investigated: time analysis and time frequency analysis. The accuracy of the various decoding strategies has been compared at various levels:
(a) the EEG recordings: intracortical EEG (iEEG) and scalp EEG
(b) robustness to artifacts and noise, with preprocessing, bipolarization methods and blinks discarding
(c) different spatial filters (large Laplacian filter and Optimized Laplacian Filter) in the time analysis and different classification methods with in time-frequency analysis (LDA and kNN for scalp EEG data; LDA, SVM, kNN and NN for iEEG data).
(d) factors influencing the features: different time windows and frequency ranges, the number of employed features,the combination of channels, and normalization.
Not surprisingly, iEEG recordings, which are less noisy and less affected by artifacts, led to better classification performances than scalp EEG signal. The detection of movement intention was performed with up to 86% of TPR (for estimated noise) for the time analysis and up to 98% with time-frequency analysis, while the classification of movement direction decoding accuracy was up to 78% (two directions classification), and up to 40% (four directions classification). The K-NN classifier with *subtraction & division* normalization was globally the one that performed better on the used datasets, while the two spatial filters, with a slight advantage for the Optimized Spatial Filter, provide similar results in the case of use of AR-estimated noise.

By using the combination of time and time-frequency analysis it is possible to first detect a motor task, and then identify the direction.
A reliable detection of human movement intention, along with the knowledge of the direction of movement, has a potential implication in the control of external devices, such prostheses or other robotic systems. Such BCI paradigm could be useful in the development of a patient-driven rehabilitation system which could induce plastic changes in the brain, or even in the context prosthetics control in amputees.

Bibliography

Allison, B., Graimann, B., and Gräser, A. (2007). Why use a bci if you are healthy. *proceedings of BRAINPLAY 2007, playing with your brain.*

Ball, T., Demandt, E., Mutschler, I., Neitzel, E., Mehring, C., Vogt, K., Aertsen, A., and Schulze-Bonhage, A. (2008). Movement related activity in the high gamma range of the human eeg. *Neuroimage*, 41(2):302–310.

Ball, T., Schulze-Bonhage, A., Aertsen, A., and Mehring, C. (2009). Differential representation of arm movement direction in relation to cortical anatomy and function. *Journal of neural engineering*, 6:016006.

Bashashati, A., Mason, S., Ward, R., and Birch, G. (2006). An improved asynchronous brain interface: making use of the temporal history of the lf-asd feature vectors. *Journal of neural engineering*, 3:87.

Besserve, M. (2007). Analyse de la dynamique neuronale pour les interfaces cerveau-machines: un retour aux sources. *PhD Thesis*, 18:43.

Birbaumer, N. (2006). Breaking the silence: brain–computer interfaces (bci) for communication and motor control. *Psychophysiology*, 43(6):517–532.

Boye, A., Kristiansen, U., Billinger, M., Nascimento, O., and Farina, D. (2008). Identification of movement-related cortical potentials with optimized spatial filtering and principal component analysis. *Biomedical Signal Processing and Control*, 3(4):300–304.

Bradshaw, L. and Wikswo, J. (2001). Spatial filter approach for evaluation of the surface laplacian of the electroencephalogram and magnetoencephalogram. *Annals of Biomedical Engineering*, 29(3):202–213.

Chaplais, F. (1998). A wavelet tutorial adapted for the web.

Dai, D. and Yuen, P. (2003). Regularized discriminant analysis and its application to face recognition. *Pattern Recognition*, 36(3):845–848.

Dalal, S., Vidal, J., Hamamé, C., Ossandón, T., Bertrand, O., Lachaux, J., and Jerbi, K. (2011). Spanning the rich spectrum of the human brain: slow waves to gamma and beyond. *Brain Structure and Function*, pages 1–8.

De Hoon, M., Van der Hagen, T., Schoonewelle, H., and Van Dam, H. (1996). Why yule-walker should not be used for autoregressive modelling. *Annals of Nuclear Energy*, 23(15):1219–1228.

Duda, R., Hart, P., and Stork, D. (2001). Pattern classification. *John Willey & Sons*.

Georgopoulos, A., Kalaska, J., Caminiti, R., and Massey, J. (1982). On the relations between the direction of two-dimensional arm movements and cell discharge in primate motor cortex. *The Journal of Neuroscience*, 2(11):1527–1537.

Graps, A. (1995). An introduction to wavelets. *Computational Science & Engineering, IEEE*, 2(2):50–61.

Hawkins, D. (2004). The problem of overfitting. *Journal of chemical information and computer sciences*, 44(1):1–12.

Hudson, D. and Cohen, M. (1999). *Neural networks and artificial intelligence for biomedical engineering*. Wiley-IEEE Press.

Jahanshahi, M. and Hallett, M. (2003). *The Bereitschaftspotential: movement-related cortical potentials*. Springer.

Jerbi, K., Ossandón, T., Hamamé, C., Senova, S., Dalal, S., Jung, J., Minotti, L., Bertrand, O., Berthoz, A., Kahane, P., et al. (2009). Task-related gamma-band dynamics from an intracerebral perspective: Review and implications for surface eeg and meg. *Human brain mapping*, 30(6):1758–1771.

Jerbi, K., Vidal, J., Mattout, J., Maby, E., Lecaignard, F., Ossandon, T., Hamamé, C., Dalal, S., Bouet, R., Lachaux, J., et al. (2011). Inferring hand movement kinematics from meg, eeg and intracranial eeg: From brain-machine interfaces to motor rehabilitation. *IRBM*.

Kandel, E., Schwartz, J., Jessell, T., et al. (2000). *Principles of neural science*, volume 4. McGraw-Hill New York.

Krepki, R., Blankertz, B., Curio, G., and Müller, K. (2003). The berlin brain-computer interface (bbci). *IEEE Transactions on Automatic Control*, 23(4):538–544.

Krepki, R., Blankertz, B., Curio, G., and Müller, K. (2007). The berlin brain-computer interface (bbci)–towards a new communication channel for online control in gaming applications. *Multimedia Tools and Applications*, 33(1):73–90.

Leeb, R., Friedman, D., Müller-Putz, G., Scherer, R., Slater, M., and Pfurtscheller, G. (2007). Self-paced (asynchronous) bci control of a wheelchair in virtual environments: a case study with a tetraplegic. *Computational intelligence and neuroscience*, 2007:7.

Leuthardt, E., Miller, K., Schalk, G., Rao, R., and Ojemann, J. (2006). Electrocorticography-based brain computer interface-the seattle experience. *Neural Systems and Rehabilitation Engineering, IEEE Transactions on*, 14(2):194–198.

Leuthardt, E., Schalk, G., Wolpaw, J., Ojemann, J., and Moran, D. (2004). A brain–computer interface using electrocorticographic signals in humans. *Journal of Neural Engineering*, 1:63.

Lotte, F., Congedo, M., Lécuyer, A., Lamarche, F., and Arnaldi, B. (2007). A review of classification algorithms for eeg-based brain–computer interfaces. *Journal of neural engineering*, 4:R1.

Martini, F. (2006). *Fundamentals of anatomy and physiology*. Prentice Hall.

Mehring, C., Nawrot, M., de Oliveira, S., Vaadia, E., Schulze-Bonhage, A., Aertsen, A., and Ball, T. (2004). Comparing information about arm movement direction in single channels of local and epicortical field potentials from monkey and human motor cortex. *Journal of Physiology-Paris*, 98(4-6):498–506.

Middendorf, M., McMillan, G., Calhoun, G., and Jones, K. (2000). Brain-computer interfaces based on the steady-state visual-evoked response. *Rehabilitation Engineering, IEEE Transactions on*, 8(2):211–214.

Millan, J., Rupp, R., Muller-Putz, G., Murray-Smith, R., Giugliemma, C., Tangermann, M., Vidaurre, C., Cincotti, F., Kubler, A., Leeb, R., et al. (2010). Combining brain-computer interfaces and assistive technologies: state-of-the-art and challenges. *Frontiers in neuroscience*, 4.

Mirkin, B. (2011). Data analysis, mathematical statistics, machine learning, data mining: Similarities and differences. In *Advanced Computer Science and Information System (ICACSIS), 2011 International Conference on*, pages 1–8. IEEE.

Niazi, I., Jiang, N., Tiberghien, O., Nielsen, J., Dremstrup, K., and Farina, D. (2011). Detection of movement intention from single-trial movement-related cortical potentials. *Journal of neural engineering*, 8:066009.

Noble, W. et al. (2004). Support vector machine applications in computational biology. *Kernel methods in computational biology*, pages 71–92.

Pfurtscheller, G., Muller-Putz, G., Scherer, R., and Neuper, C. (2008). Rehabilitation with brain-computer interface systems. *Computer*, 41(10):58–65.

Press, W., Teukolsky, S., Vetterling, W., and Flannery, B. (2007). *Numerical Recipes Source Code CD-ROM 3rd Edition: The Art of Scientific Computing*. Cambridge University Press.

Ramoser, H., Muller-Gerking, J., and Pfurtscheller, G. (2000). Optimal spatial filtering of single trial eeg during imagined hand movement. *Rehabilitation Engineering, IEEE Transactions on*, 8(4):441–446.

Rickert, J., de Oliveira, S., Vaadia, E., Aertsen, A., Rotter, S., and Mehring, C. (2005). Encoding of movement direction in different frequency ranges of motor cortical local field potentials. *The Journal of neuroscience*, 25(39):8815–8824.

Schalk, G., McFarland, D., Hinterberger, T., Birbaumer, N., and Wolpaw, J. (2004). Bci2000: a general-purpose brain-computer interface (bci) system. *Biomedical Engineering, IEEE Transactions on*, 51(6):1034–1043.

Shibasaki, H. and Hallett, M. (2006). What is the bereitschaftspotential? *Clinical Neurophysiology*, 117(11):2341–2356.

Soekadar, S., Birbaumer, N., and Cohen, L. (2011). Brain-computer interfaces in the rehabilitation of stroke and neurotrauma. *Systems Neuroscience and Rehabilitation*, pages 3–18.

Standring, S., Ellis, H., Healy, J., Johnson, D., Williams, A., Collins, P., and Wigley, C. (2005). Gray's anatomy: the anatomical basis of clinical practice. *American Journal of Neuroradiology*, 26(10):2703.

Waldert, S., Pistohl, T., Braun, C., Ball, T., Aertsen, A., and Mehring, C. (2009). A review on directional information in neural signals for brain-machine interfaces. *Journal of Physiology-Paris*, 103(3-5):244–254.

Waldert, S., Preissl, H., Demandt, E., Braun, C., Birbaumer, N., Aertsen, A., and Mehring, C. (2008). Hand movement direction decoded from meg and eeg. *The Journal of Neuroscience*, 28(4):1000–1008.

Yom-Tov, E. and Inbar, G. (2003). Detection of movement-related potentials from the electro-encephalogram for possible use in a brain-computer interface. *Medical and Biological Engineering and Computing*, 41(1):85–93.

Appendix A

The brain

A brief introduction to brain anatomy is described below. The following pages are based on [Martini, 2006] and [Standring et al., 2005].

The brain is one of the most complex parts of a human being. It accounts for up to 98% of the neural tissue within the entire body and has a weight of about 1.4 kg with large individual variance.

A.1 Protection and support

The brain tissue is tender and delicate and so it needs protection from potential damage. Its protection is ensured by three layers: the cranial bones, the cranial meninges and the cerebrospinal fluid. The bones of the cranium supply a hard encapsulation of the brain. As show in figure A.1, the cranial meninges consist of multiple layers: dura mater, arachnoid mater and pia mater, in order of deepness. The dura mater has two fibrous layers, or lamellae, with tissue fluids and blood vessels in between. The arachnoid mater provides a smooth surface covering the entire brain, which follows the brain down into its sulci, as does the pia mater. The pia mater is a thin fibrous tissue, anchored to every fold of the brain, which encloses cerebrospinal fluid in order to protect the brain and allows blood vessels to pass through and feed the brain cells.
The cerebrospinal fluid has both a role in the transport of nutrients, as a vehicle for chemical messengers and other substances, and in protecting the brain from mechanical stress, partially preventing the brain from beating against the skull.

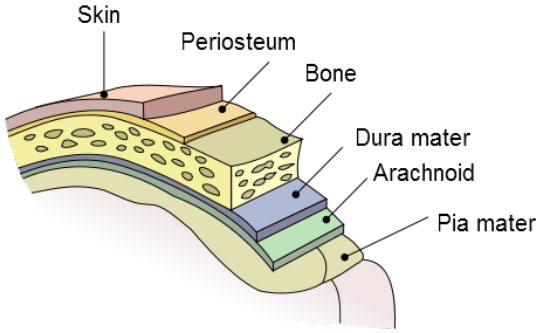

Figure A.1: Meninges surrounding the brain (adapted for own use from [Standring et al., 2005]).

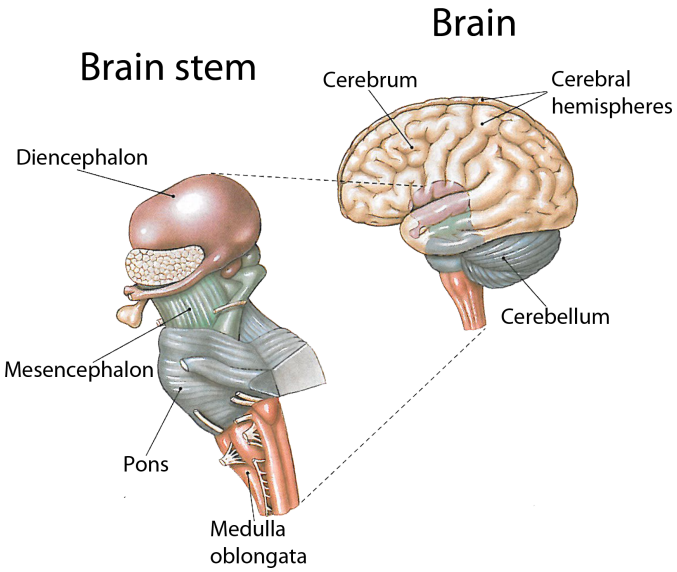

Figure A.2: Gross anatomy of the brain (adapted for own use from [Martini, 2006]).

A.2 Structure

The brain can be anatomically divided into four parts (see figure A.2): the brain stem, the diencephalon, the cerebellum and the cerebrum. The brain stem is located in the inferior part of the brain, connected and superior to the spinal cord.

A.2.1 The brain stem

The brain stem consists of several parts, which, starting superior from the spinal cord, are: medulla oblongata, pons, mesencephalon. Sometimes the diencephalon is regarded as part of the brain stem.
The medulla oblongata transmits sensory information to the superior parts of the brain stem and regulates autonomic functions, such as heart rate and blood pressure. The pons connects the cerebellum to the brain stem and is involved in visceral and somatic motor control and transmits sensory information to superior parts of the brain stem and the cerebellum. The mesencephalon controls auditorily and visually triggered reflexes and helps maintaining consciousness.

A.2.2 The diencephalon

The diencephalon is a region composed by a left and right thalamus both relaying and processing sensory information. The inferior part is called hypothalamus and is involved in hormone production, emotions and autonomic functions.

A.2.3 The cerebellum

The second largest part of the brain is the cerebellum, located posterior at the level of the mesencephalon and covered by the cerebellar cortex. The main function of the cerebellum is to adjust the ongoing movements and to help to coordinate repeated advanced somatic motor patterns by receiving sensory information and comparing it to previously experienced movements, allowing to make smooth movements.

A.2.4 The cerebrum

The cerebrum consists of two highly folded cerebral hemispheres covered with neural cortex. In general, each one controls the contralateral side of the body. Even if the hemispheres look similar, they do not have the same functionality neither the same size. The cerebrum plays a role in most higher mental functions, such as attention, awareness, thought, intellect, memory, highly complex movements, sensations and speech. The superficial layer of the cerebrum is the cerebral cortex, which together with the deeper basal nuclei, is part of the grey matter (formed from neurons and their unmyelinated fibers) and superficial to the white matter (formed predominantly by myelinated axons). The surface of the cerebral cortex is folded into the so called "sulci" and organized in different layers. The cerebral cortex can be topographically subdivided into four lobes: frontal, parietal, occipital and temporal lobe (see figure A.3), and is commonly

described as comprising three parts: sensory, motor, and association areas, depending on the functionality. Below follows a short explanation of the main areas that compose the cortex.

Cortices

The primary motor cortex (M1) is located in the posterior part of the frontal lobe and is involved in performing voluntary movements, whereas the primary sensory cortex (S1), which is a part of the parietal lobe, il located posteriorly. It allows conscious sensation of vibration, touch, pressure, pain etc. The two cortices are named "primary" because they have a specifically defined topographic mapping of the body, so that a specific area of the primary motor cortex is related to motion of a corresponding group of muscles or organ (for example a limb). The regions of the primary sensory and motor cortex are not of the same size: as the size increases, a finer control and sensitivity is allowed. The gustatory cortex, the visual cortex, the auditory and olfactory cortex are also worth to be mentioned.

Association centres

To each of the cortices mentioned above corresponds an association centre, which interprets signals and coordinates the motor response. The somatic motor association area stimulates the neurons of the primary motor cortex in order to achieve the planned movement, while the primary motor cortex initiates the actual movement. Moreover, the association area stores a pattern of stimulation, which matches the corresponding movement pattern.

Integrative centres

The integrative centres collect information from the association centres in order to perform highly complex motor or analytical tasks. The prefrontal cortex located in the frontal lobe, which integrates information from sensory association centres and Wernicke's area, while allowing coordinated access to visual and auditory memory.

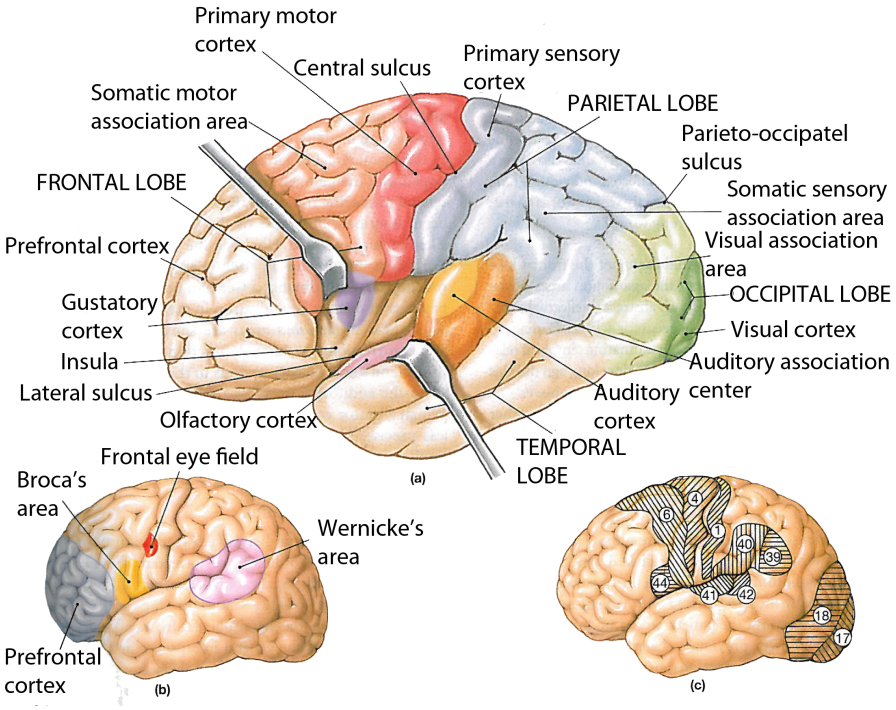

Figure A.3: The figure shows a) the major anatomical landmarks of the left cerebral hemisphere, b) the areas mainly involved in speech and c) histological distinct areas (adapted for own use from [Martini, 2006]).

Appendix B

Organization of movement

In this chapter a general overview about organization of movement and motor control is given. The following is mainly based on [Martini, 2006] and [Kandel et al., 2000] unless specified differently.

B.1 Motor cortices and motor planning

The cerebral cortex, the brain stem and the spinal cord are the most important parts of the nervous system involved in movement. Skeletal muscles can be controlled from many places in the central nervous system (CNS): the spinal cord, the pons, the basal ganglia, the cerebellum and the motor cortex, each part having its own role. The spinal cord can be described as the main path trough which signals from the brain are transmitted to the periphery of the body and the opposite. The structure is more complex than this schematic description, though: the spinal cord consists of several cord centres, which are commanded by the upper levels of the nervous system. These neuronal circuits in the cord are also responsible for walking movements or different reflexes. Pons, basal ganglia and cerebellum belong to the lower brain and control automatic, instantaneous muscle responses to sensory stimuli.
As it has already been said, the cerebral cortex is involved in processing and integrating sensory information and establishing motor commands. The motor cortex is, more specifically, in charge of complex movements that are controlled by thought processes and also functions as a storage of information for future control of motor activities. Each part of the body receiving somatosensory input corresponds to a specific area in the cortex; this is often represented with a somatosensory homonculus, as shown in figure B.1(a). In the same way, the primary motor cortex (M1) is organised in a topographical manner, containing a representation of each part of the body (see figure B.1(b)). Besides M1 and S1, a complete map of the body is present in the premotor areas too. However, while stimulation in the M1 evokes simple movements of single joints, stimulation of the premotor cortex results in more complex movement involving multiple joints and resemble natural coordinated movements. The premotor areas consist of the premotor

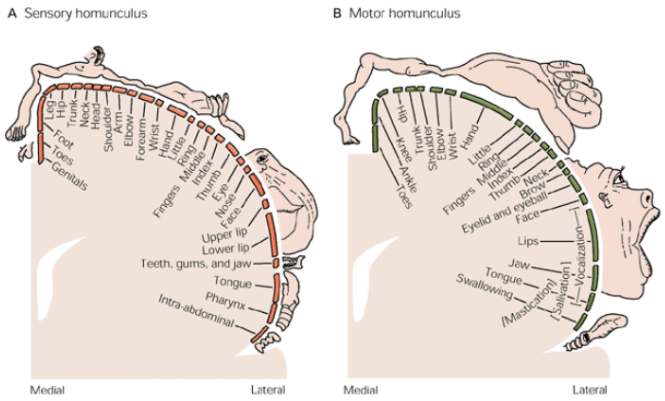

Figure B.1: The figure shows a) The somatotopic representation of the body in somatosensory cortex b) the topographic representation of the body in the motor cortex (adapted for own use from [Kandel et al., 2000]).

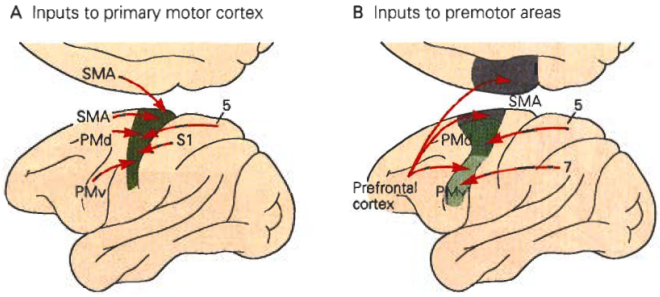

Figure B.2: The major inputs to the motor cortex in monkeys.
A. The major inputs to the primary motor cortex. (**PMd** = dorsal premotor area; **PMv** = ventral premotor area; **S1** = primary sensory cortex; **SMA** = supplementary motor area.)
B. The major inputs to the premotor areas. Dense interconnections between the premotor areas are not shown here. (adapted for own use from [Kandel et al., 2000]).

cortex and the supplementary motor area and are mainly involved in coordination and planning of movements.
All these areas in the brain are interconnected to each other in a complex network (see figure B.2).

B.2 Types of movement

The corticospinal tract is considered as the direct pathway of voluntary movements. In the spinal cord, the projection neurons are connected either with interneurons or directly with motor neurons, which in turn transmit the signals to the skeletal muscles. Three types of movements may occur with respect to ascending and descending signals via different pathways and at different levels: voluntary movement, reflexes and rhythmic movement.

Reflexes are performed subconsciously and can occur exclusively at a spinal level, though they may also be modulated by subcortical or cortical commands. A reflex is started by a sensory stimulus which then leads to excitations of motor neurons at a spinal level, resulting in a muscle contraction or relaxation, possibly even before sensation occurs. Distinct reflexes are initiated by different stimuli of the same sensory receptors or by stimuli of different receptors and can be modulated throughout excitation or depression of the level of the post-synaptic neuron excitability.
Rhythmic movements, instead, are characterized by a stereotyped action involving repetitions of the same movements (e.g. walking, running, swimming, crawling, flying) and allow control of movement at a 'low', spinal level without involvement of higher cortical control (conscious control). These can be triggered by peripheral stimuli that activate the underlying circuits or from higher cortical centres, which can also overrule them.
Here, though, we will focus on the voluntary movement planning, control and execution.

B.2.1 Voluntary movement

Voluntary movement is usually goal directed and therefore fully conscious. It arises in the motor cortex and is delivered by the spinal cord. When a voluntary movement is started, neurons in the M1 send commands to upper and lower motor neurons. Neurons in the M1 are responsible for a specific somatic location respectively (see figure B.4); for example, the leg components are situated in the middle, the face components are located laterally and so on. The largest representations belong to muscles which imply finest movement control (e.g. arms, legs and face, see figure B.3 and B.4).
Typically, the performance of a voluntary movement is based on movements the person has done several times before. In this case, the cortical motor area uses the pattern already memorised in deeper layers of brain stem, basal ganglia, cerebellum or spinal cord and combines it with the information that comes from the S1. This constant feedback from the S1 enables a finer control and adjustment of the voluntary movement before and during the execution. The cerebellum, instead, plays an essential role as important control centre for unknown motor activities. When a new unknown movement is needed (*motor learning*), the cerebellum is not only in charge of the adaptation of the motor task to the new movement sequence, but it is also associated in planning, execution, controlling and refining of the movement execution.
The neuronal activity in the cortex and the subsequent effect in the muscles is specific. More precisely, it has been shown that the force of a movement is proportionally related to the firing rate of the associated cortical neurons: when the load opposing a movement increases, the firing rate of the active neurons increases as well.

Direction of the movement

One of the first and most relevant studies regarding the direction of movement coding mechanism in the brain was achieved by Georgopoulos et al., who conducted studies on the primates' brain. Georgopoulos et al. trained monkeys to move a joystick toward

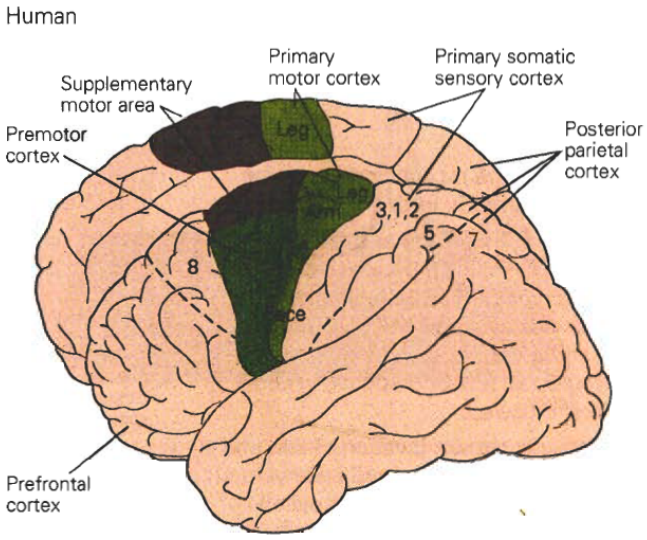

Figure B.3: The figure shows the motor cortices in humans. The sequence of representation of body parts is similar. The ankle control area is medial while the face, mouth, and mastication control areas are lateral. The face and fingers in the human motor cortex have much larger representations because of the greater degree of cortical control of these areas (adapted for own use from [Kandel et al., 2000]).

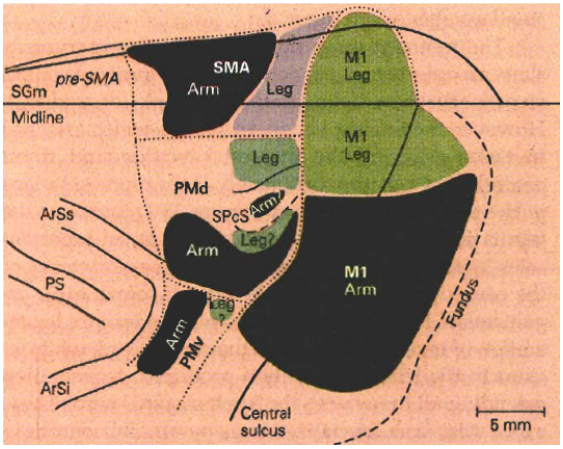

Figure B.4: Somatotopic oraganization of the medial and laterl motor cortex in the monkey, showing the arm and leg representations. **ArSi**, arcuate sulcus, inferior limb; **ArSs** = arcuate sulcus, superior limb; **CS** = central sulcus; **M1** = primary motor cortex; **PMd** = dorsal premotor area; **PMv** = ventral premotor area; **PS** = precentral sulcus; **SGm** = superior frontal gyrus, medial wall; **SMA** = supplementary motor area; **pre-SMA** = presupplementary motor area; **SPcS** = superior precentral sulcus. (adapted for own use from [Kandel et al., 2000])

visual targets located in different directions and recorded the associated changes in activity in the primary motor cortex. The experiment indicated that all neurons fired both before and during movement in a wide range of directions. It appears that motor cortical neurons are tuned to the direction of movement, but individual cells fire preferentially in connection with movement in certain a direction. The raster plots in figure B.5 show the firing pattern of a single neuron during movement in eight directions. The cell fires at relatively higher rates during movements in the range from 90 to 225 degrees, pointing out that different cells have different preferred movements directions. Cortical neurons with different preferred directions are all active during movement in a particular direction and the entirety of this activity results in a population vector that closely matches the direction of movement vector.
This means that movement in a particular direction is determined not by the actions of the single neurons, but by the net action of a large population of neurons, where the contribution of each neuron to movement in a particular direction can be represented by a vector, the length of which indicates the level of activity during the movement in that direction and where the contributions of individual cells can be added vectorially to produce a population vector.
Georgopoulos et al. also found a strong dependence between directionally tuned cell's firing rate and external load, suggesting that the activity of neurons in the primary motor cortex varies with the direction. This modulation depends on the amplitude of the force required to displace the limb; the neuron's firing rate increases if the load opposes the movement of the arm in the cell's preferred direction, while it decreases if the load pulls the arm in the cell's preferred direction.

Movement planning

In order to initiate a voluntary movement, The M1 needs to be stimulated by neurons from the premotor cortex and the supplementary motor area (SMA), which support and coordinate the M1. The preparatory activity of a movement is performed in the premotor areas and the primary motor cortex. This planning results in a motor program (or *movement pattern*) describing extent, angle and velocity of movement of the joints involved. Thus, the premotor cortex is in charge of providing sensory guidance of movement, while the SMA is responsible for planning and coordination of complex movements. The premotor cortex and the SMA are able to receive information from different decisional centres within the brain; these areas interpret the information, coordinate the execution commands and send it to the M1, which subsequently controls the actual signals sent to the muscles (effectors). A movement is the consequence of triggering of a pattern more that of the stimulation of each neuron separately, thus allowing to perform the movement more easily when it has been repeated.
A possible measure of the activity in the motor cortex of the brain, prior and during voluntary muscle movement, is called Bereitschaftspotential or BP (from German, "readiness potential"), which is covered more extensively in chapter C.

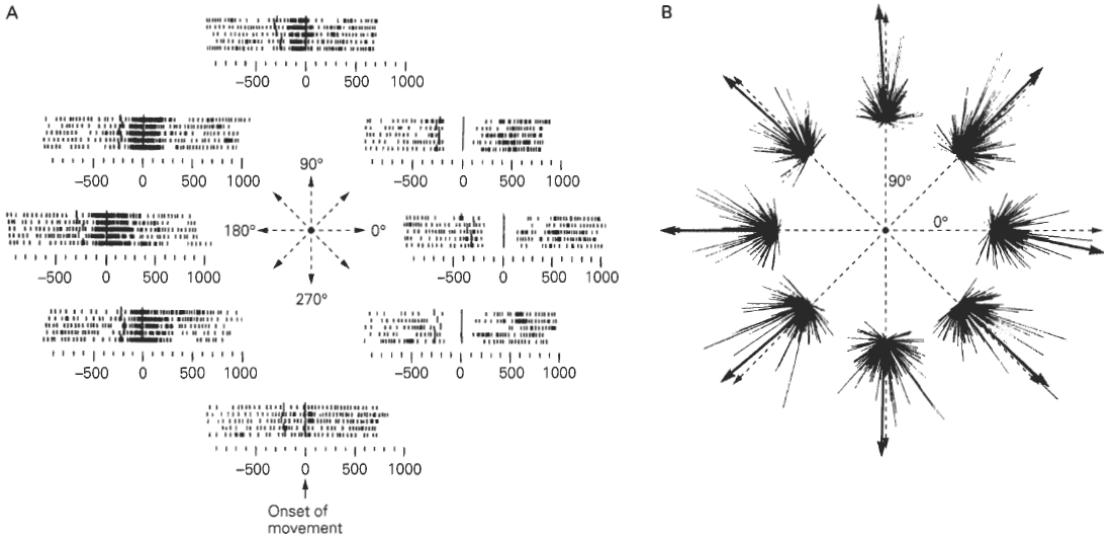

Figure B.5: The raster plots of the firing pattern of a single neuron during movement in eight direction. The cell fires at higher rates during movements in the range fro 90 degrees to 225 degrees. For these recordings a monkey was trained to move a handle to eight locations arranged radially in one plane around a central starting position. Each row of tics in each raster plot represents activity in a single trial. The rows are aligned at the onset of movement (zero time) (adapted for own use from [Georgopoulos et al., 1982]).

Appendix C

The Bereitschaftpotential

A comprehensive book which describes in detail the Bereitschaftspotential was published in 2003 ([Jahanshahi and Hallett, 2003]). It is hereby used as main reference, but also integrated with more recent findings, trying, when possible, to focus on hand movements in electroencephalographic recordings.

The first report of electroencephalographic (EEG) activity preceding voluntary movement in humans was made by Kornhuber and Deecke in 1964, who recorded EEG and electromyogram (EMG) activity, with the aim of connecting in some respect the activity of the brain with the one of the muscles involved in the movement on a temporal scale. The experiment was conducted using an off-line averaging technique and led to the identification of two main components of the BP, one before and one after the EMG onset: the actual Bereitschaftspotential (BP), also known as readiness potential (RP), and the reafferente potential. Later they found two more components which appear before the movement onset: the pre-motion positivity (PMP) and the motor potential (MP). Although a relatively high number of studies have been conducted on the movement-related cortical potentials (MRCPs), the actual physiological significance of each component, among others that of BP, has not been fully clarified yet [Shibasaki and Hallett, 2006].
In its original formulation by Kornhuber and Deecke, the BP was seen as 'readiness potential', an index of motor preparation. Further experiments have shown new and wider interpretations of the BP, which involve its influence in activities such as anticipation and expectancy, attention, preparatory activity, intention to act, resource mobilization, effort, timing of movements and degree of effort associated with movement. Jahanshahi and Hallett proposed that it is possible to differentiate the contributions to BP associated with cognitive, motivational and motor processes among the different areas of the motor cortex, rising the hypothesis that while prefrontal areas may be involved in the decision-making process necessary for response selection timing and initiation of the motor action, the pre-SMA motor areas and lateral premotor cortex may take care of preparatory precesses [Jahanshahi and Hallett, 2003].
The BP has become a common tool in motor physiology laboratory in the past years, not

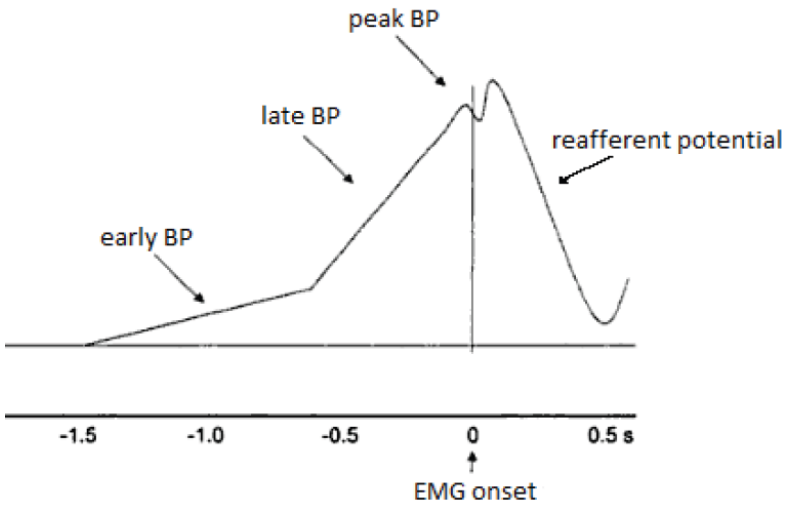

Figure C.1: A schematic representation of the time course and the Bereitschaftpotential (BP) prior to movement (adapted for own use from [Jahanshahi and Hallett, 2003])

only to investigate movement parameters such as force, rate, movement complexity and mode of movement, but its latency and/or shape have been reported to change in case of neurological disorders. Various methods are used to record BPs, e.g. scalp electroencephalography (EEG), magnetoencephalography (MEG), intracranial EEG recordings, combined EEG and positron emission tomography (PET), combined EEG and MEG, combined EEG and functional magnetic resonance imaging (fMRI).

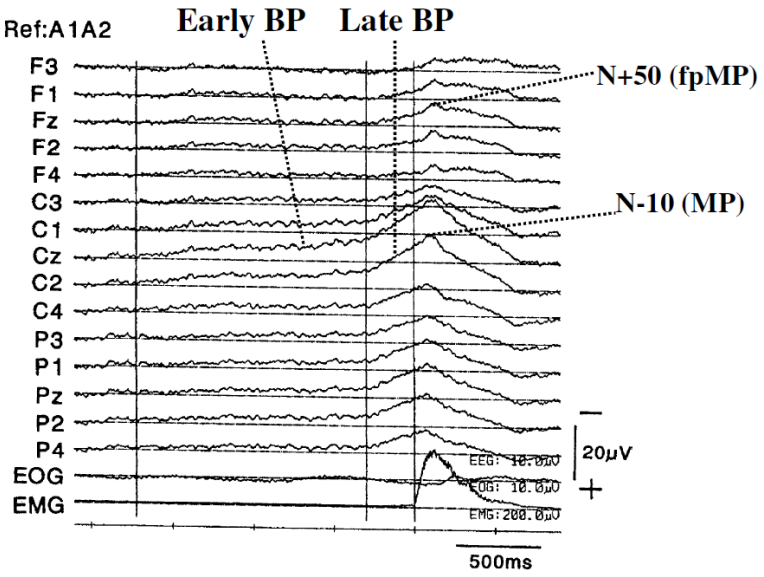

Figure C.2: Waveforms and terminology of MRCPs from a single normal subject in self-iniated left wrist extention. Avarage of 98 trials.
Reference: linked ear electrodes ((Ref:A1A2). Early pre-movement negativity (early BP) starts 1.7 s before the onset of the averaged, rectified EMG of the left wrist extensor muscle, and is maximal at the midline central electrode (Cz) and widely and symmetrically distributed on both hemispheres. The late negative slope (late BP) starts 300 ms before the EMG onset and is much larger over the right central region (contralateral to the movement). A negative peak localized at the contralateral central area (C2) is N-10 or motor potential (MP). Another negative peak occurring shortly after N-10 is localized over the midline frontal region and corresponds to N+50 or the frontal peak of motor potential (fpMP).
(adapted for own use from [Shibasaki and Hallett, 2006])

C.1 Morphology of BPs

BPs are considered to represent neuronal activation, which is the outcome of an increase of extracellular K^+ concentration and decrease of Ca^{++} concentration. This activation of brain regions result in negative slow potentials, such as the BP. More specifically, the BP is a negative cortical potential which develops beginning about 1.5 to 1 s prior the onset af a self-placed movement (see figure C.1 and C.2), although the onset of BP with respect to the movement onset significantly differs among diverse conditions of movement and among subjects. For example, when the subject is requested to repeat the same movement, the BP starts much earlier as compared to the same movement executed in natural conditions, because in such experimental conditions the subject has a longer time to prepare for the movement. It is important to stress that the BP is related to an actual, intended or imaginary voluntary movement. Thus, the BP can be defined as a movement-related cortical potential (MRCP).
Initially a distinction between the slowly rising phase of BP waveform and change in the steepness of the slope, which suddenly occurs around 400 to 500 ms prior to movement onset, was made (see figure C.1). The early and late BP differ in term of distribution over the scalp: the early BP is bilaterally symmetrical, but the late and peak BP are asymmetrically distributed and maximal over the contralateral precentral areas [Jahanshahi and Hallett, 2003]. The early slow, rising negativity has been usually referred as early BP, BP1, and NS1 (negative slope 1), whereas BP2, NS' and NS2 stand for the second phase of negativity [Jahanshahi and Hallett, 2003]. The late BP was thought to be more specific for the site of movement while the early BP was thought to represent the more general preparation for the forthcoming movement because of its diffuse distribution, but neither the physiology nor the functional significance of change of steepness is currently completely known (see section C.2).
Later, a third negative component was distinguished, occurring 50 to 60 ms prior to movement onset, the 'motor potential' (MP, peak BP or peak NS'), which is the point of maximum negativity over the hand area contralateral to the moving hand. The BP midline maximal, symmetric distribution is likely due to the summation of electrical fields generated from homologous areas of both hemispheres [Shibasaki and Hallett, 2006].
Different groups have proposed wide range of different terminologies, according to their findings and different opinions about origin, location and physiological meaning of BP components (see table C.3 for details), however, in this report, in order to avoid confusion about the use of the term BP, we call the early segment 'early BP' and the late, steeper segment 'late BP', and just BP for the early BP and the late BP inclusive (see figure C.2).

	Pre-movement components				Post-movement components			
Kornhuber and Deecke (1965)	BP		PMP	MP				RAP
Vaughan et al. (1968)	N1		P1	N2 (?)	N2 (?)			P2
Shibasaki et al. (1980a)[a]	BP	NS′	P−50	N−10	N+50	P+90	N+160	P+300
Dick et al. (1989)	NS1	NS2						
Lang et al. (1991)	BP1	BP2						
Tarkka and Hallett (1991)	BP	NS′	PMP	isMP ppMP	fpMP			
Kristeva et al. (1991)[b]	RF			MF	MEFI	MEFII	MEFIII	PMF
Cui and Deecke (1999)	BP1	BP2		MP		PMPP	MEPI	MEPII

[a] Peak of each component, except for BP and NS′, was measured from the peak of averaged, rectified EMG.
[b] Based on movement-related magnetic fields.

Figure C.3: Terminology used to describe the components of movement-related cortical potentials (adapted for own use from [Shibasaki and Hallett, 2006])

C.2 Generator sources of MRCPs

The generator sources of MRCPs have to be fully understood yet. In order to achieve this challenge, various dipole source localization techniques have been applied, as already mentioned above. The identification of generators of single MRCP components is a controversial topic in the existing literature. The complexity of the problem occurs due to several different factors, such as the specific localization technique which was used, the type of movement under investigation, the movement performance and the investigated time frame. However, it is common opinion among the literature that the BP is mainly generated by sources located in the supplementary motor area (SMA) (both the proper SMA as well as the cingulate motor area (CMA) should be considered in this context) and in the M1 (particularly in the contralateral motor cortex) to a lesser or greater extent. [Shibasaki and Hallett, 2006]. Moreover, also regarding the time course of activation of the SMA and M1, there are still doubts. Some suggest that the BP reflects serial activation of the SMA preceding M1, others propose that SMA and M1 are activated in parallel [Jahanshahi and Hallett, 2003].
The current consensus on the generator source of each MRCP component is summarized in table C.4. At least regarding self-paced repetition of simple movements at slow rate, the early BP begins about 2 s before the movement onset in the pre-SMA with no site-specificity and is bilaterally generated from the localized area of the SMA according to the somatotopic organization and shortly thereafter in the lateral premotor cortex bilaterally, again with relatively clear somatotopy. About 400 ms before the movement onset, the steepness of the waveform suddenly changes and the late BP occurs in the contralateral M1 and lateral premotor cortex with precise correspondence to a somatotopic organization. The generator sources of post-movement components have not been clearly identified yet [Shibasaki and Hallett, 2006].

Shibasaki and Hallett, in their review, have reported some experiments concerning the case of hand movements. SMA and lateral precentral gyrus were shown to be the main generator sources for early BP. It has been proposed that there are three dipole sources of the early BP, one in the SMA and two others in bilateral M1, and that only the source recorded in the SMA was influenced by the mode of movement selection in such a way that it was larger before freely selected movements than fixed ones. Based

Component	Generator sources
Early BP	
Earliest	Pre-SMA (bilateral)
	SMA proper (bilateral)[a]
Next earliest	Area 6 (bilateral)[a]
Late BP (NS′)	Area 6 (mainly contralateral)[b]
	Area 4 (mainly contralateral)[b]
MP (N−10)	Area 4 (contralateral)[b]
fpMP (N+50)	Area 3 (contralateral)[b]

[a] Somatotopically organized to some degree.
[b] Somatotopically organized precisely.

Figure C.4: Generator sources of each component of movement-related cortical potentials (MRCP) (adapted for own use from [Shibasaki and Hallett, 2006])

on the high-resolution DC-EEG analysis, it has been estimated that BP occurs earlier in the SMA and cingulate motor areas, after in the contralateral M1, and finally in the ipsilateral M1. Principal component analysis and fMRI-constrained EEG dipole source analysis were used, determining that the main source of early BP was the crown of the precentral gyrus bilaterally (specifically hand area of area 6), the source of late BP in both area 4 and area 6, and MP in area 3. Most studies have localized the source of MP or N-10 in the M1 hand area.
For this report, it is important to record EEG from multiple electrodes, including C1 and C2, because the late BP is maximal over the contralateral central area (approximately C1 or C2 of the International 10-20 System) for hand movements.

C.3 Factors influencing BP

As reported by Shibasaki and Hallett, Lang W. reviewed extensively the factors that contribute to magnitude and time course of BP recorded in a self-paced condition. Taken together, the amplitude and the time course of the MRCP are affected by various factors, such as: level of intention; speed, precision, mode (free versus fixed), pace or repetition, discreteness, complexity of the movement; preparatory state; learning and skill acquisition; perceived effort; force exerted and pathological lesions of brain structures.
Below are listed some studies supporting the information given by table C.5, which summarizes the findings about this issue so far [Shibasaki and Hallett, 2006].

The effect of the complexity of a movement on the BPs was investigated in several studies, mostly involving comparison of single, simultaneous and sequential movements, which confirm that more complex movements translate in larger late BPs.
Comparison of isolated single finger extension with simultaneous finger extension of two fingers revealed significantly larger BP at the pre-central area contralateral to the movement. In the case of single finger activation; although only half of the muscles are

Factors	Early BP	Late BP
Level of intention	Larger[a]	
Preparatory state	Earlier onset[a]	
Movement selection	Larger	No effect
Learning	Larger during learning[a]	
Praxis movement	Start parietally[a]	
Force	Larger[a]	
Speed	Later onset[a]	
Precision	No effect	Larger
Discreteness	No effect	Larger
Complexity	No effect	Larger
Parkinsonism	Small	No change
Cerebellar lesion	Small	Small
Dystonia	No change	Small
Hemiparesis recovery	No change	Involved
Mirror movement	No change	Involved

Figure C.5: Differential influence of various factors on early and late BP in normal and pathological conditions. As for the factors in normal conditions. (adapted for own use from [Shibasaki and Hallett, 2006])

activated. This phenomena can be explained by the fact that single finger movements are finer and more discrete, therefore requiring a more 'precise' motor program and M1 activation (Kitamura et al., 1993). Another study was comparing single isotonic elbow flexion and single isometric finger flexion with sequential and simultaneous activation of these two movements, finding a larger BP for the sequential and simultaneous movements compared to single flexion (Benecke et al., 1985). Kitamura found that, when middle and index finger were moved consecutively, the negative slope started earlier, but no amplitude changes of the BP were observed, compared to simultaneously activation of the fingers. Thus, it was hypothesised that the execution of unilateral sequential movement requires a greater and earlier activation of the SMA and the primary hand sensorimotor areas (Kitamura et al.). Earlier onset and larger amplitude of BP in a sequential or more complex movement compared to a simple one, was also reported by Simonetta et al.(1991).

The exerced force is another factor that was shown to increase the BP (Slobounov et al., 2004; Masaki et al., 1998). In a study conducted by Masaki et al. (1998), when subjects were asked to produce a specific force, a larger negative slope was observed compared to movements performed in a non-purposive manner although the same amount of force was produced. This leads to think about the involvement of a planning process which is required to produce a particular force and subsequently leads to a larger BP amplitude. Again, a possible explanation can be that the preparation process in order to develop larger forces requires a higher level of activity of the involved brain areas.

As for the mode of movement, investigation showed that freely selected movements lead to higher amplitude of BP as opposed to pre-determined repetitive movements. This influence does not seem to involve all the areas of the brain, though. By using a spatio-temporal decomposition, three dipole sources of the BP were estimated: one located in the SMA and two in the M1 in each hemisphere, finding that only the source in the SMA was influenced by the mode of the movement (Praamstra et al.,1995). In contrast,

Dirnberger et al. (1998) observed a larger lateralized readiness potential for freely selected movements compared to fixed repetitive movements, considering this as a result of a greater involvement of M1 activity in the selected movement mode.
Furthermore, the BP onset is affected by the speed with which the movement is conducted. The BP starts later if the movement is performed with a higher speed (Shibasaki and Hallett, 2006). The time course of the early BP is also influenced by the level of experience of the movement under study. Libet et al.(1983), for example, observed a BP occurring 1 s earlier when the movement is associated with a preplanning or preparation time to act shortly compared to movements which are associated with a more specific or endogenous intention to act (about 500 ms prior onset).

Appendix D

Signal processing and classification background

In this chapter are explained some of the signal processing, classification and statistical techniques used during the project. The following pages do not cover all the theory; rather they give a general overview on the specific techniques that have been applied.

D.1 Time-frequency maps

Time-frequency maps were used for the movement direction classification, which was indeed base on time-frequency analysis (see example in figure D.3).
A time-frequency (TF) map is a view of a signal (taken to be a function of time) represented over both time and frequency, where the modulus represented the power spectral density of the signal. There are two main ways of computing a TF map: the windowed Fourier transform and the wavelet transform.

Windowed Fourier transform The windowed Fourier transform replaces the sinusoidal wave of the Fourier transform's with the product of a sinusoid and a window localized in time. It takes two arguments: time and frequency. It uses an atom which is the product of a sinusoidal wave with a finite energy symmetric window g. The windowed Fourier transform family of atoms is obtained by time translations and frequency modulations of the original window g, thus it has a constant time frequency resolution. This resolution can be changed by rescaling of the time window. It is a complete, stable and redundant representation of the signal (see figure D.1), hence it is invertible [Chaplais, 1998].

Wavelet transform The wavelet transform replaces the Fourier transform's sinusoidal waves by a family generated by translations and dilations of a window called a wavelet. It takes two arguments: time and scale. Its time spread is proportional to scale s, while

its frequency spread is proportional to the inverse of s [Chaplais, 1998].
The main advantage of wavelet transforms is the variation of windows length. In order to isolate signal discontinuities, one would like to use short basis functions and, at the same time, long basis functions in order to obtain detailed frequency analysis. Therefore, reformulating, short high-frequency basis functions and long low-frequency ones. This "happy medium" is exactly what is provided by wavelet transforms (see figure D.2) [Graps, 1995]. Wavelet transforms do not have a single set of basis functions like the Fourier transform, which utilizes just the sine and cosine functions. Instead, wavelet transforms have an infinite set of possible basis functions. Thus, wavelet analysis provides immediate access to information that may be obscured by other time-frequency methods such as Fourier analysis [Graps, 1995].

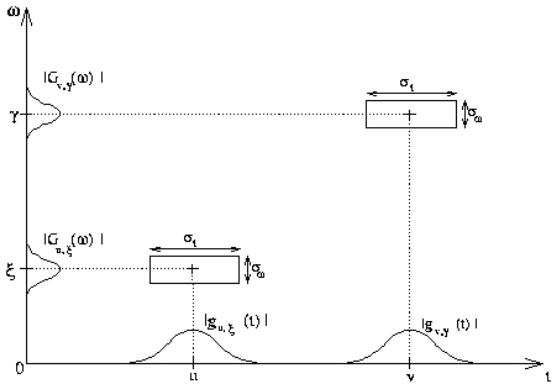

Figure D.1: Windowed Fourier transform - The boxes show the localization of an atom in the time-frequency space computed by the windowed Fourier transform. Notice that the time-frequency resolution is constant [Chaplais, 1998].

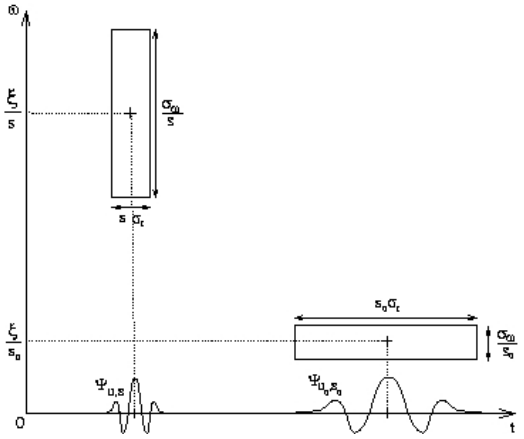

Figure D.2: Wavelet transform - The boxes show the localization of an atom in the time-frequency space computed by the wavelet transform. The time resolution is finer when punctual changes occur in the signal (high frequencies), while the frequency resolution is finer when the signal is stable in time (low frequencies) [Chaplais, 1998].

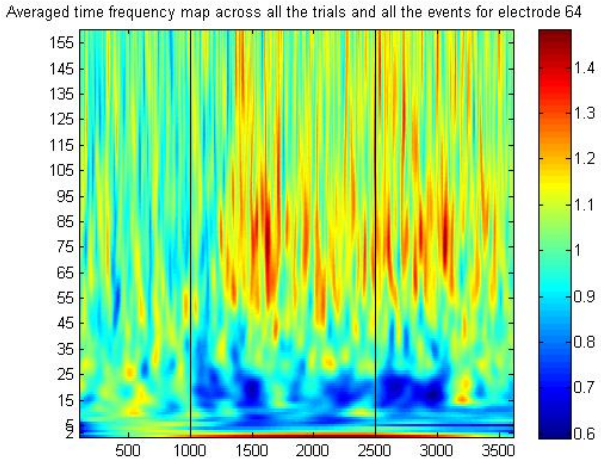

Figure D.3: Averaged TF map for channel f10-f9. The vertical black lines show respectively the visual cue and the go signal. Note the effect of wavelet transform in high frequencies (stretching) and low frequencies (crushing).

D.2 Classification

Classification algorithms were used to identify 'patterns' of brain activity. Considering the features and a classification algorithm, the BCI tries to recognize different mental states in a given data set (e.g. hand movement). As a result, the performance of a pattern recognition system depends on both the features and the specific algorithm employed [Lotte et al., 2007].

Given the features, a classifier is trained on an experimental data set so to adjust a boundary between the classes by means of a classification algorithm. Formally, classification consists in finding the true label $y*$ of a feature vector $\mathbf{x}$ using a mapping function f learnt from a training set T [Lotte et al., 2007].
A classifier can easily reach 100% of good classification on a given set of data (e.g. by learning "by heart" which sample belongs to which class) but, at the same time, provide poor performance on a new data set. It is thus important to find to evaluate the classifier performance.
The classification methods used during the project are listed in the following pages.

D.2.1 K-nearest-neighbor

The k-nearest-neighbor (kNN) rule is a supervised method for data classification. This method assumes no prior knowledge of the statistics of the data in question. kNN is sometimes referred as a 'lazy method', meaning that there it implies very little training and it does not use the training data points to do any generalization.
The k-nearest-neighbor rule classifies a sample by the majority of the number k of the nearest training samples around it, as shown in figure D.4. K is often an odd number to ensure majority, and the outcomes of the classification are strongly linked to the choice of k. E.g., a high k removes noise, but decreases the accuracy of the boundaries [Duda et al., 2001].
The distance between samples can be calculated using different measures. For this project, the Euclidean distance formula was chosen, as it is the most used:

$$D(\mathbf{a}, \mathbf{b}) = \left(\sum_{k=1}^{d} (a_k - b_k)^2 \right)^{\frac{1}{2}}$$

Where d is the dimensionality of $\mathbf{a}$ and $\mathbf{b}$.

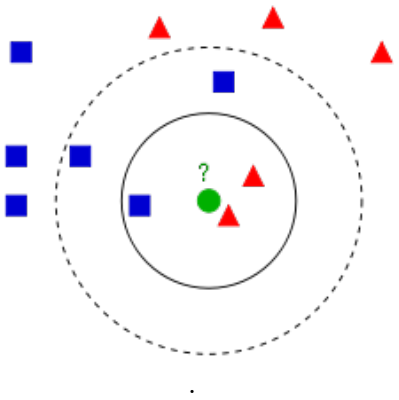

Figure D.4: The figure shows the principle behind K-Nearest-Neighbor Rule in a two dimensional feature space. The blue squares represent class 1 and the red triangles represent class two. The green dot will be classified according to the chose number k of nearest samples (image from Wikipedia)

D.2.2 Linear discriminant analysis

Linear discriminant analysis (LDA) is a method used in statistics, pattern recognition and machine learning in order to find a linear combination of features which separates two or more classes of objects or events. LDA is characterized as a supervised and parametric method and is performed under the hypothesis of multivariate normal distribution, with different mean for each class, same conditional covariance matrix and same a priori probability for each class [Duda et al., 2001].
LDA is a "fast" method compared to more complex ones but, depending on the underlying distribution of the samples, its performances may be poorer. When classes need to be classified, a decision boundary is needed: LDA looks for the linear combination of features which best describes the data and it calculates a decision boundary. The decision boundary has the form of a hyperplane $g(\mathbf{x}) = 0$ (or multiple hyperplanes to solve a N-class problem with $N > 2$) of the feature space. The discriminant function $g(\mathbf{x})$ is described as:

$$g(\mathbf{x}) = \mathbf{w}^t \cdot \mathbf{x} + w_0,$$

where $\mathbf{x}$ is the input features vector, $\mathbf{w}$ is the weight vector, which determines the direction of the decision boundary, and w_0 is the bias, which determines the location of the decision boundary.
Figure D.5 shows the result of LDA for the given set of data. It can be observed how LDA divides the two classes with a linear boundary.

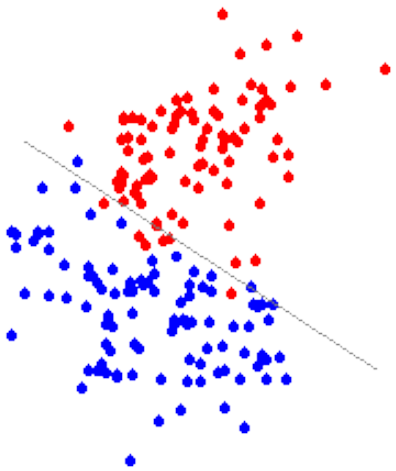

Figure D.5: LDA performed in a two dimensional feature space. The red points and the blue circles belong to different classes, the straight line is the boundary computed by LDA [Mirkin, 2011].

D.2.3 Support vector machine

Support Vector Machine (SVM) is closely related to Linear Discriminant Analysis. It uses both k-nearest-neighbor rule and linear discriminant analysis classification [Press et al., 2007]. SVM aims to find one (or several) separating hyperplane(s) between two or more classes. Differently from LDA, thought, SVM tries to find the hyperplane with the largest margin between the classes, thus it ensures a better generalization of the classifier. Furthermore, SVM does not assume multivariate normal distribution of the features [Noble et al., 2004]. A possible case is illustrated in figure D.6. The hyperplane labelled H_1 could be a result of a LDA and H_2 of SVM analysis. While $H1$ separates the classes, it is less generalizable than the hyperplane H_2, which separates the classes by a greater margin [Duda et al., 2001].
SVM finds the so-called support vectors (samples on the margin), which are the most difficult samples to classify. The hyperplane is then situated with equal distance with respect to the support vectors. As it is not realistic to expect two (or more) classes to be completely separable, the soft-margins method is introduced. It will choose a hyperplane that splits the samples, while still maximizing the margin (see figure D.7). The soft margins are introduced to allow samples of one class to push trough the margin and into the area of the other class [Noble et al., 2004].

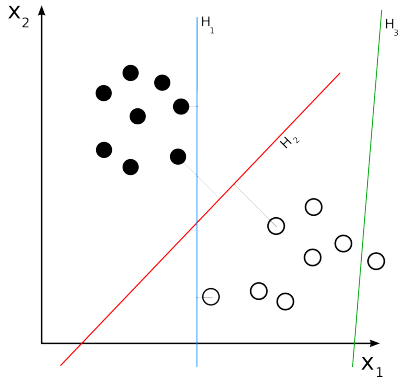

Figure D.6: The hyperplanes H_1, H_2 and H_3 lead to different separation and generalizability. H3 (green) doesn't separate the two classes. H1 (blue) does, with a small margin and H2 (red) with the maximum margin (image from Wikipedia).

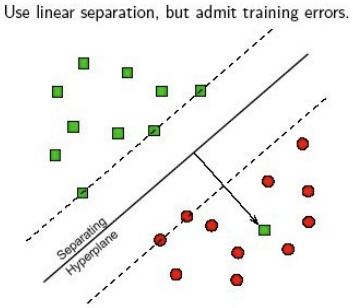

Figure D.7: Maximum-margin hyperplane and margins for an SVM trained with samples from two classes. Samples on the margin are called the support vectors (image from *dtreg.com*).

D.2.4 Neural network

Another interesting method that was used during the project, is the neural network (NN) based classification, since the architecture of neural networks is inspired by the brain. A NN is made of several simple communication processors (called 'neurons'), distributed in at least two layers. Usually, a neuron is connected to every other neuron of the following layer [Hudson and Cohen, 1999].
The inputs of the neural network are the different features, and each output is a class. Given a certain input, the sample is classified according to the output of the NN. The NN can be trained with a training data set [Hudson and Cohen, 1999].
There are three main characteristics which describe a NN: neuron model, architecture and training algorithm [Hudson and Cohen, 1999].

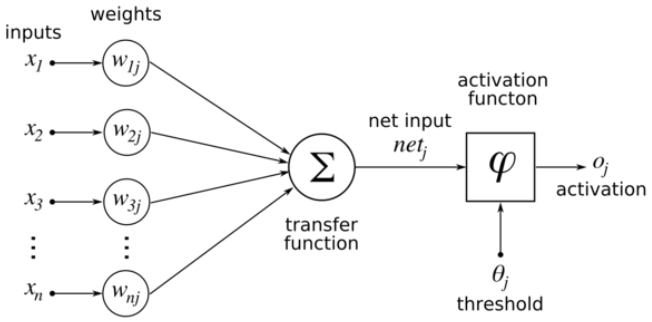

Figure D.8: Representation of a neuron using a NN (image from Wikipedia).

Neuron model As showed in figure D.8, each input is first weighted, then all the weighted inputs are summed by the so-called 'transfer function' and, finally, the 'activation function' will provide a final single output. The activation function φ can vary a lot from a NN to another. Its simplest form is a threshold which provides a binary

output (e.g. if the input $net_j > \theta_j$, then the output is 1, otherwise it is 0) or it can also be a more complex continuous functions [Hudson and Cohen, 1999].

Architecture For a supervised NN, at least three layers are usually used (as in figure D.9). The layers between the input and output layers are called hidden layers. A three-layer neural network is also usually complex enough to solve the given classification problems if the activation function is not linear[Hudson and Cohen, 1999].

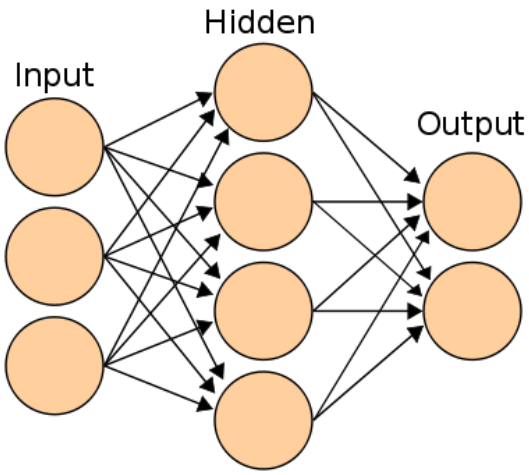

Figure D.9: Architecture of a neural network (image from Wikipedia)

However, more than three layers can be used. This enables a more adaptive NN with greater processing power at the cost of more complex training algorithm [Hudson and Cohen, 1999].
One of the most important types of NNs is the feed-forward. As illustrated in D.9 there is no feedback from a layer to the previous one. Each input represents a component of the feature vector and each output represents a class [Hudson and Cohen, 1999].

Training algorithm A widespread supervised training method is the so-called back-propagation [Hudson and Cohen, 1999]. When there is a mistake (wrong classification) in the outputs, the difference between the expected outputs and the actual outputs is computed. This difference is called error and it is propagated backwards through the hidden layers. The output of each neuron is multiplied by the error, so to get a gradient of the weight. If the gradient is negative, the weight is increased for each neuron according to a given learning rate, and vice versa [Hudson and Cohen, 1999].

D.2.5 Evaluation of classifier performance

In order to perform a classification, the first step is to train the classifier using a training set. The next step is to test the classifier and answer the question: *how well does*

the classifier perform on a new data set? There are several methods to evaluate the performance of a classifier.
A good choice is to separate the total amount of data into a training data set a testing data set and, when possible, a validation data set. In this way, the training data would never be used to test the classifier. Unfortunately, three (or even two) sets are often difficult to generate because of the required extensive amount of data. The limited amount of data makes it necessary to apply a method that reuses the training data [Hawkins, 2004]. One of these methods is cross validation, and the leave-one-out cross validation is in turn its best-known particular case.
The leave-one-out cross-validation trains the classifier on the entire set of samples, except one. The left-out sample is then used to test the classifier. This operation is iterated for every sample and provides a final confusion matrix [Duda et al., 2001].